



Různé přístupy k predikci pevnosti tryskové příze

Disertační práce

Studijní program: P3106 – Textile Engineering
Studijní obor: 3106V015 – Textile Technics and Materials Engineering
Autor práce: **Moaaz Ahmed Samy Moustafa Eldeeb**
Vedoucí práce: Ing. Eva Moučková, Ph.D.





TECHNICAL UNIVERSITY OF LIBEREC
Faculty of Textile Engineering



Different Approaches for Predicting Air Jet Spun Yarn Strength

Dissertation

Study programme: P3106 – Textile Engineering
Study branch: 3106V015 – Textile Technics and Materials Engineering
Author: **Moaaz Ahmed Samy Moustafa Eldeeb**
Supervisor: Ing. Eva Moučková, Ph.D.



Prohlášení

Byl jsem seznámen s tím, že na mou disertační práci se plně vztahuje zákon č. 121/2000 Sb., o právu autorském, zejména § 60 – školní dílo.

Beru na vědomí, že Technická univerzita v Liberci (TUL) nezasahuje do mých autorských práv užitím mé disertační práce pro vnitřní potřebu TUL.

Užiji-li disertační práci nebo poskytnu-li licenci k jejímu využití, jsem si vědom povinnosti informovat o této skutečnosti TUL; v tomto případě má TUL právo ode mne požadovat úhradu nákladů, které vynaložila na vytvoření díla, až do jejich skutečné výše.

Disertační práci jsem vypracoval samostatně s použitím uvedené literatury a na základě konzultací s vedoucím mé disertační práce a konzultantem.

Současně čestně prohlašuji, že tištěná verze práce se shoduje s elektronickou verzí, vloženou do IS STAG.

Datum:

Podpis:

Acknowledgment

First and foremost, I'm thankful to my God who gave me the capability, courage, and opportunity to complete my Ph.D. thesis, a very long journey full of hardships. The list of those that I would like to acknowledge seems to be endless. However, there are those who provided support, without which this thesis would not have been possible. I would like to thank my wife, son, parents, and parents-in-law for their sincere love, enormous support, and patience, for being away from them during the last four years.

I would like to thank my respected supervisor Ing. Eva Moučková, Ph.D., the person who helped me to see it through to the end. I'm thankful for her continued encouragement, advice, prompt response, inclusion, patience, support, invaluable guidance and confidence in my abilities. I'm also very grateful to my Ph.D. study consultant Prof. Ing. Petr Ursíny, DrSc.

It is a great pleasure to thank all those people who helped me during this journey. I will always be grateful to all members of the Textile Technology Department, including my first supervisor, (the late) Prof. Ing. Sayed Ibrahim Ali, CSc., Ing., Prof. Ing. Bohuslav Neckář, DrSc., Ing. Bc. Monika Vyšanská, Ph.D., Ing. Petra Jirásková, Ing. Jana Špánková, Ing. Muhammad Zubair, M.Sc., and Šárka Řezníčková. Without the help of all these people, this thesis would have never been completed.

I will always be grateful to Rieter CZ s.r.o team in Usti Nad Orlici as well as dean's office of the faculty especially Mrs. Bohumila Keilová and Mrs. Hana Musilova. Last, but certainly not least, I am thankful to the Faculty of Textile Engineering for their financial assistance as well as my home University, Mansoura University, Egypt, for granting me the study leave.

Abstract

Air jet spinning process has reached an industrial acceptance stage having developed through half a century. This study aims to contribute to the knowledge of air-jet yarn formation process by investigating the influence of selected technological parameters of the Rieter air-jet spinning machine on yarn properties, especially its strength. Furthermore, to shed light on the problem of the prediction of yarn strength. A three-dimensional numerical simulation of the airflow field inside Rieter air jet spinning nozzle has been presented. The velocity and pressure distribution were analyzed to describe the principle of yarn formation. The analysis of velocity components and static pressure revealed how the air vortices are created inside the nozzle as well as how the yarn is spun.

A numerical simulation along with experimental verification were performed to investigate the influence of nozzle pressure on air jet yarn tenacity and the results were in good agreement. The results show that increasing nozzle pressure resulted initially in improving yarn tenacity, but at high-pressure, tenacity deteriorates.

Different approaches have been used to predict the tenacity of air jet yarn. One of these approaches is a statistical model, where the effect of yarn linear density, delivery speed and nozzle pressure on yarn strength were investigated and a multiple regression model was used to study the combined effect of these parameters and response surfaces were obtained. Based on the different combinations of processing variables, optimal running conditions for tested materials were obtained.

As a second possible approach to predict yarn strength, a mathematical model that predicts the strength of Viscose and Tencel air jet spun yarn at short gauge length has been presented which is based on an earlier model. The model is based on calculating the core fiber strength as a parallel bundle of fibers. Also, calculating the wrapper fiber strength as a bundle of fibers in the form of helical path and considering the interaction effect between the wrapper and core fibers. Fiber parameters in addition

to yarn structural parameters were used to obtain the theoretical yarn tenacity at short gauge length. Results showed that the accuracy of the proposed model is satisfactory for the tested yarns set.

As an alternative approach to predict air jet yarn strength, a statistical model has been presented. By using this model, the influence of the tensile tester gauge length on the ring, rotor, and air jet spun yarn tenacity and its coefficient of variation has been investigated. The model correlates yarn tenacity and coefficient of variation of yarn tenacity to gauge length. The model is based on Peirce model and assuming the 3-parameter Weibull distribution of yarn strength values. A reasonable agreement has been shown between the experimental and the predicted values. The model successfully captured the change in yarn strength and its coefficient of variation at different gauge lengths. Results confirmed that at longer gauge lengths, yarn strength decreases and its coefficient of variation decreases as well.

Keywords

Numerical simulation; mathematical modeling; statistical modeling; fibers; Rieter air jet spinning; airflow; wrapper ratio; strength prediction; Viscose; Weibull distribution; gauge length; linear density; nozzle pressure; delivery speed; structure.

Abstrakt

V současné době tryskové dopřádání dosáhlo po půlstoletí svého vývoje průmyslového uznání a zaujalo své místo na trhu. Cílem této práce je přispět k poznání procesu tvorby příze, zmapovat vliv vybraných technologických parametrů tryskového dopřádacího stroje na vlastnosti příze, zejména její pevnost a především poskytnout širší náhled na problematiku predikce pevnosti tryskové příze. V práci je provedena trojrozměrná numerická simulace průtokového pole vzduchu uvnitř spřádací trysky tryskového dopřádacího stroje Rieter Air-jet. Byla analyzována distribuce rychlosti a tlaku vzduchu s cílem popsat princip tvorby příze. Analýza složek rychlosti a statického tlaku vzduchu ukázala, jak jsou uvnitř trysky tvořeny vzduchové víry, a jakým způsobem se příze formuje.

Byla provedena numerická simulace spolu s experimentální verifikací, která zkoumala vliv tlaku krouťícího vzduchu na pevnost příze. Výsledky simulace přinesly dobrou shodu s experimentem. Výsledky ukázaly, že zvyšující se tlak v trysce vedl zpočátku ke zlepšení pevnosti příze, ale při vysokém tlaku vzduchu se pevnost zhoršila.

Ve stěžejní části práce jsou prezentovány a popsány různé možnosti přístupů k predikce pevnosti příze. Jedním z nich je statistické modelování založené na experimentálních měřeních. V rámci tohoto přístupu byl sledován vliv délkové hmotnosti příze, odtahové rychlosti a nastaveného spřádního tlaku vzduchu. Pro analýzu kombinovaného vlivu těchto parametrů pomocí responzních povrchů byl použit vícenásobný regresní model. Na základě různých kombinací mezi sledovanými technologickými veličinami byly získány optimální parametry nastavení pro testovaný materiál.

Jako druhý z možných přístupů k predikci pevnosti tryskové příze je navržen matematický model. Pomocí tohoto modelu lze predikovat pevnost 100% viskozové

a 100% tencelové tryskové příze na krátkých upínacích délkách. Model je založen na výpočtu pevnosti jádra příze, jakožto paralelního svazku vláken, výpočtu pevnosti obalové vrstvy vláken jakožto svazku vláken ovinutého ve šroubovici kolem jádra příze. V modelu je rovněž zohledněn interakční účinek mezi vlákny v obalu a vlákny v jádru příze. Jako vstupní parametry modelu pro výpočet teoretické pevnosti příze na krátkých upínacích délkách jsou použity parametry vláken i strukturální parametry příze. Výsledky ukázaly, že přesnost navrhovaného modelu je uspokojivá pro soubor experimentálních přízí.

Jako další z možných přístupů k predikci pevnosti příze (na krátkých úsečkách) je prezentován statistický model. Pomocí modelu je zkoumán vliv upínací délky příze v trhacím přístroji na pevnost a variační koeficient pevnosti tryskové, prstencové a rotorové příze. Model vychází z Peirceova modelu a předpokládá tříparametrové Weibullovo rozdělení hodnot pevnosti příze. Mezi experimentálními a predikovanými hodnotami byla zaznamenána přiměřená shoda. Model úspěšně zachytil změny pevnosti příze a její variační koeficient při různých upínacích délkách. Výsledky potvrdily, že při větších upínacích délkách pevnost příze klesá a její variační koeficient se rovněž snižuje.

Klíčová slova

Numerická simulace; matematické modelování; statistické modelování; vlákna; tryskové dopřádání Rieter; proud vzduchu; podíl obalových vláken; predikce pevnosti; viskóza; Weibullovo rozdělení; upínací délka; jemnost; tlak spřádního vzduchu; odváděcí rychlost; struktura

الملخص

لقد وصلت عملية الغزل بنفث الهواء مستوى مقبول على مستوى الصناعة بعد تطورهما خلال نصف قرن. تهدف هذه الدراسة إلى المساهمة في معرفة عملية تكوين الخيط المغزول بنفث الهواء من خلال التحقيق في تأثير متغيرات تكنولوجية مختارة لنظام الغزل بنفث الهواء "ريتر" على خصائص الخيط وخاصةً المتانة. وعلاوة على ذلك، تسليط الضوء على مشكلة التنبؤ بمتانة الخيط. تم تقديم محاكاة عددية ثلاثية الأبعاد لحقل تدفق الهواء داخل فوهة الغزل النفثة "ريتر". وتم تحليل توزيع السرعة والضغط لوصف مبدأ غزل الخيط. كشف تحليل مركبات السرعة وأيضاً الضغط الساكن كيف تتكون دوامات الهواء داخل الفوهة وأيضاً كيف يُغزل الخيط.

أجريت محاكاة عددية مع تحقق عملي لبحث تأثير ضغط الفوهة على متانة الخيط المغزول بنفث الهواء وكانت النتائج في اتفاق جيد. وأظهرت النتائج أن زيادة ضغط الفوهة أدت في البداية إلى تحسين متانة الخيط، ولكن عند الضغط العالي تتدهور المتانة.

وقد تم استخدام أساليب مختلفة للتنبؤ بمتانة الخيط المغزول بنفث الهواء وأحد هذه الطرق هو نموذج إحصائي حيث تم دراسة تأثير الكثافة الطولية للخيط، سرعة الإنتاج، وضغط الفوهة على متانة الخيط وتم استخدام نموذج الانحدار المتعدد لدراسة التأثير المشترك لهذه المتغيرات وتم الحصول على أسطح الاستجابة. وإستناداً إلى التوليفات المختلفة بين متغيرات التشغيل، تم الحصول على ظروف التشغيل المثلى للعينات المختبرة.

وكطريقة ممكنة أخرى للتنبؤ بمتانة الخيط المغزول بنفث الهواء، تم تقديم نموذج رياضي يتنبأ بمتانة خيوط "الفسكوز" و"التنسل" المغزولة بنفث الهواء عند معيار قياس قصير إستناداً إلى نموذج سابق. ويستند هذا النموذج إلى حساب متانة شعيرات القلب كحزمة متوازية من الألياف. أيضاً، حساب متانة شعيرات التحزيم كحزمة من الألياف في شكل مسار حلزوني مع مراعاة التفاعل بين شعيرات القلب والتحزيم. تم استخدام متغيرات الشعيرات بالإضافة إلى متغيرات تركيب الخيط للحصول على متانة الخيط النظرية عند معيار قياس قصير. وأظهرت النتائج أن دقة النموذج المقترح مرضية للعينات المختبرة.

وكطريقة أخرى للتنبؤ بمتانة الخيط، تختلف عن السابقة، تم تقديم نموذج إحصائي. بإستخدام هذا النموذج، تم التحقيق في تأثير طول الخيط الممسوك في جهاز إختبار متانة الشد على متانة خيوط الغزل الحلقي، الروتور، والخيوط المغزولة بنفث الهواء وأيضاً على معامل إختلاف متانتها. ويربط النموذج بين متانة الخيط ومعامل إختلاف المتانة وطول الخيط الممسوك. ويستند هذا النموذج إلى نموذج "بيرس" وعلى إفتراض توزيع "3- وبيول" لقيم متانة الخيط. وقد تم التوصل إلى اتفاق معقول بين القيم العملية والمتوقعة. ونجح النموذج في النقاط

التغير في متانة الخيط ومعامل إختلاف المتانة عند أطوال مختلفة للخيط الممسوك. وأكدت النتائج أنه عند زيادة أطوال الخيط الممسوك، تنخفض متانة الخيط وينخفض معها معامل إختلاف المتانة كذلك.

الكلمات الدالة

محاكاة رقمية؛ النمذجة الرياضية؛ النمذجة الإحصائية؛ الألياف؛ فوهة الغزل النفائثة "ريتر"؛ تدفق الهواء؛ نسبة التحزيم؛ التنبؤ بالمتانة؛ فسكوز؛ توزيع "ويبول"؛ طول الخيط الممسوك؛ الكثافة الطولية؛ ضغط الفوهة؛ سرعة الإنتاج؛ تركيب

Table of Contents

<i>Acknowledgment</i>	<i>I</i>
<i>Abstract</i>	<i>II</i>
<i>Abstrakt</i>	<i>IV</i>
<i>المخلص</i>	<i>VI</i>
<i>Table of Contents</i>	<i>VIII</i>
<i>List of Figures</i>	<i>X</i>
<i>List of Tables</i>	<i>XII</i>
<i>List of Symbols</i>	<i>XIII</i>
1. Introduction	1
2. Overview of the Current State of the Problem.....	4
2.1 Literature review	4
2.2 Purpose and aim of the thesis.....	9
3. Description of Principle of Yarn Formation Using Numerical Modeling	12
3.1 Numerical computation	12
3.2 Experimental verification	16
3.3 Numerical modeling results	18
3.3.1 Vortex creation.....	18
3.3.2 Velocity magnitude	20
3.3.3 Principle of yarn formation	21
3.3.3.1 Tangential velocity distribution	22
3.3.3.2 Radial velocity distribution	23
3.3.3.3 Axial velocity distribution	24
3.3.3.4 Static pressure distribution	24
3.3.4 Effect of nozzle pressure on structure and strength of the air jet yarn	25
4. Prediction of Air Jet Yarn Strength Based on Statistical Modeling.....	31
4.1 Materials and methods.....	31
4.2 Regression model	32
4.3 Effect of process parameters on yarn strength	32
5. Prediction of Air Jet Yarn Strength Based on Mathematical Modeling	36
5.1 Model for the failure of the air jet spun yarn	36
5.1.1 Determination of core fiber strength	37
5.1.2 Wrapper fiber strength component	41

5.2	Experimental verification	42
5.3	Results of the mathematical model.....	43
6.	<i>Prediction of Air Jet Yarn Strength at Different Gauge Lengths Based on Statistical Modeling</i>	49
6.1	Yarn strength in relation to gauge length.....	49
6.1.1	Calculating the mean yarn strength	51
6.1.2	Calculating the standard deviation of yarn strength	52
6.1.3	Calculating the coefficient of variation of yarn strength	54
6.1.4	Mathematical model validation	54
6.2	Results of the model	56
6.2.1	Yarn strength.....	56
6.2.2	Coefficient of variation of yarn strength	61
7.	<i>Conclusions and Recommendations</i>	65
7.1	Summary and conclusions	65
7.2	Recommendations for future work	70
	<i>References</i>	72
	<i>Publications</i>	81
	<i>Appendices</i>	84
	<i>Curriculum Vitae.....</i>	103

List of Figures

Figure 1.1 Schematic diagram of the yarn formation zone in MJS machine (adapted and reproduced (Rieter, 2017b)).	1
Figure 1.2 Schematic diagram of the yarn formation zone in MVS machine (adapted and reproduced (Rieter, 2017a)).	2
Figure 1.3 Schematic diagram of the yarn formation zone in Rieter air jet spinning machine (adapted and reproduced (“United States Patent and Trademark Office, US Patent 2007/0125062 A1, http://www.uspto.gov ,” 2007)).	3
Figure 2.1 Structural classes in vortex spun yarns, (a) Class 1, (b) Class 2, (c) Class 3, (d) Class 4 (Nazan Erdumlu et al., 2012a).	5
Figure 3.1 Flow chart of the numerical simulation steps in CFD.	13
Figure 3.2 Rieter nozzle, (a) 2D cross-sectional view, (b) the computational grid of the airflow field, (c) velocity components.	16
Figure 3.3 30 Tex Viscose yarn longitudinal view under SEM.	17
Figure 3.4 Core fibers in the form of a cylindrical segment.	18
Figure 3.5 Velocity vectors (m/s) for the x-x axial cross-section (at 0.5 MPa pressure).	19
Figure 3.6 Contours of the velocity magnitude (m/s) at different nozzle cross-sections.	20
Figure 3.7 The velocity vector (m/s) distribution at section D.	21
Figure 3.8 Contours of the tangential velocity (m/s) at different nozzle cross-sections.	22
Figure 3.9 The tangential velocity distribution curve at section D.	23
Figure 3.10 The radial velocity distribution at section D.	24
Figure 3.11 Contours of the axial velocity (m/s) for the x-x axial cross-section.	25
Figure 3.12 Contours of the static pressure distribution (Pa) for the x-x axial cross-section.	26
Figure 3.13 Contours of the axial velocity distribution (m/s) for the x-x axial cross-section at different nozzle pressure.	27
Figure 3.14 Contours of the tangential velocity distribution (m/s) for the x-x axial cross-section at different nozzle pressure.	27
Figure 3.15 Contours of the static pressure distribution (Pa) for the x-x axial cross-section at different nozzle pressure.	28
Figure 3.16 Effect of nozzle pressure on 23 Tex yarn tenacity.	29
Figure 4.1 Effect of (a) yarn linear density and delivery speed, (b) yarn linear density and nozzle pressure, and (c) nozzle pressure and yarn delivery speed, on yarn tenacity.	34
Figure 5.1 Simplified model of short staple air jet spun yarn.	36
Figure 5.2 Bundle of fibers gripped between two jaws (Neckar & Das, 2003).	37
Figure 5.3 Force analysis of air jet yarn before and during axial tensile loading (adapted and reproduced (Krause & Soliman, 1990)).	41
Figure 5.4 Influence of fiber (a) breaking load, (b) friction coefficient and fineness, on predicted yarn breaking load.	44
Figure 5.5 Influence of yarn (a) linear density and wrapper ratio, (b) number of wraps per meter, on predicted yarn breaking load.	46
Figure 6.1 A yarn is gripped between the jaws of a tensile tester.	49

Figure 6.2 Probability density function of the linearly transformed yarn strength.	56
Figure 6.3 The probability density function of yarn tenacity at 300 mm gauge length; (a) ring, (b) rotor, (c) air jet.	58
Figure 6.4 Theoretical and experimental values of yarn strength at different gauge lengths.	59
Figure 6.5 Twist distribution through the cross-section of yarns produced on different spinning systems. (N. Erdumlu, Ozipek, Oztuna, & Cetinkaya, 2009).....	60
Figure 6.6 Longitudinal and cross-sectional view of yarns; (a) air jet, (b) rotor.....	61
Figure 6.7 Coefficient of variation of yarn strength at different gauge lengths; (a) experimental, (b) theoretical.	63
Figure 6.8 Experimental versus calculated results of coefficient of variation of yarn strength at different gauge lengths; (a) ring, (b) rotor, (c) air jet.	64

List of Tables

Table 3.1 Yarn structural parameters at different nozzle pressures.....	30
Table 4.1 Spun yarn production parameters.....	31
Table 4.2 <i>P</i> -values of the model and its coefficients.....	32
Table 5.1 Yarn production plan.....	43
Table 5.2 Viscose and Tencel fiber properties.	46
Table 5.3 Theoretical and experimental yarn results.....	47

List of Symbols

Symbol	Description
AJS	Air jet spinning
ABC	Specific triangle during tensile loading test
ADE	Specific triangle during tensile loading test
A	1 st yarn parameter under microscope “equivalent core diameter”
a	Specific distance during tensile loading test
B	2 nd yarn parameter under microscope “equivalent wrapper diameter”
c	Shape
CFD	Computational fluid dynamics
$C_{1\epsilon}$	Constant
$C_{2\epsilon}$	Constant
C	3 rd yarn parameter under microscope “equivalent wrapper width”
CV	Coefficient of variation of yarn strength
D	4 th yarn parameter under microscope “equivalent coil length”
ds	An element of wrapper fiber
$d\theta$	An increment angle corresponding to ds
E	Expectation operator
e_f	Fiber breaking elongation
e_y	Yarn longitudinal strain
e_r	Yarn lateral strain
F	External forces
$F(p, l_o)$	The cumulative distribution function of yarn strength at gauge length l_o
f	Fiber strength
$f(p, L)$	The probability density function
$F(p, L)$	The cumulative distribution function of yarn strength at length L
G_b	Generation of turbulence kinetic energy due to buoyancy
G_k	Generation of turbulence kinetic energy due to the mean velocity gradients
h_1	1 st component of height of one coil of air jet yarn

h_2	2 nd component of height of one coil of air jet yarn
h_3	3 rd component of height of one coil of air jet yarn
h_4	4 th component of height of one coil of air jet yarn
h_5	5 th component of height of one coil of air jet yarn
h_6	6 th component of height of one coil of air jet yarn
h	Gauge length
I	Intensity tensor
i	Fiber position index
j	Bundle position index
k	Kinetic energy
l_o	Short gauge length
L	Yarn length
l_u	Average strained fiber length in unit length
l_{uo}	Average unstrained fiber length in unit length
l	Fiber length
l_{max}	Maximum fiber length
MJS	Murata jet spinning
MVS	Murata vortex spinning
m	Yarn mass
m_j	J th Partial bundle mass
m_i	Fiber mass
n_e	Total number of gripped fibers
n	Total number of fibers in yarn cross-section
n_{e_j}	Total number of fibers in the j th partial bundle gripped by the both jaws simultaneously
N	Normal forces exerted by wrapper fibers per unit length
n_j	Total number of fibers in the j th partial bundle
p	Yarn strength
P_{max}	Maximum applied force
P_{min}	Minimum applied force
$\overline{(p - \bar{p}_l)^m}$	m th central moment of yarn strength

$\overline{p^m}$	m^{th} non-central statistical moment
p_{min}	Location
$\overline{p^1}$	Mean value of yarn strength
P	Fluid pressure
p_o	Average unstrained pitch of wrapper fibers
p_i	Average strained pitch of wrapper fibers
q	Scale
Q	Yarn constant parameter
r	Average strained yarn radius
r_o	Average unstrained yarn radius
R	Gas constant
$R(p)$	Risk function
S_ϵ	User-defined source term
S_k	User-defined source term
SEM	Scanning electron microscope
T_i	Fiber linear density
T	Temperature
t	Time
T_j	Partial bundle linear density
u	Transformed value
$\overline{u^x}$	Non-central moments of the transferred value u
U	Flow velocity
V	Volume of one cylindrical section
V_c	Volume of core fibers
V_r	Volume of wrapper fibers
W	Wrapper ratio
X_i	Independent variable
X_j	Independent variable
X_k	Independent variable
X_1	Yarn linear density
X_2	Yarn delivery speed

X_3	Nozzle pressure
x	Specific distance during tensile loading test
Y	Dependent variable
Y_M	Contribution of the fluctuating dilatation in compressible turbulence to the overall dissipation rate
Z	Yarn tenacity
β_0	Regression equation constant
β_i	Linear coefficient
β_j	Linear coefficient
β_k	Linear coefficient
β_{ij}	Interaction coefficient
β_{ik}	Interaction coefficient
β_{jk}	Interaction coefficient
β_{ii}	Quadratic coefficient
β_{jj}	Quadratic coefficient
β_{kk}	Quadratic coefficient
η	Fiber length utilization factor
η_j	Fiber length utilization of the j^{th} partial bundle
ϵ	Dissipation rate of kinetic energy
μ	Fluid dynamic viscosity
ρ	Fluid density
γ_j	Mass fraction of the j^{th} partial bundle
$\gamma(l)$	Mass fraction function
μ	Fiber friction coefficient
ν	Poisson ratio
ν_f	Yarn packing density
Γx	Gamma function
$\omega(u)$	The probability density function of the transferred value u
σ^2	Dispersion (variance)
σ	Standard deviation of yarn strength
σ_k	Turbulent Prandtl number for thermal conductivity

σ_ϵ	Turbulent Prandtl number for dissipation rate of kinetic energy
σ_1	Core fibers strength
σ_2	Total frictional forces on core fibers
σ_3	Total wrapper fibers strength
α_o	Average unstrained wrapper fiber helix angle
α	Average strained wrapper fiber helix angle

1. Introduction

Air jet spinning process has reached an industrial acceptance stage having developed through half a century. Known as Fasciated spinning, air jet yarn was first introduced by DuPont Company in 1971 using the principle of air vortices to form a yarn. In 1982, Murata jet spinning "MJS" was introduced and achieved more commercial success. In this system, some control was achieved over the distribution of the wrapper fibers leading to better yarn quality.

As shown in *Figure 1.1*, the spinning unit of MJS consists of two jets rotating in opposite directions. After drafting the sliver, the pressure of the second jet is larger than that of the first jet, therefore the S twist from the second jet propagates along the false-twisted core and null the Z-twist of the first jet, leaving some S-twist to travel toward the nip line of the front rollers. Because of the reduced twist at front roller, some of the fibers in the fiber bundle get separated from the main fiber bundle and become wound around the fiber bundle (Lawrence, 2010). A twist diagram is also shown in *Figure 1.1*.

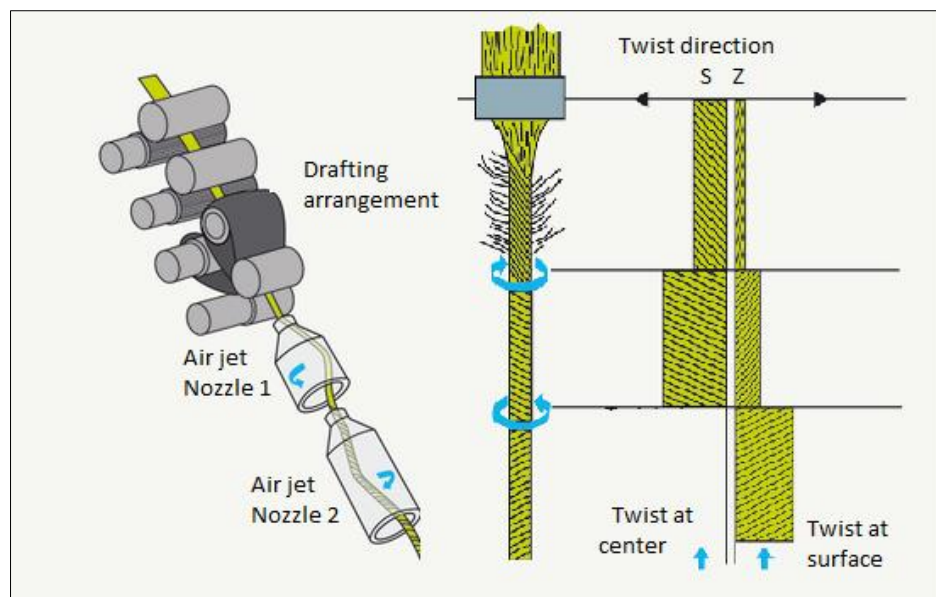


Figure 1.1 Schematic diagram of the yarn formation zone in MJS machine (adapted and reproduced (Rieter, 2017b)).

MJS has a major disadvantage of not being able to produce acceptable 100% cotton yarns. Furthermore, MJS is restricted to finer counts, since yarn tenacity reduces as the yarn becomes coarser. In 1997, Murata jet spinning "MVS" was introduced. The MVS system uses a single nozzle with an inner needle and this system became able to produce 100% carded cotton yarns (Basu, 1999).

As shown in *Figure 1.2*, the fibers come out of the front rollers in MVS, they are sucked into the spiral orifice at the entrance of the air jet nozzle, and they are then held together more firmly as they move towards the tip of the needle protruding from the orifice. At this stage, the fibers are twisted by the force of the air stream. This twisting motion tends to flow upwards. The needle protruding from the orifice prevents this upward propagation (twist penetration). Therefore, the upper portions of some fibers are separated from the nip point between the front rollers, but they are kept "open". After the fibers have passed through the orifice, the upper portions of the fibers begin to expand due to the whirling force of the jet air stream and they twine over the hollow spindle. The fibers twined over the spindle are whirled around the core fiber and spun into MVS yarn as they are drawn into the hollow spindle. The spun yarn is then wound onto a package after its defects have been removed (Demir, 2009).

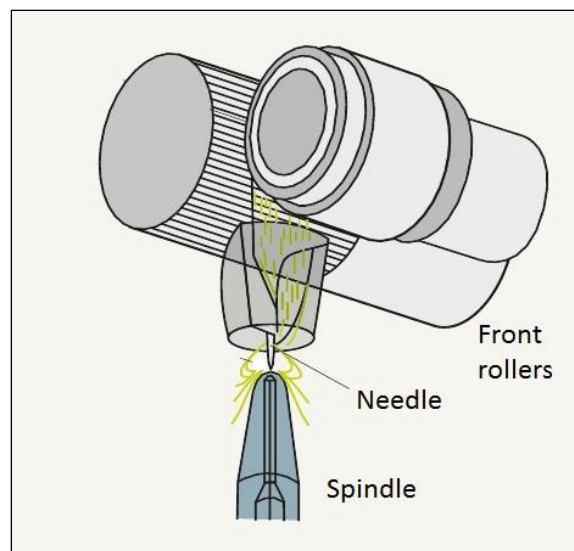


Figure 1.2 Schematic diagram of the yarn formation zone in MVS machine (adapted and reproduced (Rieter, 2017a)).

In 2009, Rieter Company presented the latest method in air jet yarn production. Both Rieter and MVS systems are based on a similar principle, but the nozzle block in Rieter system does not contain the needle holder that works as a twisting guide (Nazan Erdumlu, Ozipek, & Oxenham, 2012b).

In this system, the drafting zone consists of four over four roller drafting arrangement. As shown in *Figure 1.3*, the drafted fiber strand is fed into the vortex chamber. The channel where the yarn is withdrawn from lies above the fiber feed channel. Therefore, during fibers transportation process, some fibers are separated from the mainstream, which is nearly straight from the drafting zone to the spindle tube entrance point. Due to the air vortices inside the spindle, those fibers are twisted to wrap around the main fiber strand which becomes core, then the resultant yarn is wound by a winding device ([“http://www.rieter.com/cz/rikipedia/articles/alternative-spinning-systems/the-various-spinning-methods/air-jet-spinning/development/,”](http://www.rieter.com/cz/rikipedia/articles/alternative-spinning-systems/the-various-spinning-methods/air-jet-spinning/development/) 2016, [“http://www.textileworld.com/textile-world/features/2012/03/spinning-with-an-air-jet/,”](http://www.textileworld.com/textile-world/features/2012/03/spinning-with-an-air-jet/) 2016). The yarn structure consists of core fibers which are parallel and consolidated by wrapping fibers that incline to the yarn axis by different angles.

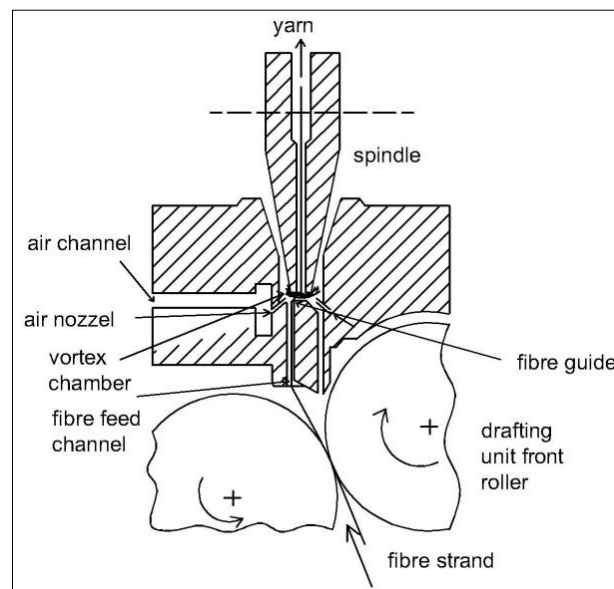


Figure 1.3 Schematic diagram of the yarn formation zone in Rieter air jet spinning machine (adapted and reproduced (“United States Patent and Trademark Office, US Patent 2007/0125062 A1, <http://www.uspto.gov>,” 2007)).

2. Overview of the Current State of the Problem

2.1 Literature review

Since the yarn structure and properties in air jet spinning technology depend on the airflow field distribution and its intensity inside the air jet nozzle, therefore, it is necessary to study this airflow. The early system of air jet spinning was introduced by MJS. Investigations were carried out to simulate numerically the airflow field on this system using computational fluid dynamics “*CFD*” software (H. F. Guo, Chen, & Yu, 2010; Huifen, Xianglong, & Chongwen, 2007; Zeng & Yu, 2003, 2004).

Other researchers performed a numerical computation of the airflow field in MVS in order to explain the principle of yarn formation (Zeguang Pei, Hu, Diao, & Yu, 2012; Zeguang Pei & Yu, 2011b). Also, different numerical along with experimental investigations were carried out to study the influence of MVS production and nozzle parameters on yarn structure and properties (Nazan Erdumlu, Ozipek, & Oxenham, 2012a; H. Guo, An, Yu, & Yu, 2008; Ishtiaque, Salhotra, & Kumar, 2006; A. Kumar, Ishtiaque, & Salhotra, 2006; A. Kumar, Salhotra, & Ishtiaque, 2006; a. Kumar, Ishtiaque, & Salhotra, 2006; Oxenham & Basu, 1993; Z Pei & Yu, 2010; Zeguang Pei & Yu, 2011a, 2011c; Salhotra, Ishtiaque, & Kumar, 2006; Suzuki & Sukigara, 2012; Zeguang Pei & Chongwen Yu, 2011).

Zou et al. (Zhuanyong Zou et al., 2009; Zou, Liu, Zheng, & Cheng, 2010) conducted numerical analyses to investigate the influence of nozzle air pressure on the flow field inside the MVS nozzle block. They concluded that the increase in pressure results in an increase in the airflow velocity, including the axial, radial and tangential velocities inside the nozzle block. This increase results in an increase in the mean angular velocity of open end fibers and increases the amount of twist inserted in the fiber bundle, i.e. fibers are tightly wrapped around the yarn structure as more forces are applied to wrapped fibers. These results were confirmed by the experimental analysis of yarn structure conducted by Tyagi et al. (Tyagi, Sharma, & Salhotra, 2004a) who observed an increase in the tight wrapping (classified as Class 1) and a decrease in the

long wrappings (classified as Class 2) and the unwrapped sections (classified as Class 4) (the different classes are shown in *Figure 2.1*).

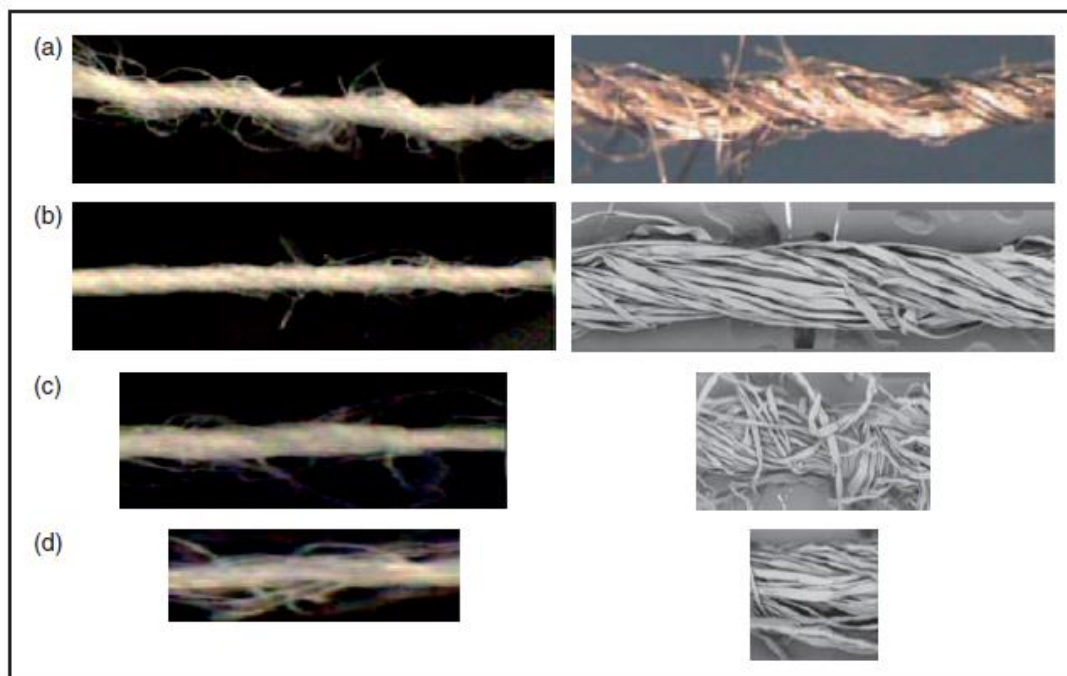


Figure 2.1 Structural classes in vortex spun yarns, (a) Class 1, (b) Class 2, (c) Class 3, (d) Class 4 (Nazan Erdumlu et al., 2012a).

However, at high air pressure, the existence of irregular wrappings (classified as Class 3) was obvious which deteriorates yarn tenacity. Another study showed that by increasing nozzle pressure, mean migration intensity (rate of change in radial position of a fiber in yarns) increases while the migration width of wrapper fibers and regular wrappers fiber decrease (Guldemet Basal, 2003).

Increasing the tangential velocity enhances the efficiency of twist insertion. Also increasing radial velocity contributes to improving the expanding effect of the fiber bundle which in turn causes more open-trail-end fibers, i.e. more wrapper fibers. However, at very high pressure, more fibers are separated from the yarn body and this results in irregularity and strength deterioration (Zhuanyong Zou, Longdi Cheng, Wenliang Xue, & Jianyong Yu, 2008; Zou et al., 2010).

There are differences between Murata and Rieter nozzle design. Therefore, it is interesting to simulate the airflow field inside the Rieter nozzle as this could give a better understanding of this new technique. Furthermore, since the pressure is an important air jet spinning process parameter, therefore its influence on airflow should be investigated. In this way, the change in yarn strength as nozzle pressure changes can be predicted.

Also, experimental investigations were carried out on the influence of MVS machine production parameters on yarn properties in order to optimize yarn quality. Those parameters are nozzle (pressure and orifice angle), the distance between spindle and front roller nip point, draft, spindle (cross-section, working period and diameter), yarn (linear density and delivery speed) and fiber composition. Most of these parameters proved to have a significant effect on final yarn properties (G. Basal, 2006; Nazan Erdumlu & Ozipek, 2010; Gordon, 2001; Sharma, 2004).

Coarser MVS yarns exhibit superior yarn properties in terms of yarn tenacity, and the nozzle pressure required is higher when spinning these yarns. Earlier studies carried out on MVS yarn showed that the tensile strength initially increases with the increase in nozzle pressure then deteriorates by any further increase in nozzle pressure. The structural integrity, tensile properties, and abrasion resistance deteriorate at high yarn delivery speeds (Johnson, 2002; H. G. Ortlek, 2005; Huseyin Gazi Ortlek, Nair, Kilik, & Guven, 2008; R. Rajamanickam, Hansen, & Jayaraman, 1998b). Although these parameters have been investigated, the slight differences in nozzle design for both Rieter and MVS systems may lead to a different trend.

Along with these experiments, response surface equations were obtained using multiple regression that relates process parameters to yarn structure and its properties (Chasmawala, Hansen, & Jayaraman, 1990; Tyagi et al., 2004a; Tyagi, Sharma, & Salhotra, 2004b). Yet no regression model has been presented for Rieter air jet spun yarns. A possible model can be presented that predicts yarn tenacity based on nozzle pressure, delivery velocity and yarn linear density, which are considered as very important air jet spinning parameters.

There is no doubt that the strength is considered as a very important yarn property that significantly influences its post-processing performance and final fabric quality. To engineer air jet yarns aiming better quality, this requires knowing the relationship between fiber properties, yarn structure, and yarn properties. The mathematical models are usually used to describe and explain such relationships (Anindya Ghosh, Ishtiaque, Rengasamy, Mal, & Patnaik, 2005).

Numerous researchers presented a good contribution to this topic. Many of them presented mathematical models for ring spun yarn (Aggarwal, 1989; Bogdan, 1956; Chu, Cummings, & Teixeira, 1950; Frydrych, 1992, 1995; Guha, Chattopadhyay, & Jayadeva, 2001; Majumdar & Majumdar, 2004; Ning, 1993; Onder & Baser, 1996; Pan, 1992; Pan, Hua, & Qiu, 2001a, 2001b; Zurek, Frydrych, & Zakrzewski, 1987) and rotor yarn (Jiang, Hu, & Postle, 2002; Muhammad Zubair, Bohuslav Neckar, Moaz Eldeeb, 2017; Neckář & Das, 2017; Ning, 1993; Zubair, Eldeeb, & Neckar, 2017). Nevertheless, mathematical models of air jet spun yarn are limited (Anindya Ghosh, Ishtiaque, & Rengasamy, 2005; Krause & Soliman, 1990; Xie, Oxenham, & Grosberg, 1986; Zeng, Wan, Yu, & He, 2005).

Krause W. et al (Krause & Soliman, 1990) proposed a set of equations that predicts the air jet yarn strength where they included the major yarn parameters, fiber strain, inter-friction, slenderness, wrapper fiber position, wrapping length, and wrapping angle. Rajamanickam et al. (R. Rajamanickam, Hansen, & Jayaraman, 1998a; Rangaswamy Rajamanickam, Hansen, & Jayaraman, 1997b) also presented mathematical models that describe the air jet yarn fracture behavior, including the failure mechanism of core and wrapper fibers and predict the air jet yarn strength accordingly. They obtained a mathematical relationship between yarn breaking load, its structural parameters, and fibers properties. The model also classified the modes of yarn failure into noncatastrophic (due to partial slippage or partial breakage), catastrophic (due to complete slippage or complete breakage). However, their model is a bit complicated as well as they obtained a prediction error which was quite high. So, it is necessary to develop a model which can be simpler and more accurate.

Generally yarn strength is measured at 500 mm gauge length, however, in fact, the yarn is exposed to stresses at longer lengths in post-spinning processes particularly in sizing, warping, and weaving. Therefore, it is interesting to know how yarn strength varies at different gauge lengths.

Substantial researches have been done to study experimentally the effect of gauge length on different spun yarn tensile properties (a. Ghosh, 2005; A Ghosh, Ishtiaque, & Rengasamy, 2005; Anindya Ghosh, Ishtiaque, Rengasamy, Mal, & Patnaik, 2004; Hussain, Nachane, Krishna Iyer, & Srinathan, 1990; Oxenham, Zhu, & Leaf, 1992; Punj, Mukhopadhyay, & Chakraborty, 1998; Seo et al., 1993). Hussain et al (Hussain et al., 1990) concluded that there are significant differences in the gauge length effect on ring and rotor spun yarn strength only at long gauge lengths (70 cm).

Realff et al (Realff, Seo, Boyce, Schwartz, & Backer, 1991) studied the effect of gauge length on the failure mechanism of the ring, open end rotor and air jet yarns. They observed that at longer gauge lengths, ring spun yarns are stronger and that was characterized by the short failure zone and more broken fibers. While at short gauge length, air jet yarn exhibits more strength because of the difference in the helix angle among the different yarns. The rotor yarn shows a change in breaking mechanism from slippage dominant failure at long gauge length to breakage dominant failure at short gauge lengths.

Oxenham et.al (Oxenham et al., 1992) found that there is a sharp drop in ring spun yarn strength as gauge length changes from 1 mm to 40 mm (40 mm is equivalent to the fiber length for this yarn). Further increase in gauge length showed no obvious differences in strength. Whereas a sharp drop in friction spun yarn strength was observed when gauge length changes from 1 mm to 20 mm (20 mm is equivalent to the fiber extent for this yarn). The strength reduction continues after 20 mm because of the existence of the discontinuity in the friction spun yarn structure.

Some other researchers studied this phenomenon theoretically and developed a model

that relates yarn tenacity to gauge length (Pan et al., 2001b; Rosen, 1983). Neckář et al. (Neckar & Das, 2003) modeled yarn strength as an ergodic, stationary, stochastic and Markovian process, and simulated yarn tenacity values at large range of gauge lengths. In their study, they calculated the autocorrelation function that related yarn strength in the adjacent sections to total yarn strength at different gauge lengths. Zurek et al. proposed empirical relationships between yarn tenacity and gauge length (Grant & Morlier, 1948; Hussain et al., 1990; J. Kapadia, 1935; Neckar & Das, 2003; Pillay, 1965; Zurek et al., 1987; Zurek, Malinowski, & Plotka, 1976).

Peirce proposed the weak link theory and concluded that yarn strength decreases with the increase of gauge length (Peirce, 1926). Spencer-Smith, J. L. (Spencer-Smith, 1947) improved Peirce's theory by including the relationship between the strength of neighboring fracture zones in yarns. In that model, average strength, variability and the serial correlogram of the fracture zones had been used.

By studying Peirce model, it can be seen that it is based on Gaussian distribution, nevertheless, by analyzing the model, it is observed that it is valid only on short gauge lengths. Therefore, a new model can be established if another type of distribution for the yarn strength values is assumed. If this distribution fits the data well, this could achieve more accurate model.

2.2 Purpose and aim of the thesis

The main aims of this thesis are to contribute to the knowledge of the air jet yarn formation process, particularly Rieter air jet spinning technology, to investigate the influence of selected technological parameters of the spinning machine on yarn properties, especially its strength. Furthermore, to shed light on the problem of the prediction of yarn strength by trying different approaches to establish models that can be used for prediction of air jet spun yarns strength. Each model, whether statistical, mathematical or numerical could contribute to understanding the air jet spinning process, yarn structure, yarn strength and the relationship between fibers and yarns.

The first part of this work includes a 3-dimensional simulation of the airflow field inside the Rieter air jet spinning nozzle using ANSYS software which is based on the finite volume method. The numerical simulation using computer aided engineering software generally has a lot of advantages, particularly time-saving as well as cost reduction. Nevertheless, the accuracy of the results can be doubted, for instance, results of simulating laminar flows are more reliable than simulating turbulent flows. On the other hand, to obtain real and accurate results of the flow field inside the nozzle, it is necessary to use special airflow measuring gauges or instruments. This is difficult due to the very tiny dimensions of the nozzle and the hollow spindle as well as the high cost of such tools.

So, before embarking on prediction process, the principle of yarn formation is initially explained using the numerical simulation approach. Afterward, the effect of nozzle pressure has been studied using the simulation process, then experiments have been conducted to verify the results obtained from the simulation process. Furthermore, predicting the change in the air jet yarn strength as nozzle pressure changes.

The second part aims to investigate some process parameters in Rieter air jet spinning technology, namely, yarn linear density, nozzle pressure, and delivery speed. These parameters were proved to influence fiber configuration and yarn structure significantly. Along with the experiment, a statistical model had been established based on multiple regression to study the combined effect of process parameter on yarn tenacity as well as to predict the air jet yarn strength.

In the third part, a mathematical model to predict the air jet yarn strength at short gauge length is presented. An earlier mathematical model for air jet yarn strength has been modified targeting simpler and more accurate model.

And in the last part, an attempt has been made to establish a statistical model to predict the air jet yarn strength at different gauge lengths. The model is based on an earlier model but used a different type of the distribution function to fit yarn strength values

at all gauge lengths, hence, obtaining the more accurate model. Moreover, the validation of the model was extended to include ring, rotor, and air jet yarns.

3. Description of Principle of Yarn Formation Using Numerical Modeling

In this chapter, a 3D simulation process has been carried out to study the principle of yarn formation of the Rieter air jet spinning machine. Along with the theoretical study, an experimental investigation was carried out to study the effect of the nozzle pressure on yarn tenacity.

3.1 Numerical computation

CFD is a term being used when solving and analyzing fluid flow using numerical methods and algorithms. The general process for performing a CFD analysis is outlined in the flow chart shown in *Figure 3.1*. All dimensions of a Rieter air jet nozzle unit were measured and the cross-sectional view of the nozzle is shown in *Figure 3.2-a*. The simulated region consists of all regions occupied by the air (the existence of yarn was ignored seeking simplification). The mesh of the fluid field was constructed using an unstructured tetrahedral grid because the computational domain of the studied nozzle is considered as a complex geometry and such grid type allow the change of resolution over the domain. The computational grid of the airflow field in Rieter air jet spinning nozzle is shown in *Figure 3.2-b*. Afterward, the mesh quality was adjusted using inflation sizing and edge sizing to adopt the dense and wide zones accordingly, taking into consideration the flow gradient from jet orifices which have very fine dimensions to the vortex chamber that has comparatively larger dimensions. The constructed mesh contains 500,802 mesh elements and the steady state was employed in the modeling process.

The characteristics of the flow in this nozzle pertain to the high swirling instruments which have anisotropic airflow. Therefore, the realizable k - ε model was used to simulate this turbulent airflow and it considers turbulent viscosity, adverse pressure, recirculation and separation which provides more calculation accuracy than the traditional k - ε model particularly when simulating planar and round jets. Since nozzle inlet pressure is very high and the internal airflow speed is very high, the air

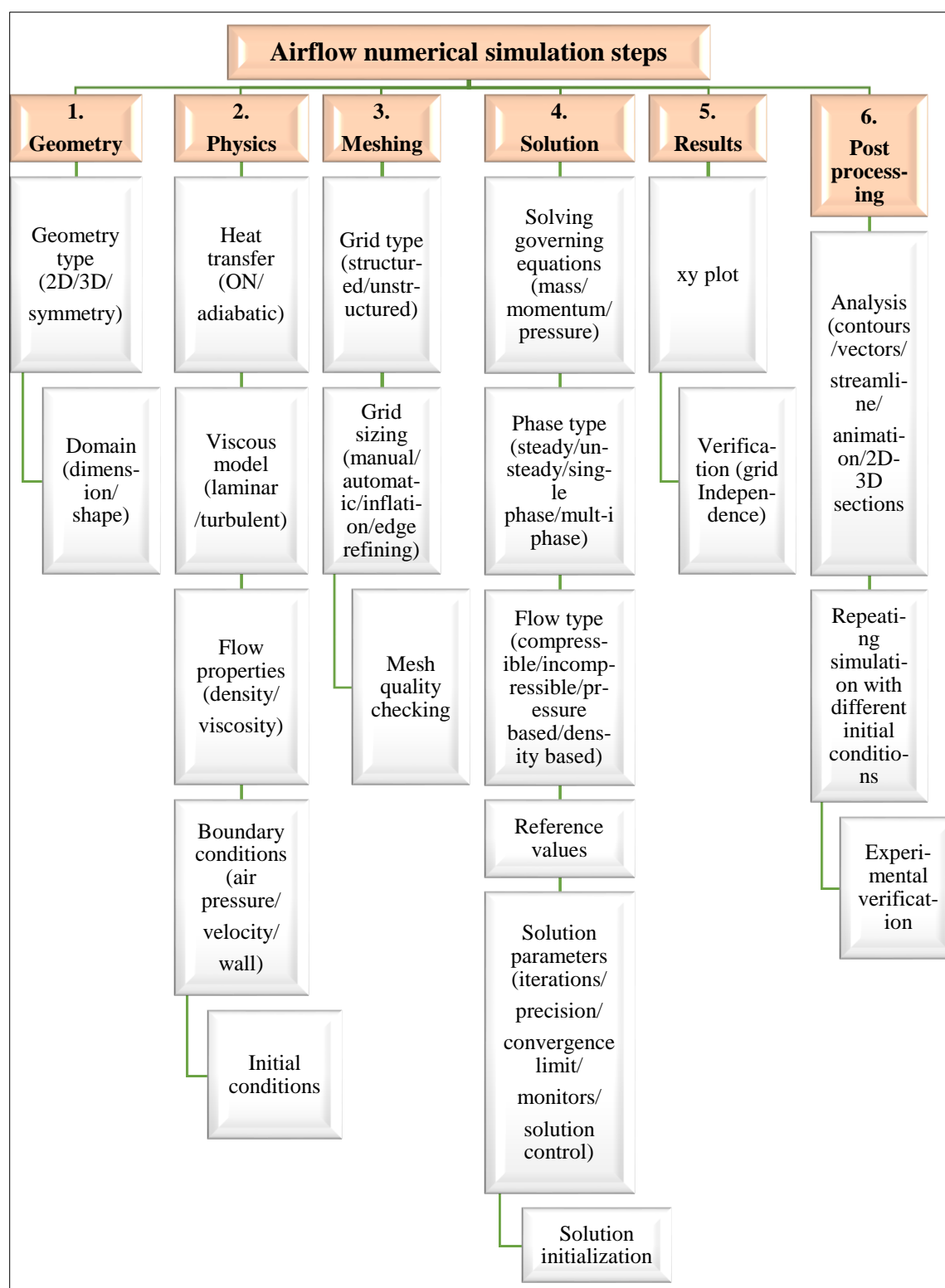


Figure 3.1 Flow chart of the numerical simulation steps in *CFD*.

density change cannot be ignored (compressible fluid). Therefore, the solution method in the Fluent module was density based. The governing equations are as follows; the

mass conservation equation in the differential form (Łukaszewicz & Kalita, 2016).

$$\frac{\partial \rho}{\partial t} + \nabla(\rho U) = 0 \quad (3.1)$$

Where ρ is the fluid density (kg/m^3), t is time (sec), U is flow velocity (m/sec). The momentum conservation equation in the form of Navier-Stokes equation for compressible flow (Łukaszewicz & Kalita, 2016).

$$\begin{aligned} \rho \left(\frac{\partial U}{\partial t} + U \cdot \nabla U \right) \\ = -\nabla P + \nabla \left(\mu (\nabla U + (\nabla U)^T) - \frac{2}{3} \mu (\nabla U) I \right) + F \end{aligned} \quad (3.2)$$

Where P is fluid pressure, μ is the fluid dynamic viscosity (N.s/m^2), T is temperature (K), I is intensity tensor and F is external forces (N). The ideal gas law (Zhu & Ibrahim, 2012).

$$P = \rho RT \quad (3.3)$$

Where R is the gas constant (J/mol.K). The realizable k - ϵ turbulence model was adopted and combined with the implicit solver to obtain the simulation results. The kinetic energy k (J) and its dissipation rate ϵ (J/kg) were obtained from the following transport equations.

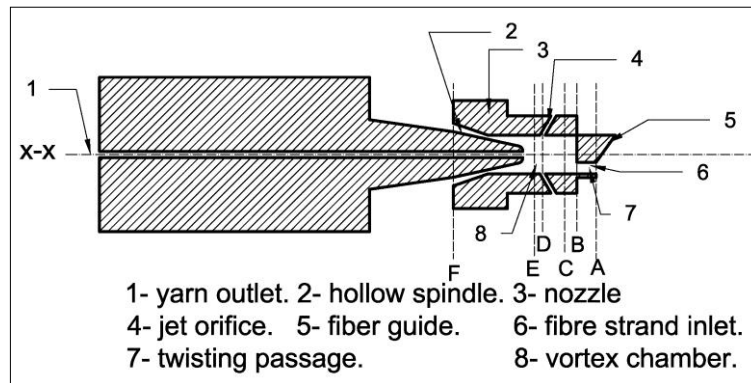
$$\begin{aligned} \frac{\partial}{\partial t}(\rho k) + \frac{\partial}{\partial x_i}(\rho k U_i) \\ = \frac{\partial}{\partial x_j} \left[\left(\mu + \frac{\mu_t}{\sigma_k} \right) \frac{\partial k}{\partial x_j} \right] + G_k + G_b - \rho \epsilon - Y_M + S_k \end{aligned} \quad (3.4)$$

$$\begin{aligned} \frac{\partial}{\partial t}(\rho \epsilon) + \frac{\partial}{\partial x_i}(\rho \epsilon U_i) \\ = \frac{\partial}{\partial x_j} \left[\left(\mu + \frac{\mu_t}{\sigma_\epsilon} \right) \frac{\partial \epsilon}{\partial x_j} \right] + C_{1\epsilon} \frac{\epsilon}{k} (G_k + C_{3\epsilon} G_b) \\ - C_{2\epsilon} \rho \frac{\epsilon^2}{k} + S_\epsilon \end{aligned} \quad (3.5)$$

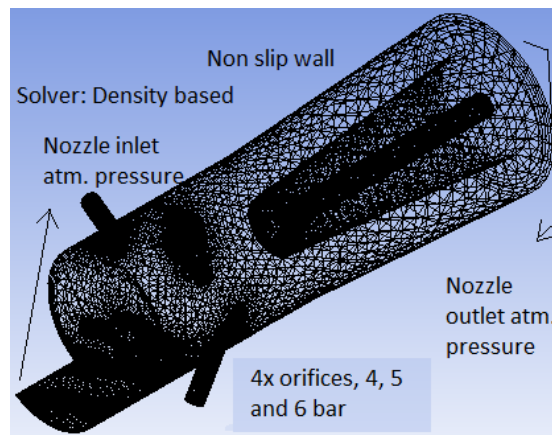
Where, G_b is the generation of turbulence kinetic energy due to buoyancy, Y_M represents the contribution of the fluctuating dilatation in compressible turbulence to the overall dissipation rate, G_k represents the generation of turbulence kinetic energy due to the mean velocity gradients, σ_k and σ_ϵ are the turbulent Prandtl numbers for k

and ϵ , respectively, S_ϵ and S_k are user-defined source terms and $C_{1\epsilon}$, $C_{2\epsilon}$ are constants (FLUENT, 2013).

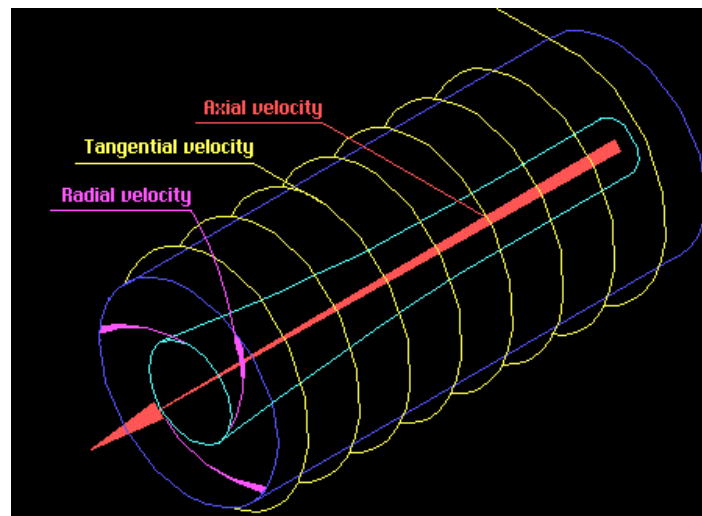
To convert the differential equations that govern the fluid flow to a set of algebraic equations that will be solved, the second order upwind spatial discretization was used for the turbulence variables and air velocity. The boundary conditions were set as follows; the solid wall has the non-slip boundary condition, nozzle outlet pressure is equal to the outside atmospheric pressure, nozzle inlet pressure is equal to the external atmospheric pressure, hollow spindle outlet pressure is equal to the external atmospheric pressure. Different pressures were applied for the four jet orifices inlets; 0.4, 0.5 and 0.6 MPa. To simplify the modeling process, the process is assumed adiabatic.



(a)



(b)



(c)

Figure 3.2 Rieter nozzle, (a) 2D cross-sectional view, (b) the computational grid of the airflow field, (c) velocity components.

3.2 Experimental verification

100% Viscose fibers of 1.3 dtex and 38 mm length were spun to produce air jet spun yarns. After carding process, sliver was drawn using three consecutive drawing passages in order to enhance fiber orientation and sliver evenness. The drawn sliver with 3.5 ktex was spun using Rieter air jet spinning machine J20 to produce 23 Tex yarns with different nozzle pressure; 4, 5 and 6 bar.

Yarn samples were conditioned for 24 hours in $20 \pm 2^\circ\text{C}$ and $65 \pm 2\%$ relative humidity. Yarn tensile properties were tested using Instron 4411 instrument. The instrument is a single yarn strength tester and operates at a constant rate of extension. Following BS EN ISO 2062:1995 (ISO, 1995), with a sample length of 50 cm, the crosshead moving speed has been adjusted to give a yarn failure time of 20 ± 3 sec. One-way ANOVA test was performed to check the significance of nozzle pressure on yarn tenacity. To verify the simulation process in a better way, yarn structure was analyzed using scanning electron microscope SEM, where the yarn wrapper ratio W was calculated for each yarn as shown in Figure 3.3. Where A is equivalent core diameter, B is equivalent wrapper diameter, C is equivalent wrapper width, and D is equivalent coil length.

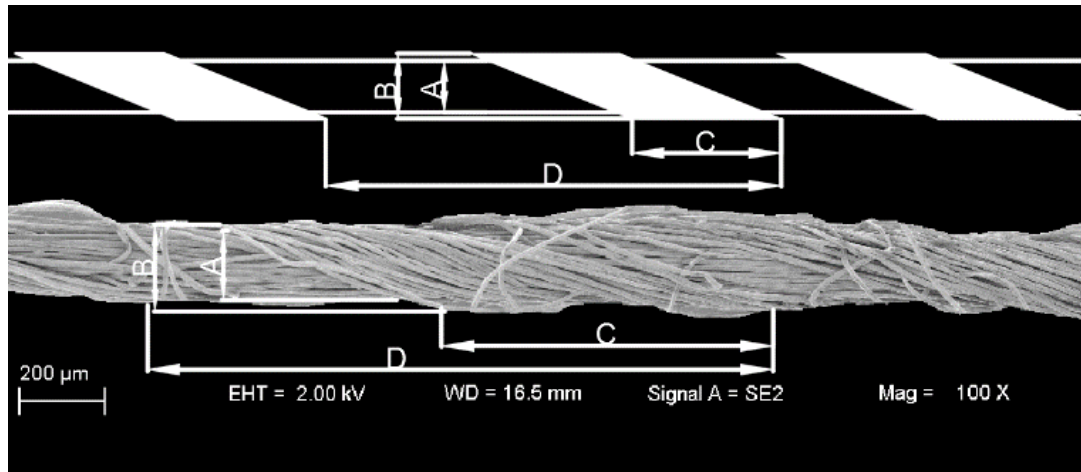


Figure 3.3 30 Tex Viscose yarn longitudinal view under SEM.

According to the ideal yarn structure shown in *Figure 3.4*, the volume of the core fibers can be calculated as a cylindrical segment from both sides (also called a truncated cylinder). The volume of one cylindrical section can be obtained by imagining that two sections are fitted together to form a cylinder of diameter A (mm) and height D (mm) (Harris & Stocker, 1998), and the total volume V (mm³) can be obtained as follows,

$$V = \frac{\pi}{4} A^2 \left(\frac{h_1 + h_2}{2} \right) + \frac{\pi}{4} A^2 \left(\frac{h_3 + h_4}{2} \right) \quad (3.6)$$

Where $h_{1,2,\dots,6}$ are components of one coil heights (mm), thus,

$$V = \frac{\pi}{4} A^2 h_5 + \frac{\pi}{4} A^2 h_6 \quad (3.7)$$

And core fiber volume V_c (mm³) can be calculated,

$$V_c = \frac{\pi}{4} A^2 D \quad (3.8)$$

Analogously, the total volume of the wrapper fibers V_r (mm³) can be obtained as follows,

$$V_r = \frac{\pi}{4} (B^2 - A^2) C \quad (3.9)$$

Therefore, the wrapper ratio (%) can be obtained assuming that the packing density of the core fibers strand is approximately equal to the packing density of the wrapper fibers strand

$$W = \frac{C(B^2 - A^2)}{C(B^2 - A^2) + A^2 D} \cdot 100 \quad (3.10)$$

As shown in *Figure 3.3*, the longitudinal yarn view under the microscope for 70 yarn section was captured, then merged to create the whole yarn image. The images were then analyzed and parameters A , B , C and D were obtained.

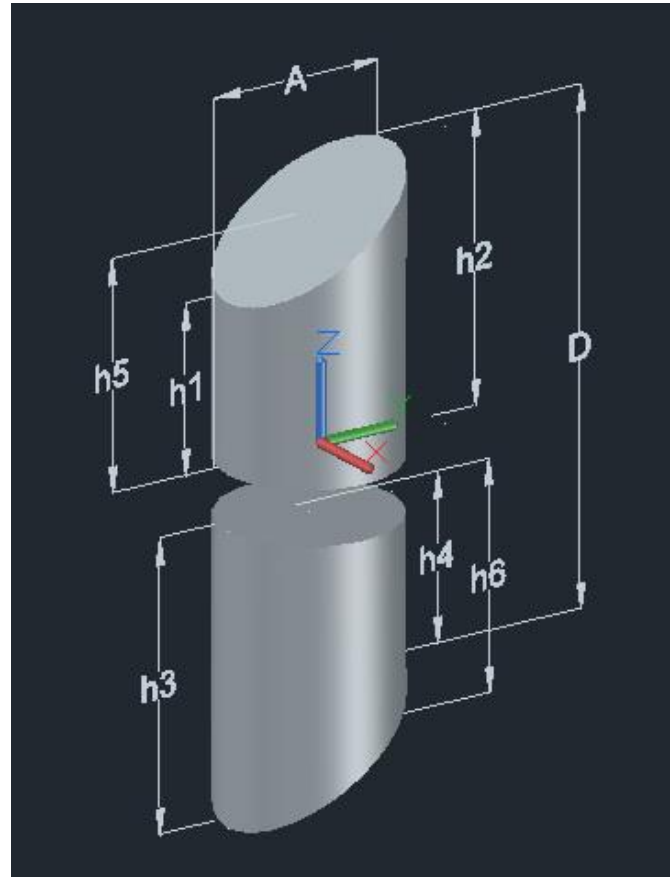


Figure 3.4 Core fibers in the form of a cylindrical segment.

3.3 Numerical modeling results

3.3.1 Vortex creation

Figure 3.5 shows the velocity vectors for the x-x axial cross-section. The air stream is ejected from the 4 jet orifices at a speed exceeding 650 m/s. This speed decreases when it reaches the vortex chamber to become less than 320 m/s. As a result, a swirling airflow is generated in a thin layer near the vortex chamber wall. This airflow whirls inside the nozzle and move downstream and finally is expelled from the nozzle outlet. In the twisting passage, a suction airflow is created and flows into the vortex chamber enabling the drafted fiber strand to enter the nozzle.

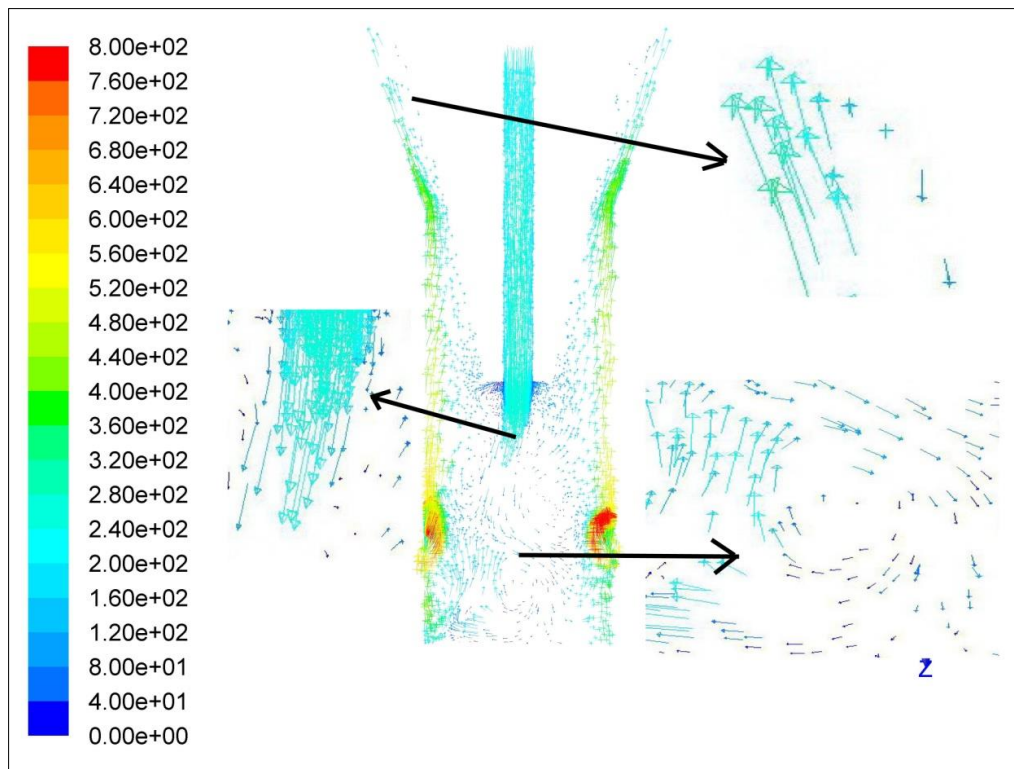


Figure 3.5 Velocity vectors (m/s) for the x-x axial cross-section (at 0.5 MPa pressure).

It can be noticed also that another airflow is created inside the hollow spindle and flows from the hollow spindle outlet upstream to the vortex chamber and this can help in controlling the trailing ends of the spun yarn. Afterward, these two mentioned airflows meet and become a single airflow. At this stage, the velocity of the airflow reduced to approximately 80 m/s near the nozzle inlet and 200 m/s near the hollow spindle inlet. Finally, the vortex is created inside the nozzle. This result agrees with the earlier research findings (Zeguang Pei & Yu, 2009).

As shown in *Figure 3.2-a*, because of the specific geometry of the Rieter nozzle, the fiber strand is not sucked uniformly at the nozzle inlet where fibers strand enters the nozzle inclined to the nozzle axis so a certain number of fibers are separated from the main fiber strand. These fiber ends are then twisted around the non-rotating yarn core at the entry of the hollow spindle by the action of the mentioned air vortex (Eldeeb & Moučková, 2017).

3.3.2 Velocity magnitude

Figure 3.6 shows the velocity magnitude at different nozzle cross-sections. As shown in section A, the air stream enters the nozzle from its inlet with a speed of about 40 m/s. The inlet area is much smaller than the whole nozzle diameter. Afterward, the air reaches section B where it enters from one side with a speed of approximately 160 m/s and the remaining part of nozzle in this section still has zero velocity and this difference in the air velocity magnitude along the nozzle cross-section at the entrance helps in separating the outer fibers layer of the strand which will turn later into wrapper fibers. In section C, the airflow velocity distribution is asymmetric because of the effect of the geometry in the preceding sections A and B.

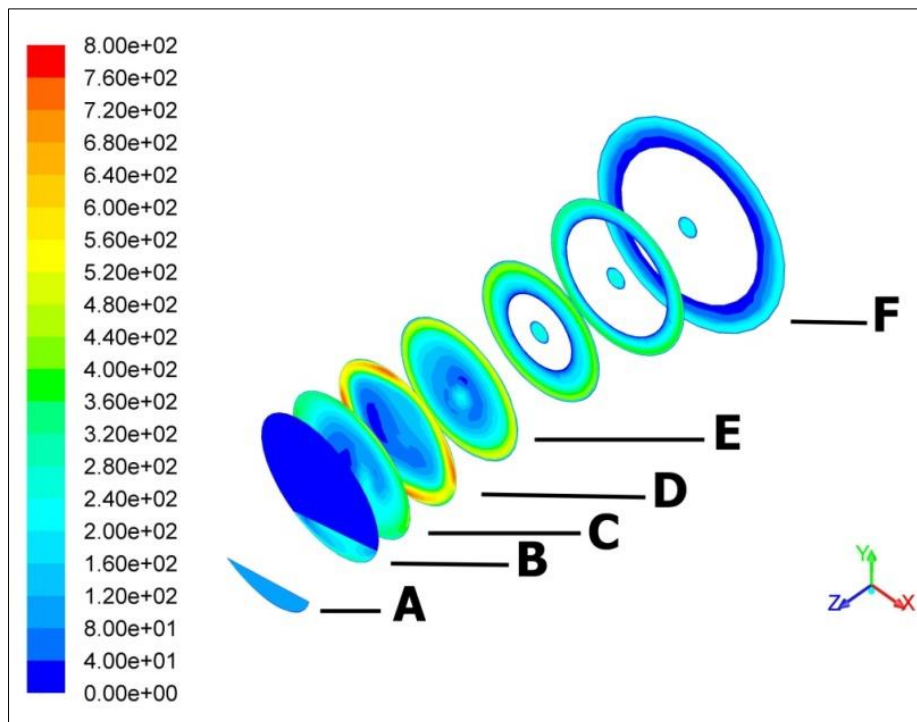


Figure 3.6 Contours of the velocity magnitude (m/s) at different nozzle cross-sections.

In section D, the swirling airflow has been ejected from jet orifices and high air velocity in the outer thin region is created while the inner region relatively has very slow airflow. This also can be observed in the velocity vector distribution for this section shown in Figure 3.7. The airflow afterward spins downstream as can be seen in section E and its intensity decreased and its distribution became almost

symmetrical. On section F, the airflow swirls in the gap between the hollow spindle outer wall and the nozzle inner wall to leave the nozzle from its outlet to the external atmosphere. Obviously, the airflow velocity reduced significantly at this stage.

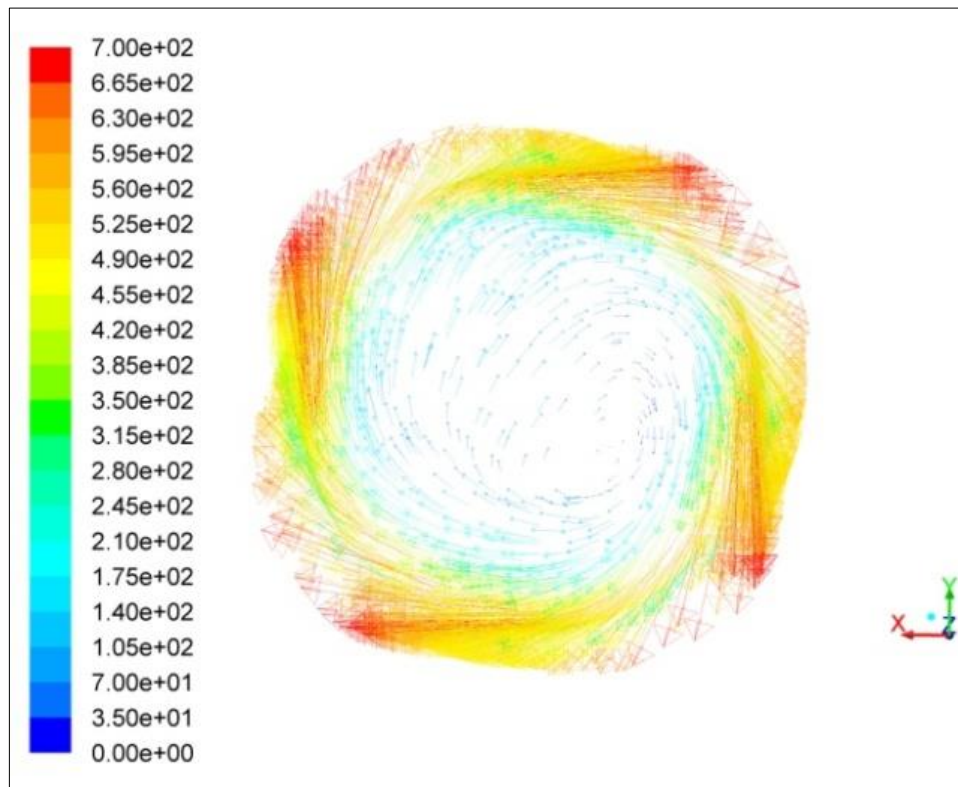


Figure 3.7 The velocity vector (m/s) distribution at section D.

3.3.3 Principle of yarn formation

The above-motioned velocity magnitude is the resultant velocity of three velocity components; the axial velocity component that forces the fibers to move downstream towards the hollow spindle outlet; the tangential velocity component that causes the fibers trailing ends to rotate tangentially to the nozzle inner wall leading to fiber twisting, hence, yarn wrapping; and the radial velocity component that separates the fibers and affects the yarn compactness. Results revealed that the tangential velocity component has the maximum value, followed by the axial velocity, then the radial velocity and this is ascribed to a big inclination angle of the jet orifices to nozzle axis (around 60°). These three components will be discussed separately in the next sections. The quality of the air jet yarn depends mainly on the wrapping process, i.e. higher number of wrapper fibers along with tighter and regular wrapping contribute

to better yarn structure. The mentioned fiber separation process at the nozzle inlet is very important to achieve yarn quality. After the wrapping process takes place inside the vortex chamber, the yarn is formed and drawn through the hollow spindle.

3.3.3.1 Tangential velocity distribution

Figure 3.8 shows the tangential velocity at different nozzle cross-sections. It can be remarked that the value of the tangential velocity in the vicinity of the hollow spindle outer wall is high while the tangential velocity value inside the hollow spindle is low and its direction is opposite to the former. Because of this difference in value and direction, the hairs on yarn surface could be embedded into the yarn body or blown away, consequently, yarn hairiness and tenacity improve. This justifies that the air jet yarn is known for its relatively low hairiness (Li, Yu, & Shang, 2013).

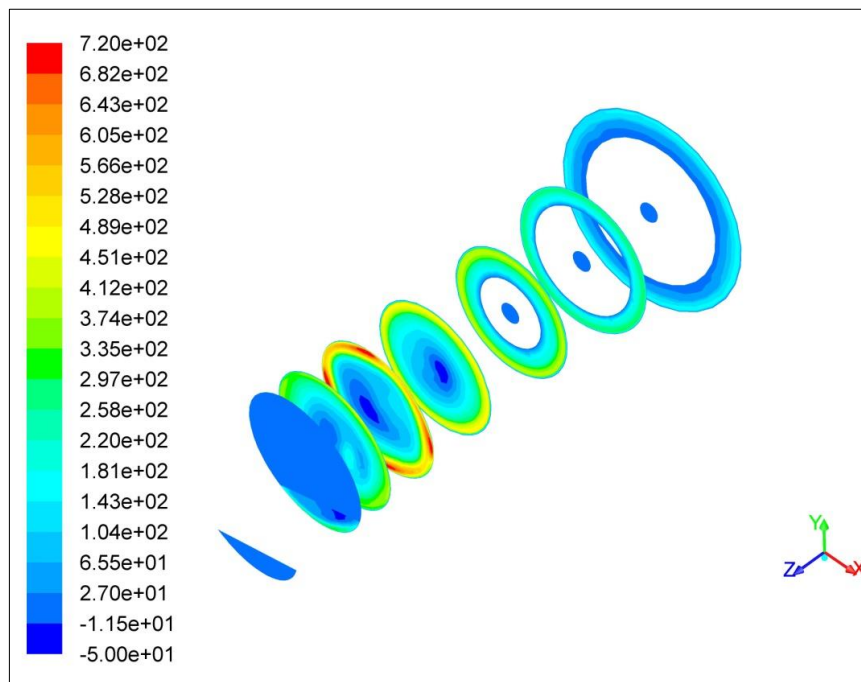


Figure 3.8 Contours of the tangential velocity (m/s) at different nozzle cross-sections.

Generally, sufficient tangential velocity could reduce hairiness but excessive tangential velocity could blow a lot of fibers away from the yarn body and increases fly fibers, floating fibers, consequently, yarn quality deteriorates. Figure 3.9 shows the tangential velocity distribution curve at section D. It can be seen that the tangential

velocity increases slowly from the nozzle axis towards outside in both directions, then a sudden and sharp increase in the tangential velocity takes place near the edges of the nozzle wall. In the inner region, the core fibers strand is exposed and affected slightly by this slow airflow, therefore, the core fibers in the final spun yarn have almost no twist. While the fibers in the periphery of the strand are affected greatly by the high tangential velocity that forces them to twist.

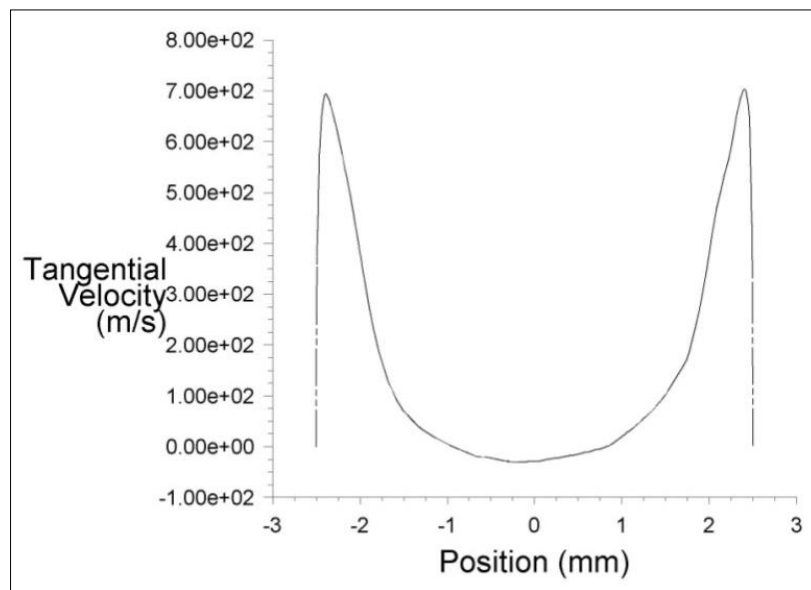


Figure 3.9 The tangential velocity distribution curve at section D.

3.3.3.2 Radial velocity distribution

Figure 3.10 shows the radial velocity distributions at section D. The fiber separation process is more likely in this zone. Results showed that the values of the radial velocity near the nozzle wall are higher than that in the vicinity of the nozzle axis and this forces the fibers in the strand periphery to be embedded towards the yarn axis. It is also clear that the values of the radial velocity are less than the corresponding tangential velocity and its distribution is not symmetric as the tangential velocity and this is due to the influence of the vortex.

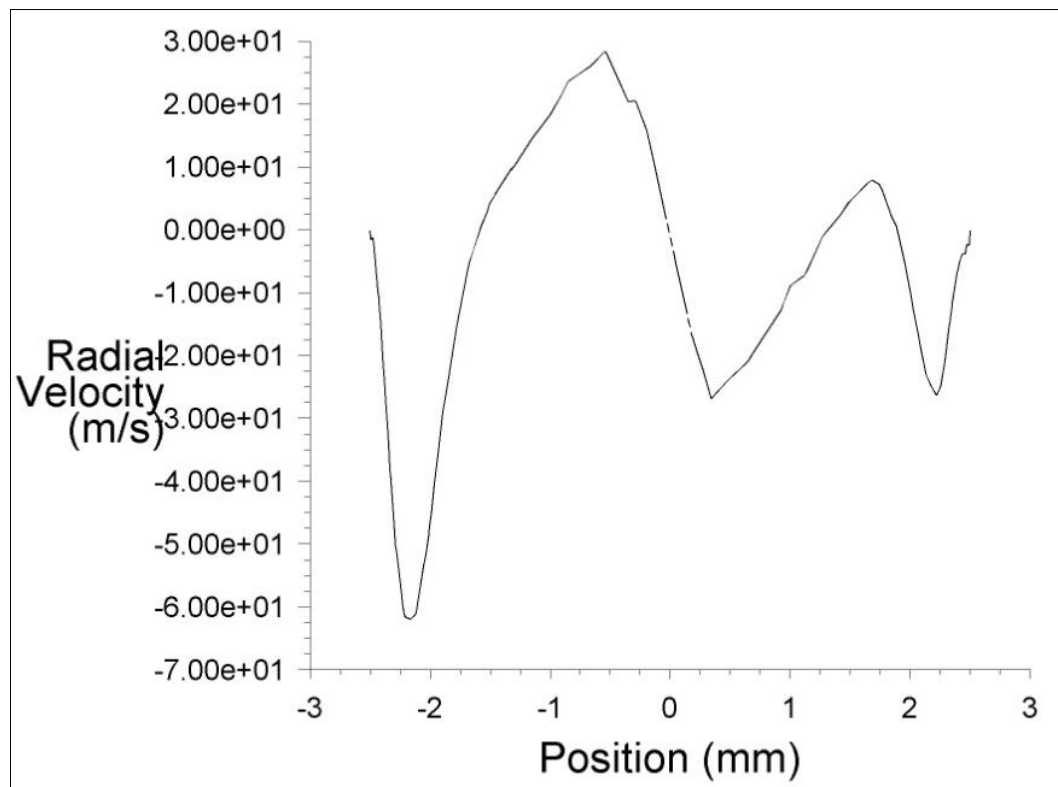


Figure 3.10 The radial velocity distribution at section D.

3.3.3.3 Axial velocity distribution

Figure 3.11 shows the axial velocity for the x-x axial cross-section. Similar to the tangential velocity distribution, the axial velocity direction inside the hollow spindle is in the opposite direction of the axial velocity direction outside the hollow spindle. The reverse flow is evident inside the hollow spindle from its inlet to its outlet.

3.3.3.4 Static pressure distribution

Figure 3.12 shows the static pressure distribution for the x-x axial cross-section. As can be seen, a negative air pressure is created as a result of the entrainment effect of airflow via the jet orifices and it covers the region from the nozzle inlet to the hollow spindle internal area. On the other hand, there is a positive air pressure near the nozzle outer wall. Therefore, the few fibers that were separated previously at the entrance of

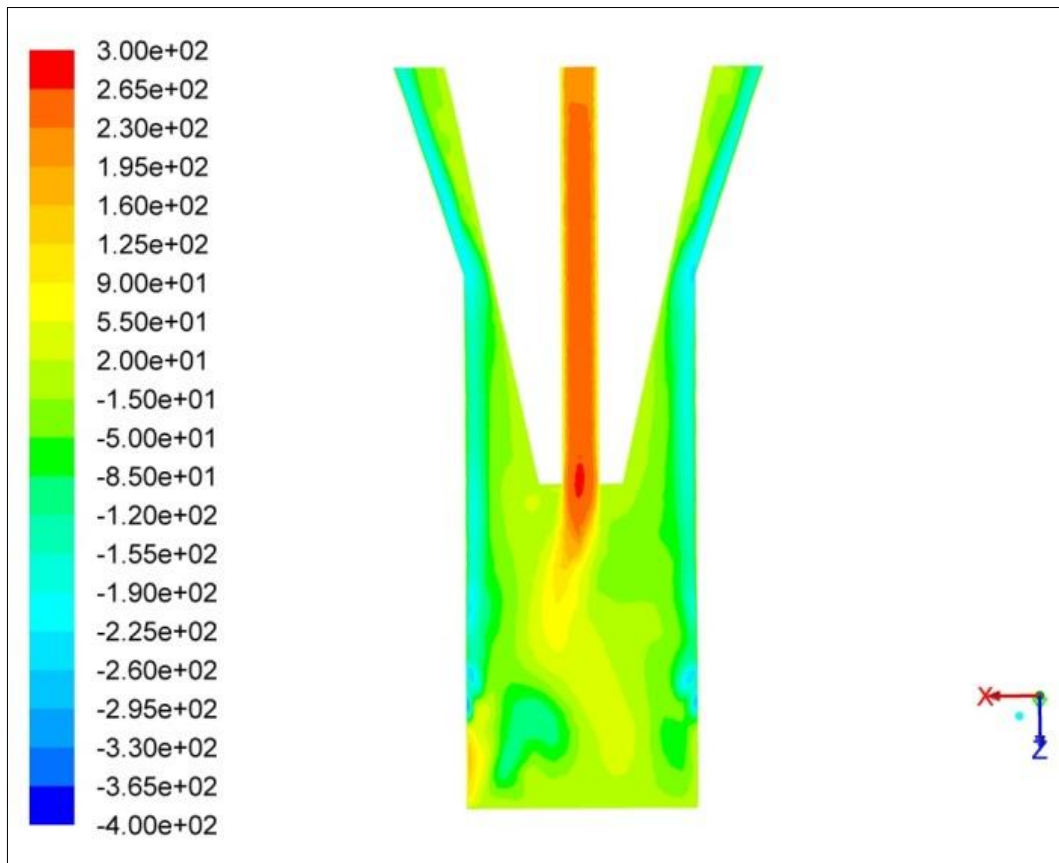


Figure 3.11 Contours of the axial velocity (m/s) for the x-x axial cross-section.

the nozzle (using the fiber guide) are sucked into the vortex chamber and reside on the outer wall surfaces of the nozzle taking the open end form. The intensity of this negative pressure is important for the formation process of these open end fibers. The higher the negative pressure value, the higher the fiber separation process and the more formed open end fibers. In the meantime, as mentioned earlier, the high tangential velocity exists in this region causes these open end fibers to twist and wrap the core fibers constructing the air jet yarn with its distinctive structure.

3.3.4 Effect of nozzle pressure on structure and strength of the air jet yarn

Figure 3.13 shows the contours of the axial velocity distribution at different nozzle pressure. It can be seen that the intensity of above-mentioned reverse flow in the hollow spindle which contributes to the vortex creation increases with the increase of

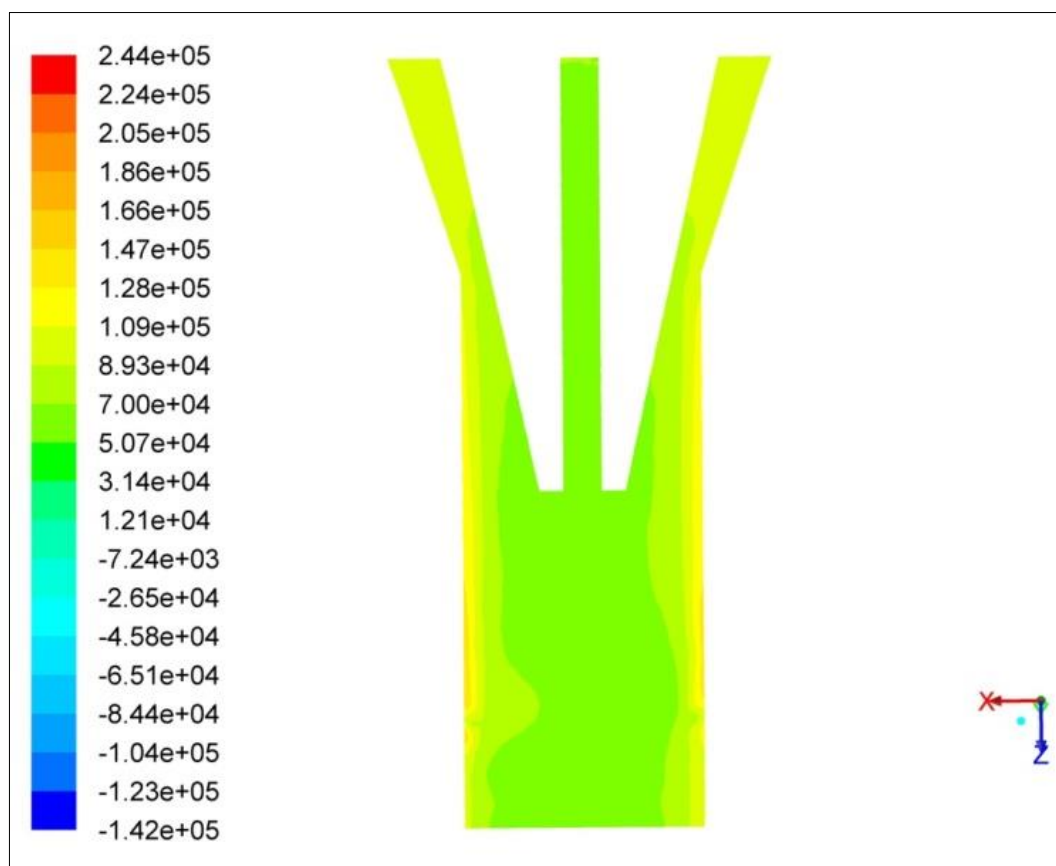


Figure 3.12 Contours of the static pressure distribution (Pa) for the x-x axial cross-section.

the nozzle pressure from 4 to 6 bar. When the pressure became 6 bar, it is obvious that the reverse flow reached the nozzle inlet which obstructs the spinning process because its direction is opposite to the strand movement direction.

Figure 3.14 shows the contours of the tangential velocity distribution at different nozzle pressure. The fiber separation process takes place in the region near to the nozzle entrance. By increasing nozzle pressure, the tangential velocity in this area increases gradually which is good for fiber separation and twist. But at high pressure, the tangential velocity becomes very high and fiber control could be deteriorated as the number of regular wrapper fiber decreases while the irregular wrapping increases. Also, by increasing the nozzle pressure to 6 bar, the tangential velocity in the region between the wall of the hollow spindle and the inner wall of the nozzle increases and

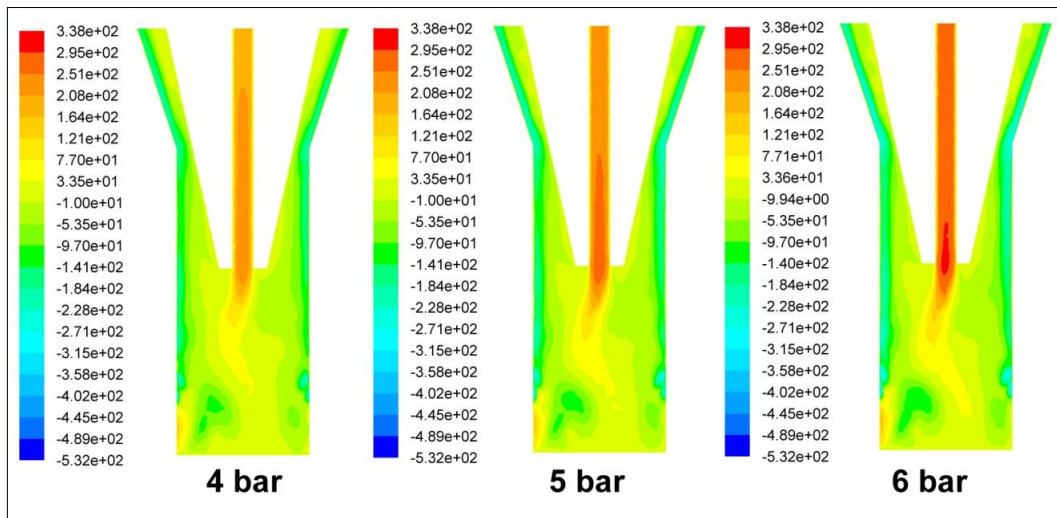


Figure 3.13 Contours of the axial velocity distribution (m/s) for the x-x axial cross-section at different nozzle pressure.

its area enlarges. This can lead to turbulence in this zone, which consequently could affect yarn quality. This trend is also found similar when MVS nozzle was investigated (Z Pei & Yu, 2010).

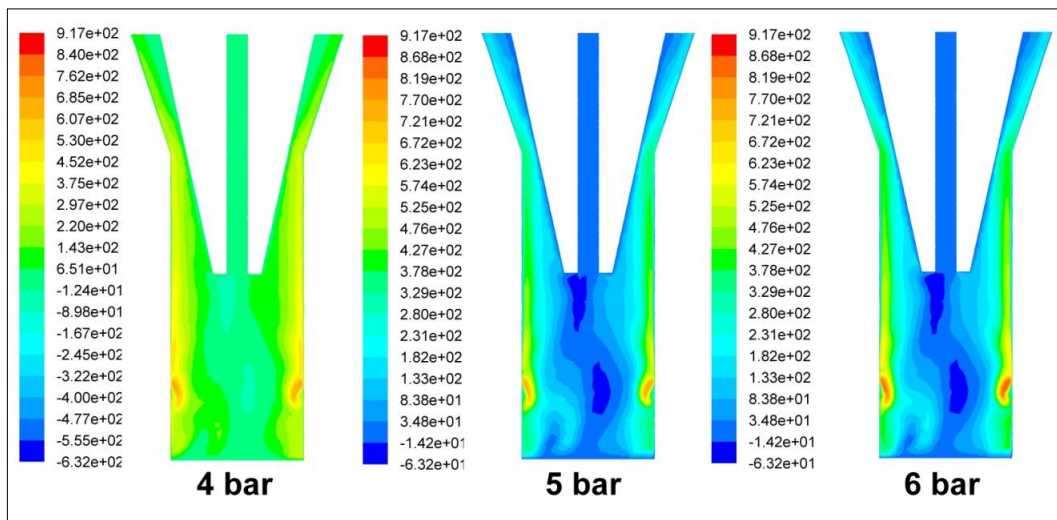


Figure 3.14 Contours of the tangential velocity distribution (m/s) for the x-x axial cross-section at different nozzle pressure.

The contours of the static pressure distribution at different nozzle pressure are shown in *Figure 3.15*. By increasing the nozzle pressure, the negative pressure in the area in the vicinity of the vortex chamber outlet increases and its area shifts towards outside,

this is beneficial to the fiber separation process. On the other hand, increasing the nozzle pressure resulted in increasing the positive air pressure exists in the area between the outlets of the jet orifices toward the hollow spindle outer wall. This could obstruct the fibers movement influencing yarn formation process negatively. By combining the results presented in *Figure 3.13*, *Figure 3.14*, and *Figure 3.15*, the optimum yarn strength is anticipated when using a nozzle pressure of 5 bar.

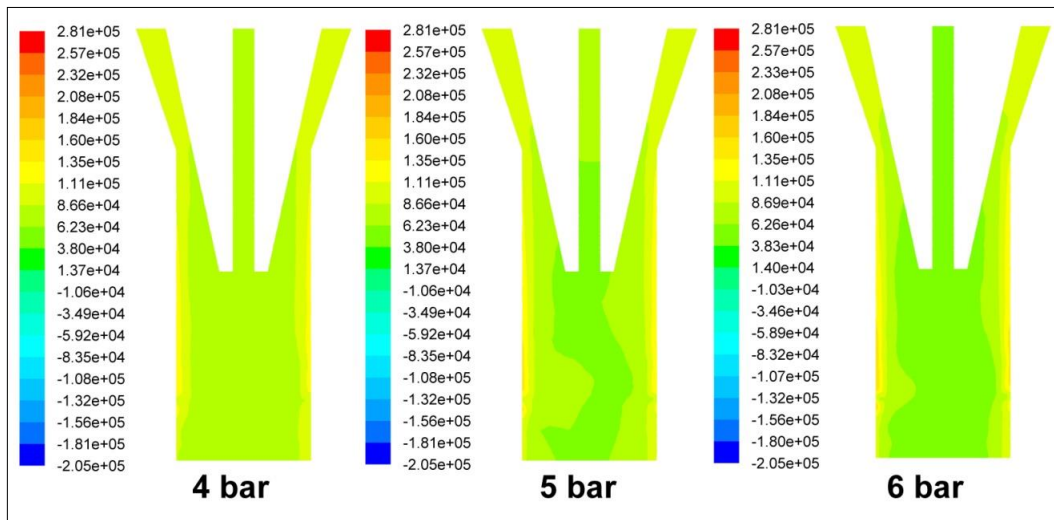


Figure 3.15 Contours of the static pressure distribution (Pa) for the x-x axial cross-section at different nozzle pressure.

Figure 3.16 shows the experimental results of the yarn tenacity at different nozzle pressure (the individual values of tenacity and one way-ANOVA results are given in Appendix 1). Statistical analyses showed that the differences in yarn tenacity are statically significant at 95% confidence level. It is clear that yarn tenacity increases when nozzle pressure increases from 4 to 5 bar, then tenacity decreases gradually when it reaches 6 bar.

The structural analyses shown in *Table 3.1* revealed that when spinning using nozzle air pressure of 4, 5 and 6 bar, the corresponding wrapper fiber ratio is 30.7, 32.7 and 29.3% respectively. The statistical analyses showed that the differences in wrapper ratio are statically significant at 95% confidence level. However, the coefficient of variation is quite high (24.51-29.44%) (the individual values of wrapper ratio and one-way ANOVA results are given in Appendix 2). Nevertheless, considering the values

of C and D, it can be seen that the coefficient of variation is less (08.93-19.59%). Therefore, C/D ratio was calculated (it is the ratio between one wrap width to the pitch at this yarn section). The values of C/D support the previous results of wrapper ratio where it followed the same trend. When spinning using nozzle air pressure of 4, 5 and 6 bar, the corresponding C/D ratio is 21.81, 33.33, and 26.94% respectively.

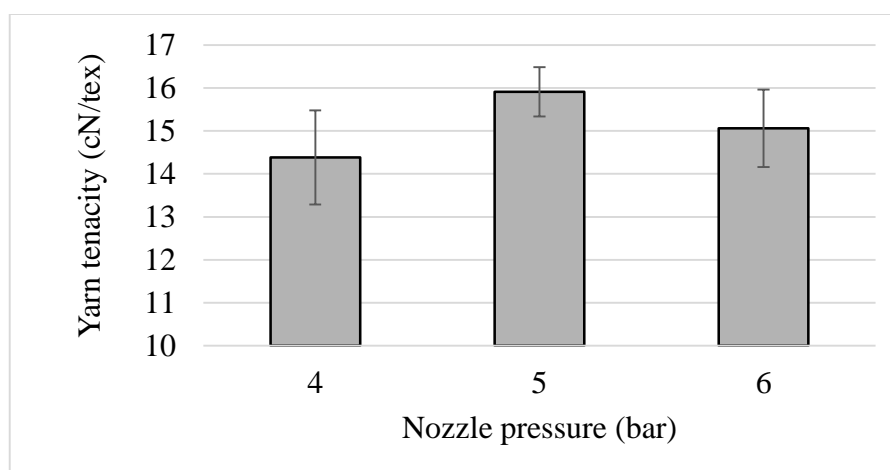


Figure 3.16 Effect of nozzle pressure on 23 Tex yarn tenacity.

The initial increase in air pressure (4 and 5 bar) increases the intensity of the above-mentioned reverse flow in the hollow spindle which contributes to the vortex creation, the tangential velocity in the region near the nozzle entrance increases gradually, the negative pressure in the area in the vicinity of the vortex chamber outlet increases and its area shifts towards outside. All these factors contribute to fiber separation process and the regular twist. Consequently, the yarn structure has tight regular wrappings and more wrapped portions (more wrapper ratio 32.7%).

On the other hand, When the pressure reaches 6 bar, it is obvious that the reverse flow reached the nozzle inlet which could obstruct the spinning process because its direction is opposite to the strand movement direction, the tangential velocity becomes very high, the tangential velocity in the region between the wall of the hollow spindle and the inner wall of the nozzle increases and its area enlarges. This can lead to turbulence in this zone. All these factors contribute to less fiber control and obstruction of fibers movement influencing yarn formation process negatively. Consequently, the yarn structure contains wild fibers, irregular wrapping, and less

wrapped portions (less wrapper ratio 29.3%). By comparing the above-mentioned results, it can be concluded that the experimental findings agree with the numerical simulation results.

Table 3.1 Yarn structural parameters at different nozzle pressures.

Nozzle pressure	4 bar		5 bar		6 bar	
	Average (μm)	CV%	Average (μm)	CV%	Average (μm)	CV%
A	175	32.29	105	36.82	168	34.17
B	241.5	31.74	133	36.04	207.9	24.29
C	287	18.12	273	9.16	431.9	16.23
D	1316	13.11	819	8.93	1603	19.59
C/D (%)	21.81		33.33		26.94	
Wrapper ratio (%)	30.7	29.39	32.7	29.44	29.3	24.51

4. Prediction of Air Jet Yarn Strength Based on Statistical Modeling

In this chapter, some process parameters of Rieter air jet spinning machine, namely, yarn linear density, nozzle pressure, and delivery speed have been investigated. Along with the experiment, a statistical model had been established based on multiple regression to study the combined effect of those parameter on yarn tenacity as well as to predict the air jet yarn strength.

4.1 *Materials and methods*

100% Viscose fibers were spun to produce air jet yarns with different counts and machine parameters. The Box-Behnken factorial experimental design is an efficient method to reduce the number of experiments required to study the parameters and their combined effect and it was used to obtain the combination of yarn count, delivery speed, and nozzle pressure. *Table 4.1* shows the chosen parameters and their levels. It is notable to mention that spinning one sample with the level coded (-1, 1, 0) was impractical because the end breakage rate was very high which obstructed the spinning process. A total of 12 yarns were spun then placed in the standard conditions prior to testing.

Table 4.1 Spun yarn production parameters.

Parameters	The levels and their codes		
	-1	0	1
Yarn count (Tex)	16	23	30
Delivery speed (m/min)	350	400	450
Nozzle pressure (bar)	4	5	6

The yarn tenacity was tested using Instron 4411. The instrument is a single yarn strength tester and operates at a constant rate of extension. Following BS EN ISO 2062:1995 (ISO, 1995), with a sample length of 50 cm, the crosshead moving speed

has been adjusted to give a yarn failure time of 20 ± 3 sec and taking the average of 50 observations for each yarn sample. Ordinary least squares regression model was used to analyze the test results and to obtain the regression equation (4.1).

$$Y = \beta_0 + \beta_i X_i + \beta_j X_j + \beta_k X_k + \beta_{ij} X_i X_j + \beta_{ik} X_i X_k + \beta_{jk} X_j X_k + \beta_{ii} X_i^2 + \beta_{jj} X_j^2 + \beta_{kk} X_k^2 \quad (4.1)$$

Where Y is the dependent variable, X_i, X_j, X_k are independent variables, β_0 is the regression equation constant, $\beta_i, \beta_j, \beta_k$ are the linear coefficients, $\beta_{ij}, \beta_{ik}, \beta_{jk}$ are the interaction coefficients and $\beta_{ii}, \beta_{jj}, \beta_{kk}$ are the quadratic coefficients.

4.2 Regression model

Equation (4.2) Indicates the response surface equations for yarn tenacity obtained by using multiple regression (the squared multiple regression coefficient $R^2=95.5\%$).

$$Z = -22.4652 + 0.7800X_1 + 0.0808X_2 + 4.1643X_3 + 0.0005X_1X_2 + 0.0079X_1X_3 + 0.0068X_2X_3 - 0.01637X_1^2 - 0.0002X_2^2 - 0.6931X_3^2 \quad (4.2)$$

By using this model, it is possible to predict air jet yarn tenacity Z based on yarn count X_1 , yarn delivery speed X_2 and nozzle pressure X_3 . All regression coefficients and their P -values are shown in *Table 4.2*.

Table 4.2 P -values of the model and its coefficients.

Coefficient	β_0	β_i	β_j	β_k	β_{ij}	β_{ik}	β_{jk}	β_{ii}	β_{jj}	β_{kk}	Regression model F(P-value)
P-value	0.08	0.00*	0.09	0.02*	0.27	0.62	0.00*	0.00*	0.01*	0.00*	0.01*

(*): Statistically significant at 95% confidence level.

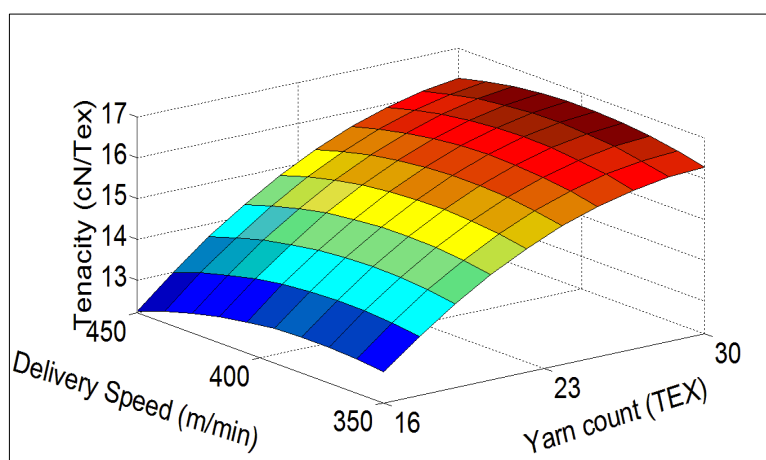
4.3 Effect of process parameters on yarn strength

Figure 4.1 shows the influence of linear density, delivery speed and nozzle pressure on yarn tenacity. It is obvious that the linear density has the maximum effect on yarn

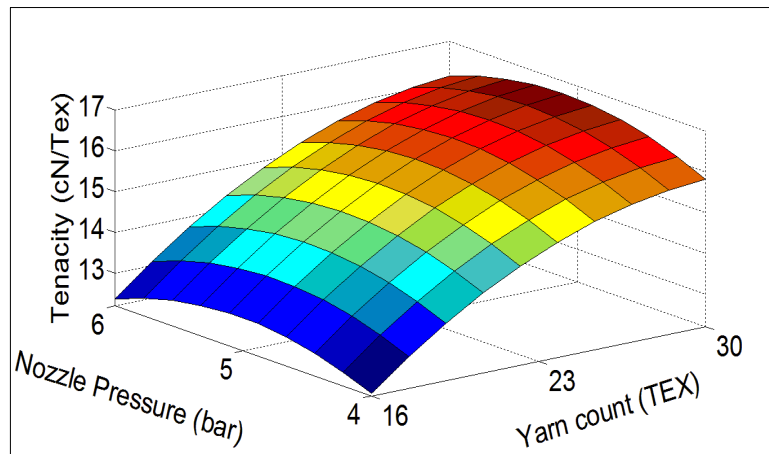
tenacity. As shown in *Figure 4.1-a* and *b*, coarser yarns 30 Tex have higher tenacity by about 29% than finer yarns 16 Tex and this is due to the increase in the number of fibers in yarn cross-section, thus, the number of core and wrapper fibers in yarn cross-section that bear the load exerted on the yarn. Nevertheless, results shown later in *Table 5.3* reveal that wrapper ratio increases slightly at coarser counts. The same trend also exists for MVS yarn (Tyagi et al., 2004b).

Increasing the yarn delivery speed from 350 to 400 m/min results in increasing yarn tenacity, but when using high delivery speed of 450 m/min a deterioration in yarn tenacity occurs by about 3.5% and this is a consequent of the insufficient time for the whirling action to take place in the vortex chamber which could result in an increment of the number of the wild fibers and the regions of unwrapped core fibers (Tyagi et al., 2004a). This effect is more obvious when producing 16 Tex yarn at 400 and 450 m/min where yarn tenacity is very low.

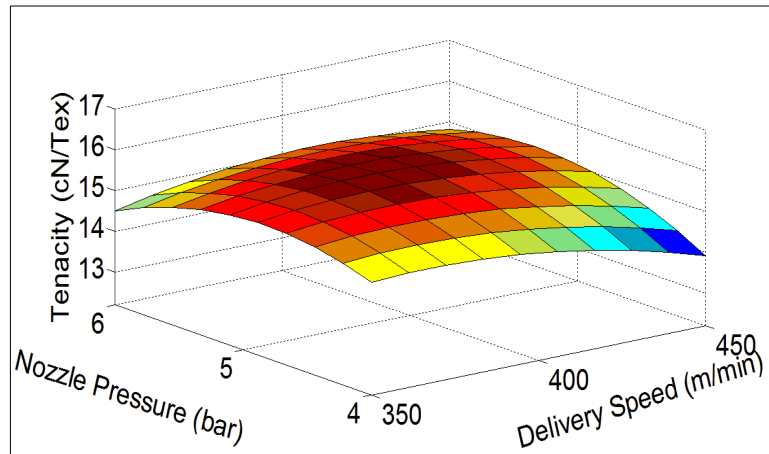
Yarn tenacity increases when nozzle pressure increases from 4 to 5 bar, then decreases gradually when it reaches 6 bar and this is because the increase in air pressure initially causes tight regular wrappings and more wrapped portions of the yarn (more wrapper ratio), but higher air pressure creates irregular wrappings and increases the wild fibers (less wrapper ratio), (elaborate explanation is given in section 3.3.4). The same trend is also confirmed for MVS yarn (Tyagi et al., 2004b).



(a)



(b)



(c)

Figure 4.1 Effect of (a) yarn linear density and delivery speed, (b) yarn linear density and nozzle pressure, and (c) nozzle pressure and yarn delivery speed, on yarn tenacity.

In addition to yarn tenacity, other yarn properties were investigated including breaking elongation, imperfections, hairiness, and abrasiveness. Average values of the tested yarn properties are given in Appendix 3, a set of stress-strain curves for one yarn sample is given in Appendix 4, and response surfaces are presented in Appendix 5.

It is clear that coarser counts have better yarn evenness, abrasiveness, and fewer yarn imperfections. Increasing nozzle pressure results in increasing tight regular wrappings and more wrapped portions, consequently, total imperfections reduce initially but later

on, abrasiveness deteriorate and total imperfections increase at higher pressures because of the incidence of irregular wrappings and increase of wild fibers and fibers loss. Using high delivery speeds deteriorates yarn abrasiveness, hairiness, and imperfections because of the insufficient time for the whirling action to take place in the vortex chamber which could result in an increment in the number of wild fibers as well as the regions of unwrapped core fibers.

Response surface equations showed that yarn count range taken has the maximum effect on yarn breaking elongation, evenness, and total imperfection while the delivery speed has the maximum effect on yarn hairiness.

5. Prediction of Air Jet Yarn Strength Based on Mathematical Modeling

In this chapter, a prediction of air jet spun yarn strength at short gauge length has been presented. Different models have been modified, combined and a new model has been proposed and validated.

5.1 Model for the failure of the air jet spun yarn

Air jet yarn structure can be divided into the core which is almost parallel fibers and the wrapper which is in a helical form. In the current model, the core strand strength has been calculated as a parallel bundle of fibers. This strand is also subjected to the normal forces of the wrapper fibers. Therefore, the frictional forces applied to the core fibers strand have been calculated. In addition, the strength of the wrapper fiber strand has been calculated.

It is worth mentioning that the strength of the core fiber strand has been calculated based on the assumption that the fibers are gripped between two jaws and the gauge length of the yarn tensile tester is less than fiber length. Consequently, to verify the model, the air jet yarn strength has been measured at a gauge length shorter than the fiber length. The yarn structure is assumed to be ideal as shown in *Figure 5.1*. It is assumed that; wraps width and height are constant and distributed regularly along the yarn axis, helix angle is constant, and core fibers are straight and parallel to yarn axis.

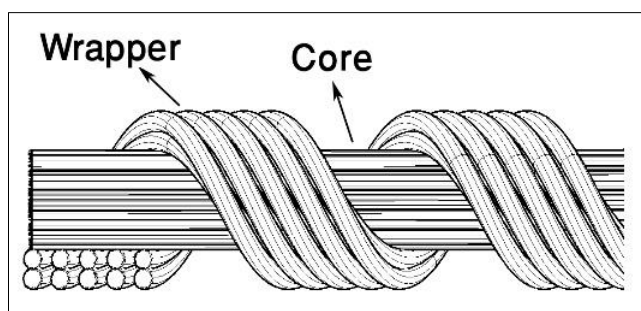


Figure 5.1 Simplified model of short staple air jet spun yarn.

5.1.1 Determination of core fiber strength

The strength of the core fiber strand is the summation of the strength of a parallel bundle of fibers gripped between two jaws of the tensile testing instrument and the strength of that bundle originated from a fiber-to-fiber frictional force caused by the normal forces from the wrapper fiber strand during the extension process.

Assuming a short staple spun yarn is gripped between tensile tester jaws with a gauge length less than fiber length. This yarn is spun using short staple fibers. Assuming that these fibers are straight, parallel to yarn axis, have equal circular diameters, no slippage occurs between core fibers due to the usage of short gauge length, inter-fiber friction is so small that can be ignored and individual fiber position in the yarn is random. Therefore, Neckář theory of parallel fiber bundle can be used to find the strength of this parallel fiber bundle (Neckar & Das, 2003). The derivation steps are given below. During the tensile testing process, and due to the random distribution of fibers in the bundle, some fibers are gripped between the jaws while some others aren't as shown in *Figure 5.2*. Fiber length utilization factor η is the ratio between the total number of gripped fibers n_e and the total number of fibers in yarn cross-section n .

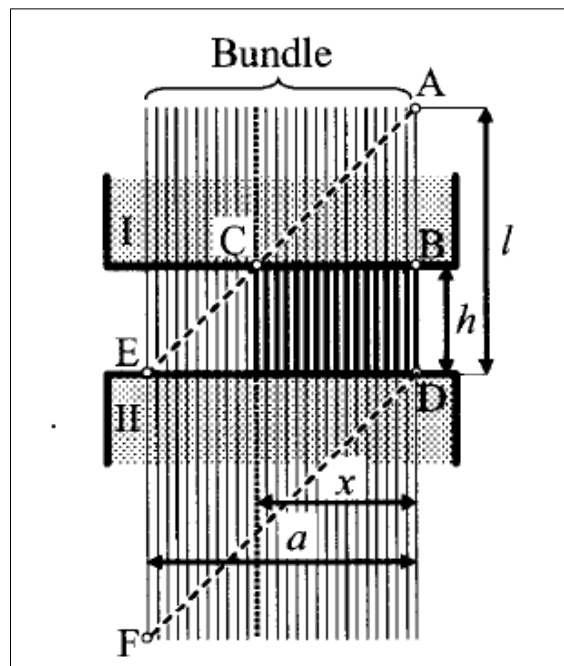


Figure 5.2 Bundle of fibers gripped between two jaws (Neckar & Das, 2003).

From *Figure 5.2*, it is valid that the distance a is proportional to n while the distance x is proportional to n_e and comparing the triangles ABC and ADE leads to the following relationship.

$$\eta = \frac{n_e}{n} = \frac{x}{a} = \frac{l-h}{l} = 1 - \frac{h}{l}, h < l_{max} \quad (5.1)$$

Where h denotes the gauge length (mm), l is fiber length (mm), and l_{max} is maximum fiber length (mm). Assuming a yarn has mass m (gm) and linear density X_1 (Tex). The yarn consists of several bundles of fibers, each bundle has mass m_j (gm), linear density T_j (Tex) and number of fibers in cross-section n_j . Each bundle consists of fibers have mass m_i (gm) and linear density T_i (Tex). Therefore, it is valid that,

$$m = \sum_{j=1}^k m_j, \quad X_1 = \sum_{j=1}^k T_j, \quad n = \sum_{j=1}^k n_j \quad (5.2)$$

Given that, γ_j is the mass fraction of the j^{th} partial bundle and it is the ratio of its mass m_j to the yarn mass m . Therefore,

$$n_j = \frac{T_j}{T_i} = \frac{m_j}{lT_i} = \frac{m\gamma_j}{lT_i} = \frac{X_1\gamma_j}{T_i} = n\gamma_j \quad (5.3)$$

Evidently, fiber length utilization factor η can be expressed as follows,

$$\eta = \frac{n_e}{n} = \frac{\sum n_{ej}}{n} = \frac{\sum (n_j \eta_j)}{n} = \frac{\sum (n \gamma_j \eta_j)}{n} = \frac{n \sum \gamma_j \eta_j}{n} = \sum \gamma_j \eta_j \quad (5.4)$$

Where n_{ej} is the number of fibers in the j^{th} partial bundle gripped by both jaws simultaneously and η_j is fiber length utilization of the j^{th} partial bundle. Intuitively,

$$\eta = \int_0^{l_{max}} \eta_j \gamma(l) dl \quad (5.5)$$

Using equation (5.1),

$$\eta = \begin{cases} \int_0^{l_{max}} \left(1 - \frac{h}{l}\right) \gamma(l) dl, & h < l_{max} \\ 0, & h \geq l_{max} \end{cases} \quad (5.6)$$

$\gamma(l)$ is the mass fraction function which is the summation of the partial mass fractions of each fiber in the yarn and it can be calculated using equation (5.7).

$$\gamma(l) = \sum_{i=1}^k \frac{m_i}{m} \quad (5.7)$$

The value of $\gamma(l)$ ranges from 0 to 1. If all fibers in the yarn have the same fiber length and equal to the maximum fiber length, then $\gamma(l)$ will be equal to 1 and the parallel bundle strength will be a function of gauge length only. Thus, we can deduce the core fibers strength σ_1 as a parallel bundle gripped between two jaws (cN) using equation (5.6) and (5.7) as follows,

$$\sigma_1 = f \frac{(100 - W) X_1}{100} \frac{1}{T_i} \eta \quad (5.8)$$

Where f denotes fiber breaking load (cN) and W denotes wrapper fibers percentage (%). The yarn wrapper ratio W can be considered as the average volumetric ratio between wrapper fibers and yarn at different yarn sections, thus, it can be obtained using equation (3.10).

Assuming that the yarn cross-section is circular and remains circular till break. To obtain the normal forces on core fibers, Krause et al. model (Krause & Soliman, 1990) was used and modified. The derivation steps are given below. By analyzing the forces acting on an element of a wrapper fiber as shown in *Figure 5.3*, the following relationship is valid,

$$\sin \frac{d\theta}{2} = \frac{N ds / 2}{f \sin \alpha} \quad (5.9)$$

Where ds is an element of wrapper fiber, $d\theta$ is an increment angle corresponding to ds , N is normal forces exerted by wrapper fibers per unit length (cN/mm) and α is the average strained wrapper fiber helix angle (rad). Also, from *Figure 5.3*, the following relationship is valid,

$$\sin \alpha = \frac{r d\theta}{ds} \quad (5.10)$$

Where r is the average strained yarn radius (mm). From equation (5.9) and (5.10),

$$N = \frac{2f(\sin \alpha)^2}{r} \cdot \frac{\sin(d\theta/2)}{d\theta} \quad (5.11)$$

The value of $\sin(d\theta/2)$ is approximately equal to the value of $(d\theta/2)$ when $d\theta$ value approaches 0, hence,

$$N = \frac{f(\sin \alpha)^2}{r} \quad (5.12)$$

By analyzing the yarn before and after axial loading, it is valid that,

$$l_u = l_{uo}(1 + e_f) \quad (5.13)$$

Where l_u is the average strained fiber length in unit length (mm), l_{uo} is the average unstrained fiber length in unit length (mm) and e_f is fiber breaking elongation (%).

$$pi = p_o(1 + e_y) \quad (5.14)$$

Where pi is the average strained pitch of wrapper fibers (mm), p_o the average unstrained pitch of wrapper fibers (mm), and e_y expresses yarn longitudinal strain (%).

$$r = r_o(1 + e_r) \quad (5.15)$$

Where r_o is the average unstrained yarn radius (mm) and e_r represents yarn lateral strain (mm). It is valid from *Figure 5.3* that,

$$\sin \alpha = \frac{2\pi r}{l_u} \quad (5.16)$$

And

$$\sin \alpha_o = \frac{2\pi r_o}{l_{uo}} \quad (5.17)$$

Where α_o is the average unstrained wrapper fiber helix angle (rad). From equations (5.13), (5.15), (5.16) and (5.17),

$$\sin \alpha = \left(\frac{1 + e_r}{1 + e_f} \right) \sin \alpha_o \quad (5.18)$$

It is known that Poisson ratio ν (the ratio between yarn extension and its corresponding diameter deformation) is approximately equal to -1 (Krause & Soliman, 1990; Xie et al., 1986). Hence,

$$e_r = -e_y \quad (5.19)$$

Using equation (5.13), (5.19), *Figure 5.3*, and following the steps which are given in Appendix 6, the following formula has been obtained.

$$e_y = 2(\sin \alpha_o)^2 - 1 + \sqrt{(2(\sin \alpha_o)^2 - 1)^2 + e_f(2 + e_f)} \quad (5.20)$$

We can then deduce the total frictional forces on core fibers σ_2 (cN) as a result of the total normal forces exerted by wrappers fiber strand as follows,

$$\sigma_2 = v_f \mu \frac{f(\sin \alpha)^2}{r} \frac{W}{100} \frac{X_1}{T_i} pi \quad (5.21)$$

Where μ is the fiber friction coefficient, and v_f is yarn packing density (assumed constant=0.6 (Neckar & Das, 2003)).

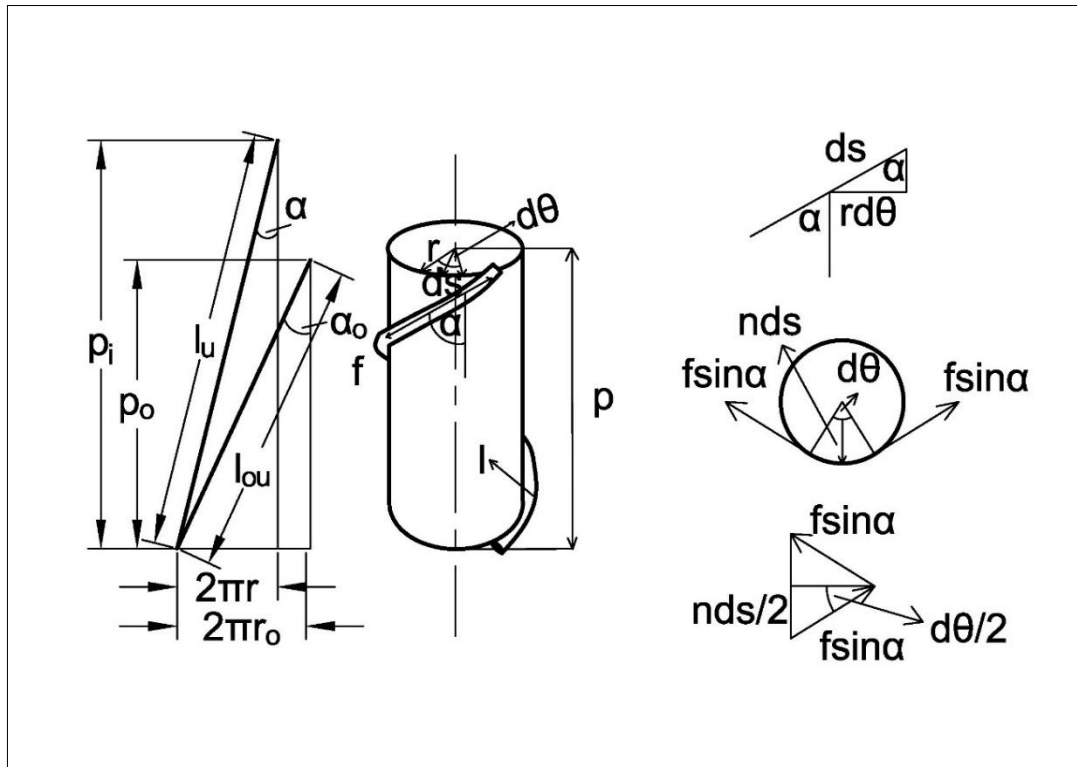


Figure 5.3 Force analysis of air jet yarn before and during axial tensile loading (adapted and reproduced (Krause & Soliman, 1990)).

5.1.2 Wrapper fiber strength component

Hypothesizing the existence of uniform normal pressure on core fibers due to the wrapping effect, constant wrapping angle and fibers are breaking simultaneously due to extension at a gauge length less than fiber length, total wrapper fibers strength σ_3 (cN) can be deduced from Krause et al. model (Krause & Soliman, 1990).

$$\sigma_3 = f \cos \alpha \frac{W}{100} \frac{X_1}{T_i} \quad (5.22)$$

It is worth mentioning that during a tensile test, the stress or load is a complicated function of the elongation. The effects of the variability should be considered. One important factor is the variability in the fiber breaking elongation. It is assumed that all fibers break at the same elongation. On the other hand, there are two different types of fibers orientation. As the elongation continues, the core parallel fibers reach to the breaking point. After that point, there is no contribution of these fibers to the load-elongation process of the yarn while the helical wrapper fibers elongate up to their

breaking point. On short gauge length, the effect of this phenomenon diminishes so that it is ignored in the current model.

Therefore, for a tensile drawing in a short nip gauge, the total tensile strength of air jet yarn is contributed by the core fiber strength, the wrapper fiber strength and the friction force between fibers. According to the proposed assumptions in the current model and using equations (5.8), (5.21) and (5.22), it is possible to obtain yarn strength p (cN) as follows,

$$p = \sigma_1 + \sigma_2 + \sigma_3 \quad (5.23)$$

5.2 Experimental verification

Air jet yarns were spun using different materials and machine parameters as shown in *Table 5.1*. Fibers strength and fineness were measured using Lenzing Vibrodyn-400 according to EN ISO1973 (*ISO 1973:1995, Textile fibres, determination of linear density, gravimetric method and vibroscope method*, 1995). Fiber length distribution was obtained using Sinus instrument according to ASTM D1447 (*ASTM D 1447, Standard test method for length and length uniformity of cotton fibers by photoelectric measurement*, 2012). SEM analyses were performed to analyze the yarn structure where samples were coated by gold sputtering for 45 sec and analyzed for yarn longitudinal view using Carl Zeiss – EVO-LS10 SEM operated at a voltage of 2 kV. Yarn number of wraps per meter, helix angle and parameters A, B, C and D were obtained.

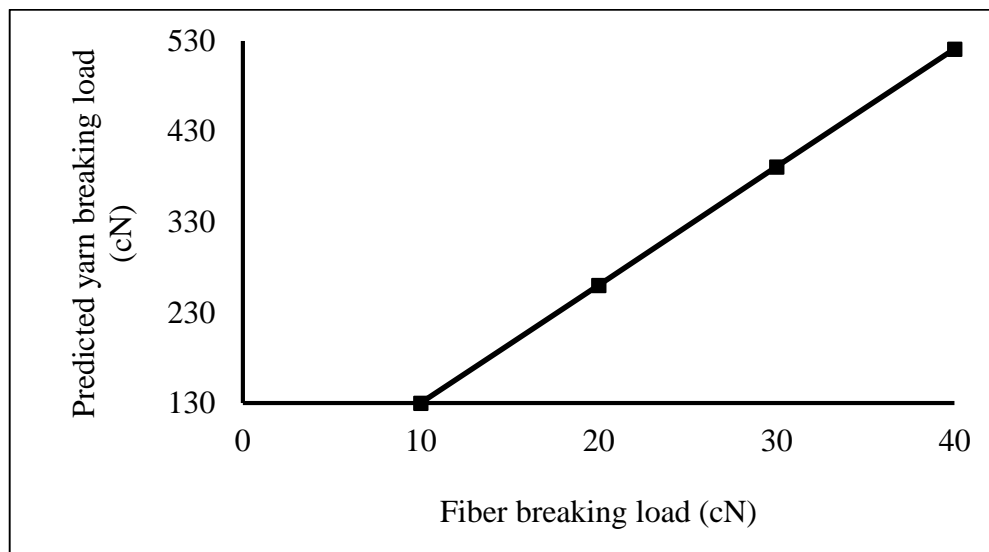
Yarn diameter was measured using Uster tester according to ASTM D1425 (*ASTM D1425, Standard test method for evenness of textile strands using capacitance testing equipment*, 2009). Yarn strength was measured at short gauge length using Labortech instrument according to ASTM D2256 (*ASTM D2256 - 10(2015), Standard test method for tensile properties of yarns by the single-strand method*, 2015), (Gauge length 30 mm, 1 cN preload, constant rate of elongation principle, mechanical jaws and keeping the 17-23 sec breakage time).

Table 5.1 Yarn production plan.

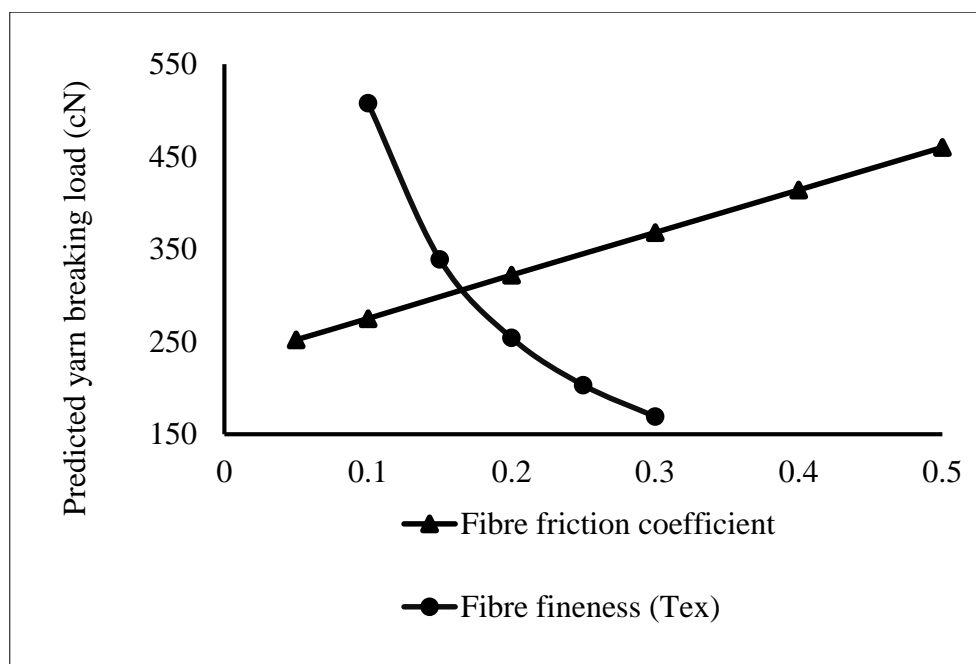
Sample No.	Material type	Yarn count (Tex)	Delivery speed (m/min)	Nozzle pressure (bar)
1	Viscose	16	350	5
2	Viscose	30	350	5
3	Viscose	30	450	5
4	Viscose	16	400	4
5	Viscose	30	400	4
6	Viscose	16	400	6
7	Viscose	30	400	6
8	Viscose	23	350	4
9	Viscose	23	450	4
10	Viscose	23	350	6
11	Viscose	23	450	6
12	Viscose	23	400	5
13	Viscose	20	400	6
14	Viscose	25	400	6
15	Tencel	23	400	6

5.3 Results of the mathematical model

By using the proposed model, it is possible to investigate theoretically the effect of both fibers and yarn parameters on yarn breaking load as shown in *Figure 5.4* and *Figure 5.5*. *Figure 5.4-a* depicts the direct proportionality between fiber strength and yarn strength. It can be seen from *Figure 5.4-b* that yarn strength improves significantly with the increase of interfiber friction coefficient. Because the increase in friction reduces the slippage in the wrapper and core fibers, hence, increases the number of the wrapper and core fibers that resist loading then break during the extension process (Rangaswamy Rajamanickam, Hansen, & Jayaraman, 1997a). When spinning air jet yarn using coarser fibers, the overall number of fibers in yarn cross-section decreases and yarn strength drops significantly.



(a)



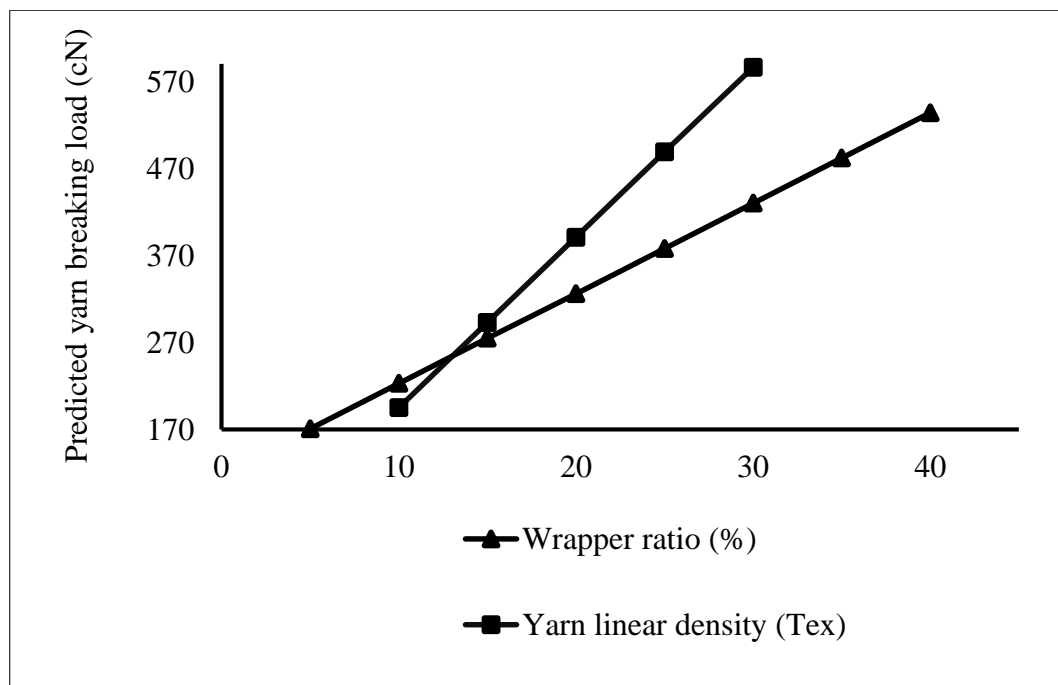
(b)

Figure 5.4 Influence of fiber (a) breaking load, (b) friction coefficient and fineness, on predicted yarn breaking load.

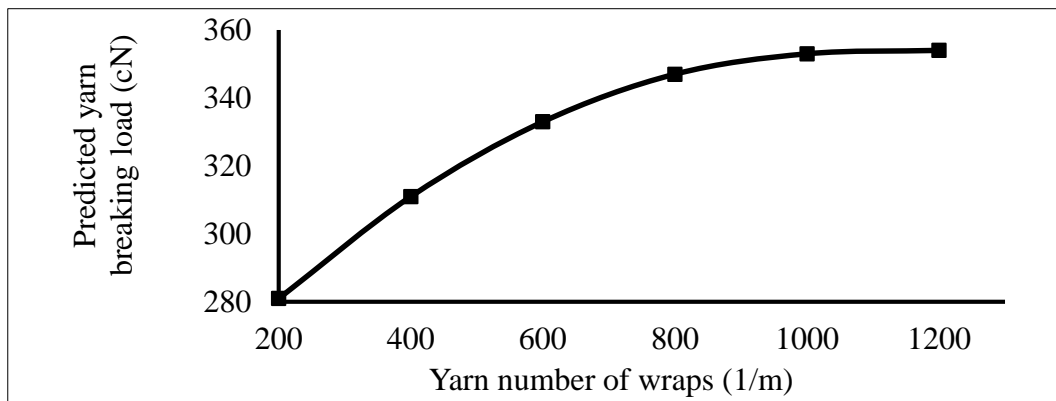
Results in *Figure 5.5-a* show that yarn strength improves by increasing the wrapper ratio as this increases the total number of wrapper fibers that exert the above-mentioned normal forces on the core fiber strand causing more frictional forces that resist the tensile load. Generally, higher wrapper fiber ratio is desired, but it is mainly

limited to the spinning technology. During spinning, when fibers separation from the bundle occurs everywhere in the entire outer periphery of the fiber bundle, the wrapper ratio increases. That is why, the wrapper fibers ratio in AJS is approximately 05-15% (Demir, 2009), the wrapper fibers ratio in MJS is approximately 28-40% (Bhortakke, Nishimura, & Matsuo, 1999; Chasmawala et al., 1990), while the wrapper fibers ratio in MVS is approximately 35-45% (Günaydin & Soydan, 2017). Results also show that when the yarn gets coarser the breaking load increases. All those theoretical findings agree with the experimental results of Tygai et al. (H. G. Ortlek, 2005; Tyagi et al., 2004b).

As shown in *Figure 5.5-b*, when wraps per meter increase, yarn breaking load increases. However, unlike ring and rotor yarns, the strength of air jet yarn does not decrease much, but it levels off at high twist (wraps per meter). This is because approximately 70% of the yarn structure is untwisted core fibers, this result also agrees with the finding of Krause et al. (Krause & Soliman, 1990).



(a)



(b)

Figure 5.5 Influence of yarn (a) linear density and wrapper ratio, (b) number of wraps per meter, on predicted yarn breaking load.

The 15 yarn samples theoretical strength was calculated by obtaining the fiber length distribution, fiber properties, yarn parameters under SEM and using equations (3.10), (5.6), (5.7), (5.8), (5.14), (5.15), (5.18), (5.19), (5.20), (5.21), (5.22) and (5.23). Fiber parameters, measured yarn parameters under the microscope along with the predicted and experimental values of yarn strength are shown in *Table 5.2* and *Table 5.3*. The individual results of the fibers tensile properties and fineness are presented in Appendix 7.

Table 5.2 Viscose and Tencel fiber properties.

Property	Viscose	Tencel
Fiber friction coefficient (-)	0.35	0.21
Fiber breaking elongation (%)	19.40	8.10
Fiber fineness (Tex)	0.13	0.13
Fiber breaking load (cN)	3.28	5.20
Fiber length utilization factor (-)	0.199	0.188

It is important to point out the disadvantage of the method used to calculate the wrapper ratio W . Firstly, the proposed method assumed equal core and wrapper fibers packing density while in fact it could be different as fiber orientation of each bundle is different. Secondly, while analyzing the longitudinal yarn view under SEM, due to the irregular nature of air jet yarn structure and the existence of irregular and wild

wraps, where the twists are inserted pneumatically rather than mechanically as in ring spun yarn, there is a variation in the measured values of wrapper fiber pitch, helix angle and the height of the core and wrapper bundle.

The obtained yarn structural parameters and calculations of wrapper ratio for one yarn are shown in Appendix 8. Results presented in *Table 5.3* show that the proposed model exhibited good agreement with the experimental results of yarn breaking load where the prediction error varies from (1.62-16.17%). The higher values of prediction error could be ascribed to the variation ($CV\%$) in the measured values of wrapper fiber helix angle ($CV\%=08-31\%$), the measured values of pitch ($CV\%=05-43\%$) and wrapper fiber ratio ($CV\%=09-42\%$).

By comparing the breaking load of 23 Tex Viscose (samples 04-08) and Tencel yarn (sample 15) in *Table 5.3*, the Tencel yarn is stronger than the Viscose yarn. The fiber length utilization factor of Viscose fiber shown in *Table 5.2* is greater than that for Tencel fibers, nevertheless, the fiber breaking load of Tencel (5.2 cN) is greater than Viscose fiber (3.28 cN). The influence of this difference surpasses the influence of the former difference which affects the core and wrapper fiber strength, σ_1 , σ_2 and σ_3 , and consequently the final yarn strength (Eldeeb, 2016). The method for calculating Viscose fiber length utilization factor is given in Appendix 9.

Table 5.3 Theoretical and experimental yarn results.

Sample	Actual yarn count (Tex)	Wrapper fiber ratio (%)	Yarn diameter (mm)	Average unstrained wrapper fiber helix angle (rad)	Average unstrained pitch (mm)	Yarn wraps per meter	Predicted yarn breaking load (cN)	Experimental yarn breaking load (cN)	Prediction error (%)
1	15.9	33.36 (19)	0.20	0.45 (23)	1.17 (42)	825	224.41	237.85	5.65
2	15.6	28.82 (42)	0.23	0.40 (31)	1.38 (40)	714	195.42	214.95	9.09

3	16.4	33.25 (18)	0.21	0.45 (19)	1.45 (18)	700	237.64	241.55	1.62
4	22.4	34.3 (21)	0.24	0.55 (13)	1.46 (34)	668	347.37	401.99	13.59
5	22.6	31.82 (27)	0.23	0.53 (18)	1.29 (43)	698	329.07	370.19	11.11
6	22.6	32.85 (28)	0.28	0.51 (22)	1.56 (38)	635	323.97	372.39	13.00
7	22.7	37.01 (20)	0.25	0.54 (16)	1.34 (29)	658	366.74	377.68	2.89
8	22.4	37.74 (15)	0.25	0.55 (15)	1.34 (30)	685	366.83	404.85	9.39
9	29.4	37.14 (18)	0.27	0.59 (17)	1.45 (35)	629	490.97	552.92	11.20
10	29.4	39.42 (9)	0.29	0.61 (18)	1.64 (24)	562	525.39	551.58	4.75
11	29.5	35.96 (18)	0.29	0.62 (19)	1.74 (22)	545	502.52	522.89	3.89
12	29.4	36.4 (21)	0.27	0.64 (10)	1.45 (37)	619	502.49	562.38	10.65
13	20	35.92 (25)	0.23	0.47 (20)	1.05 (15)	692	303.13	361.60	16.17
14	25	37.36 (21)	0.28	0.56 (16)	1.24 (5)	634	404.79	453.21	10.68
15	22.6	34.56 (18)	0.25	0.66 (8)	1.26 (24)	515	566.97	612.53	7.43

* The values in brackets indicate the coefficient of variation (*CV%*) of the measured parameter.

6. Prediction of Air Jet Yarn Strength at Different Gauge Lengths Based on Statistical Modeling

In this chapter, step by step derivation of a statistical model that predicts air jet yarn strength at different gauge length has been presented. The model has been derived by Neckář B. et al. (Neckar B. and Das D., 2016) in which, the yarn strength, as well as its coefficient of variation at different gauge length, are being calculated. Moreover, the model has been validated by Eldeeb M. et al. (Eldeeb & Neckář, 2017).

6.1 Yarn strength in relation to gauge length

The current model uses the same assumptions of Peirce model which implies that the principle of weakest link theory is valid and the probability that one short part of yarn breaks is independent to the probabilities of breakage of all other short parts, i.e., the probability of breakage of all short parts is mutually independent. But unlike Peirce model, it is assumed that the yarn strength p (cN) at a short gauge length l_o (mm) follows the Weibull distribution (Neckar B. and Das D., 2016). Let us assume a yarn is gripped between two jaws as shown in *Figure 6.1*. And let us assume that the function $F(p, L)$ is the probability that a yarn of a given length L (mm) breaks by a force p and this function is non-decreasing function because if the value of p is high, $F(p, L)$ value becomes high as well.

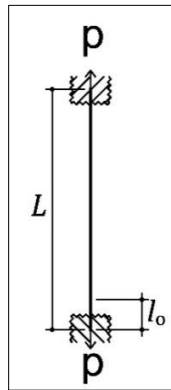


Figure 6.1 A yarn is gripped between the jaws of a tensile tester.

The probability of non-breaking of the long length L can be formulated as follows,

$$1 - F(p, L) = (1 - F(p, l_{o1})) * (1 - F(p, l_{o2})) \\ * \dots \dots \dots (1 - F(p, l_{on})) = (1 - F(p, l_o))^n \quad (6.1)$$

It can be said that,

$$1 - F(p, L) = (1 - F(p, l_o))^{L/l_o} \quad (6.2)$$

Where, $F(p, l_o)$ is the cumulative distribution function of yarn strength at gauge length l_o (i.e. the probability that a yarn with a given (short) gauge length l_o breaks by a force p). Since $F(p, L)$ is a non-decreasing function ranges from $F(p \leq p_{min}, L) = 0$ to $F(p \geq p_{max}, L) = 1$, so, $1 - F(p, L)$ is non-increasing function ranges from $1 - F(p \leq p_{min}, L) = 1$ to $1 - F(p \geq p_{max}, L) = 0$. In addition, equation (6.2) is a function of p only. Thus, let us introduce the risk function $R(p)$ in the way that,

$$(1 - F(p, L))^{1/l_o} = e^{-R(p)}, \quad L > 0 \quad (6.3)$$

Hence,

$$(1 - F(p, L))^{L/l_o} = e^{-LR(p)}, \quad L > 0 \quad (6.4)$$

And,

$$R(p) = \left(\frac{p - p_{min}}{Q} \right)^c \quad (6.5)$$

Where $R(p) \in (0, \infty)$, $p_{min} \geq 0$, $Q \geq 0$ and $c \neq 0$ are constants for a yarn. Then the cumulative distribution function can be formulated by using equation (6.4) and (6.5),

$$F(p, L) = 1 - e^{-L \left(\frac{p - p_{min}}{Q} \right)^c} \quad (6.6)$$

The unit of p_{min} and p is (cN) and the unit of Q is $(cN \cdot m^{1/c})$, consequently, the cumulative distribution function is a dimensionless unit. Let us assume a parameter of gauge length q where,

$$q = \frac{Q}{L^{1/c}} \quad (6.7)$$

Furthermore, the probability density function $f(p, L)$ is the differentiation of the cumulative distribution function $F(p, L)$, therefore, by differentiating equation (6.6) in respect to p ,

$$f(p, L) = e^{-L} \frac{Lc}{Q} \left(\frac{p - p_{min}}{Q} \right)^c \left(\frac{p - p_{min}}{Q} \right)^{c-1} \quad (6.8)$$

From equation (6.7) and (6.8),

$$f(p, L) = \frac{c}{q} \left(\frac{p - p_{min}}{q} \right)^{c-1} e^{-\left(\frac{p - p_{min}}{q} \right)^c} \quad (6.9)$$

Equation (6.9) characterizes the distribution of random variable p by the parameters p_{min} , q and c which can be expressed by 3-parameters Weibull distribution. Where p_{min} represents location, c is shape and q is scale. The variable p also can be transformed in the way that,

$$u = \left(\frac{p - p_{min}}{q} \right)^c, u \in (0, \infty) \quad (6.10)$$

The random variable p can be calculated using equation (6.10),

$$p = qu^{1/c} + p_{min} \quad (6.11)$$

By differentiating equation (6.11),

$$dp = \frac{q}{c} u^{\frac{1}{c}-1} du \quad (6.12)$$

In Peirce model, the probability density function for the transformed value u was obtained assuming a Gaussian distribution. This distribution can't fit the data at all cases of gauge length. On the other hand, the Weibull distribution is one of the most widely used distribution in survival and life time analyses because of its flexibility and versatility among other distributions by changing the value of its shape parameter. Therefore, in the present model, the 3-parameter Weibull distribution was assumed which could be valid at most of the cases, hence, giving better accuracy (Eldeeb & Neckář, 2017).

6.1.1 Calculating the mean yarn strength

The m^{th} non-central statistical moment can be calculated as follows,

$$\overline{p^m} = \int_{p_{min}}^{\infty} p^m f(p, L) dp \quad (6.13)$$

From equation (6.9) and (6.13),

$$\overline{p^m} = \int_{p_{min}}^{\infty} p^m \frac{c}{q} \left(\frac{p - p_{min}}{q} \right)^{c-1} e^{-\left(\frac{p - p_{min}}{q} \right)^c} dp \quad (6.14)$$

Substituting equations (6.10), (6.11), (6.12) in equation (6.14),

$$\overline{p^m} = \int_{p_{min}}^{\infty} \left(qu^{\frac{1}{c}} + p_{min} \right)^m e^{-u} du \quad (6.15)$$

And using the binomial theorem yields,

$$\overline{p^m} = \sum_{i=0}^m \left(\binom{m}{i} q^{m-i} p_{min}^i (1)^i \int_0^{\infty} u^{\frac{m-i}{c}} e^{-u} du \right) \quad (6.16)$$

As Gamma function $\Gamma x = \int_0^{\infty} u^{x-1} e^{-u} du$, Therefore,

$$\Gamma(x+1) = \int_0^{\infty} u^x e^{-u} du \quad (6.17)$$

By substituting equation (6.17) in (6.16),

$$\overline{p^m} = \sum_{i=0}^m \left(\binom{m}{i} q^{m-i} p_{min}^i \Gamma\left(\frac{m-i}{c} + 1\right) \right), m = 1, 2, \dots \quad (6.18)$$

Thus,

$$\begin{aligned} \overline{p^1} &= \binom{1}{0} (+1)^0 q^{1-0} p_{min}^0 \Gamma\left(\frac{1-0}{c} + 1\right) \\ &\quad + \binom{1}{1} (+1)^1 q^{1-1} p_{min}^1 \Gamma\left(\frac{1-1}{c} + 1\right) \end{aligned} \quad (6.19)$$

Finally, the mean value of yarn strength $\overline{p^1}$ can be obtained,

$$\overline{p^1} = q \Gamma\left(\frac{1}{c} + 1\right) + p_{min} \quad (6.20)$$

As $\Gamma(x+1) = x\Gamma x$, hence,

$$\overline{p^1} = \frac{q}{c} \Gamma \frac{1}{c} + p_{min} \quad (6.21)$$

Based on equation (6.7) and (6.21), the mean yarn strength (cN) can be expressed also as follows,

$$\overline{p^1} = \frac{QL^{-1/c}}{c} \Gamma \frac{1}{c} + p_{min} \quad (6.22)$$

6.1.2 Calculating the standard deviation of yarn strength

Assume that $\omega(u)$ is the probability density function of the transferred value u , therefore it is valid that,

$$\omega(u)du = f(p, L)dp \quad (6.23)$$

Using equations (6.9), (6.10), (6.12) and (6.23), the probability density function can be obtained,

$$\omega(u)du = e^{-u}du \quad (6.24)$$

Analogically, the non-central moments of the transferred value u is,

$$\overline{u^x} = \int_0^\infty u^x e^{-u} du \quad (6.25)$$

From equation (6.24) and (6.25),

$$\overline{u^x} = \int_0^\infty u^x \omega(u) du \quad (6.26)$$

Also, from equation (6.17) and (6.25),

$$\overline{u^x} = \Gamma(x + 1) \quad (6.27)$$

And the m^{th} central moment of yarn strength $\overline{(p - \bar{p}_l)^m}$ can be calculated using equation (6.11) and applying the expectation operator E of mean value as follows,

$$(p - \bar{p}_l)^m = E\{(p - \bar{p}_l)^m\} \quad (6.28)$$

By using equation (6.21),

$$(p - \bar{p}_l)^m = E\left(\left(qu^{1/c} + p_{\min}\right) - \left(q\overline{u^{\frac{1}{c}}} + p_{\min}\right)\right)^m \quad (6.29)$$

That is,

$$(p - \bar{p}_l)^m = q^m E\left(u^{1/c} - \overline{u^{\frac{1}{c}}}\right)^m \quad (6.30)$$

And using the binomial theorem yields,

$$(p - \bar{p}_l)^m = q^m E\left(\sum_{j=0}^m \left((-1)^j \binom{m}{j} u^{\frac{m-j}{c}} \left(\overline{u^{\frac{1}{c}}}\right)^j\right)\right) \quad (6.31)$$

And,

$$(p - \bar{p}_l)^m = q^m \left(\sum_{j=0}^m \left((-1)^j \binom{m}{j} \left(u^{\frac{m-j}{c}}\right) \left(\overline{u^{\frac{1}{c}}}\right)^j\right)\right) \quad (6.32)$$

Using the same logic in equation (6.27),

$$(p - \bar{p}_l)^m = q^m \left(\sum_{j=0}^m \left((-1)^j \binom{m}{j} \Gamma\left(\frac{m-j}{c}\right) + 1\right) \left(\overline{u^{\frac{1}{c}}}\right)^j\right) \quad (6.33)$$

The dispersion σ^2 , which is the 2nd central moment of yarn strength can be obtained,

$$(p - \bar{p}_l)^2 = q^2 \left(\sum_{j=0}^2 \left((-1)^j \binom{m}{j} \Gamma \left(\frac{m-j}{c} + 1 \right) \left(\Gamma \left(\frac{1}{c} + 1 \right) \right)^j \right) \right) \quad (6.34)$$

Intuitively,

$$\begin{aligned} \sigma^2 = q^2 & \left(\binom{2}{0} \Gamma \left(\frac{2-0}{c} + 1 \right) \Gamma \left(\frac{1}{c} + 1 \right)^0 (-1)^0 \right. \\ & + \binom{2}{1} \Gamma \left(\frac{2-1}{c} + 1 \right) \Gamma \left(\frac{1}{c} + 1 \right)^1 (-1)^1 \\ & \left. + \binom{2}{2} \Gamma \left(\frac{2-2}{c} + 1 \right) \Gamma \left(\frac{1}{c} + 1 \right)^2 (-1)^2 \right) \end{aligned} \quad (6.35)$$

And finally, the standard deviation of yarn strength can be calculated,

$$\sigma = q \sqrt{\frac{2}{c} \Gamma \frac{2}{c} - \frac{1}{c^2} \Gamma^2 \frac{1}{c}} \quad (6.36)$$

6.1.3 Calculating the coefficient of variation of yarn strength

Using the values of σ and p from equation (6.21) and (6.36), the coefficient of variation of yarn strength CV (%) can be obtained.

$$CV = \frac{\sigma}{p^1} = \frac{\sqrt{\frac{2}{c} \Gamma \frac{2}{c} - \frac{1}{c^2} \Gamma^2 \frac{1}{c}}}{\frac{1}{c} \Gamma \frac{1}{c} + \frac{p_{min}}{q}} \quad (6.37)$$

The CV can be expressed by Q parameter using equation (6.7),

$$CV = \frac{\sqrt{\frac{2}{c} \Gamma \frac{2}{c} - \frac{1}{c^2} \Gamma^2 \frac{1}{c}}}{\frac{1}{c} \Gamma \frac{1}{c} + \frac{p_{min}}{QL^{-1/c}}} \quad (6.38)$$

6.1.4 Mathematical model validation

100% Tencel fibers of 1.3 dtex and 38 mm were spun to produce 23 Tex ring, rotor and air jet spun yarns. After carding process, 4.6 ktex sliver was drawn twice to spin

rotor and ring yarns while it was drawn thrice to spin air jet yarn in order to enhance fiber orientation and sliver evenness. Instron 4411 was used to measure yarn tensile properties at different gauge lengths namely, 60, 100, 200, 300, 400, 500, 600 and 700 mm. 75 readings were taken for each yarn sample.

The structure of rotor and air jet spun yarns was investigated by analyzing the longitudinal view of these yarns using optical microscope according to the standard test method (*Recommended procedure for preparation of samples. Soft and hard sections (slices). Internal standard no. 46-108-01/01, Faculty of Textile, Technical University of Liberec, 2004*).

To examine the yarn cross-section, the yarn impregnation process was carried out in three steps of immersing the yarn into different solutions and drying it for 24 hours in the standard atmosphere after each immersion step. In the first step the solution consisted of a powerful soaking agent Spolion 8 (Sodium dialkylsulphoxanthane at concentration 5 g/l), in the second step the solution consisted of a mixture of the soaking agent and Gama Fix Henkel glue in 1:1 ratio, and in the third step the solution consisted of glue only. Afterward, a warm mixture of bee's wax and paraffin (ratio 2:3) was poured into a tub containing the sample. After cooling of the wax in the tub, the sample was placed in a freezer at -18°C for 24 hours for hardening then the hardened block was clamped to the Microtome. The thickness of the section (slice) was set to 15 µm. A drop of Xylene was applied on the slices to dissolve the wax (*Recommended procedure for preparation of samples. Soft and hard sections (slices). Internal standard no. 46-108-01/01, Faculty of Textile, Technical University of Liberec, 2004*). Then the sections were examined under the microscope.

To validate the model, the values of yarn strength at 300 mm gauge length were obtained and the Weibull distribution along with its 3-parameters, p_{min} , c and q were obtained using the modified weighed least square estimators method (Ahmad, 1994). Then the Weibull distribution was obtained using the following equation,

$$f(t) = \frac{c}{q} \left(\frac{t - p_{min}}{q} \right)^{c-1} e^{-\left(\frac{t - p_{min}}{q} \right)^c} \quad (6.39)$$

Afterward, the parameter Q was calculated using equation (6.7), then yarn tenacity, $\overline{p^1}$ and coefficient of variation of yarn strength, CV were obtained at each gauge length by using equation (6.22) and (6.38).

6.2 Results of the model

6.2.1 Yarn strength

To understand the behavior of the probability density function of the linearly transformed yarn strength as defined according to Peirce model (Peirce, 1926), it was calculated at different values of L/l_o . It can be seen from *Figure 6.2* that with the increase of gauge length, i.e. an increase of L/l_o , yarn strength decreases including its mean value, strength variability decreases where the area under the curve decreases and asymmetry of this function slightly increases. This is usually characterized by high values of kurtosis and skewness. Also, it is clear that, the distribution shape changes at different gauge lengths and it follows the Gaussian distribution approximately only at L equal to l_o .

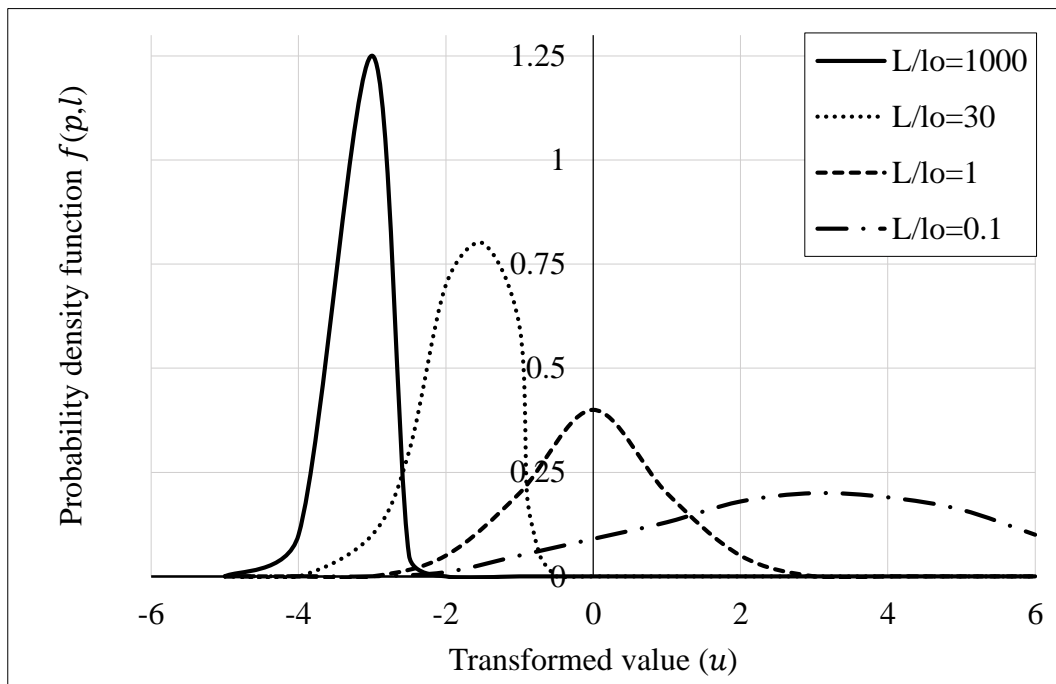
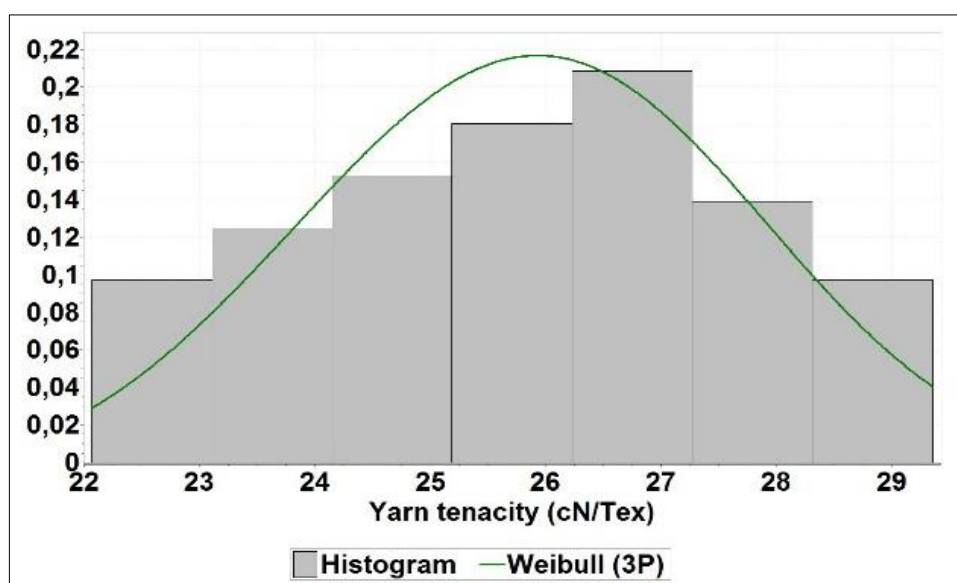


Figure 6.2 Probability density function of the linearly transformed yarn strength.

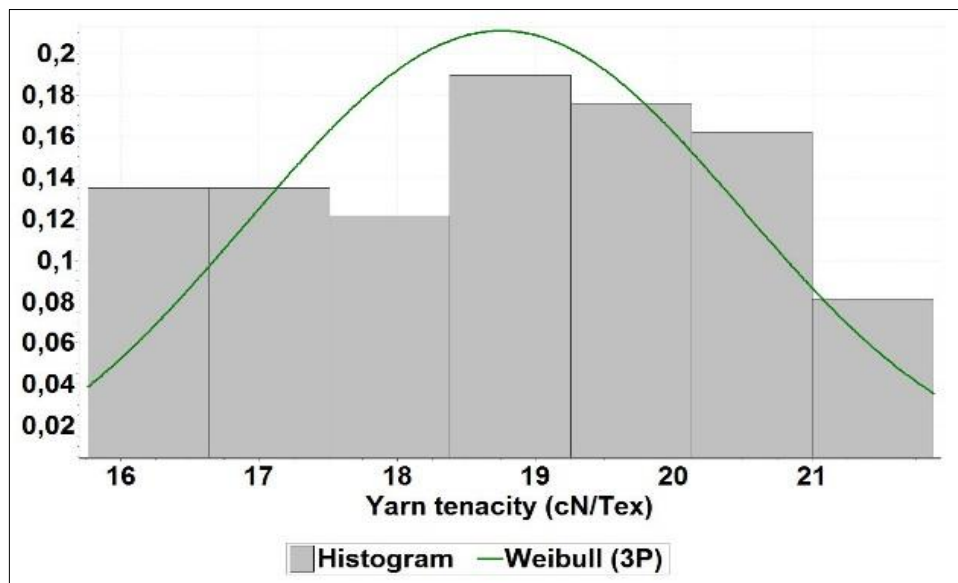
Figure 6.3 shows the histogram and the equivalent 3-parameter Weibull distribution for yarn tenacity measured at 300 mm gauge length. It is important to point out that the proposed model, as well as Peirce model, are not valid at short gauge lengths less than fiber length. That is because the theory is based on the probability that the fibers are gripped only at the upper tensile tester jaw, at the lower tensile tester jaw or not gripped by any jaw but located in-between jaws.

The values of p_{min} , c and q for each yarn were obtained and used for predicting yarn strength and its coefficient of variation. It is clear that the Weibull distribution fit well the yarn strength values at 300 mm gauge length. By observing Figure 6.3-b, it is obvious that the irregular nature and the variability in rotor yarn structure causes difficulty in obtaining the Weibull distribution accurately. Hence, another distribution could be hypothesized and investigated that may be able to fit better the data including the rotor yarn data. But this necessitates to change completely the proposed statistical model accordingly.

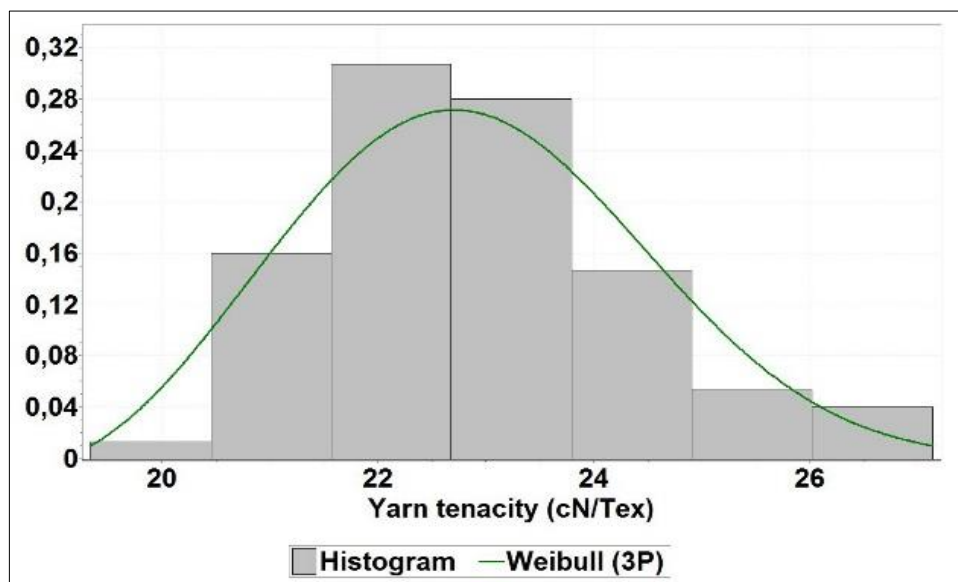
Figure 6.4 shows the theoretical and experimental values of yarn strength at different gauge lengths. Appendix 10 shows the experimental values of tenacity for the ring, rotor and air jet Tencel yarns at different gauge lengths. It is evident that the predicted



(a)



(b)



(c)

Figure 6.3 The probability density function of yarn tenacity at 300 mm gauge length; (a) ring, (b) rotor, (c) air jet.

and experimental strength values are in a good agreement for all tested spun yarns. It can be observed also that the ring spun yarn tenacity is the strongest yarn followed by the air jet yarn then rotor yarn.

The high tenacity of ring spun yarn is attributed to the uniform twist which improves fiber gripping, interlocking and migration characteristics (Huh, Kim, & Oxenham,

2002). *Figure 6.5* shows the twist distribution through the cross-section of yarns produced on different spinning systems. In ring spinning, fibers are more straightened and parallelly arranged in thin strand before they are twisted. Owing to twist, all or some of fibers take the required helical position in the yarn and twisting takes place from the outside inwards.

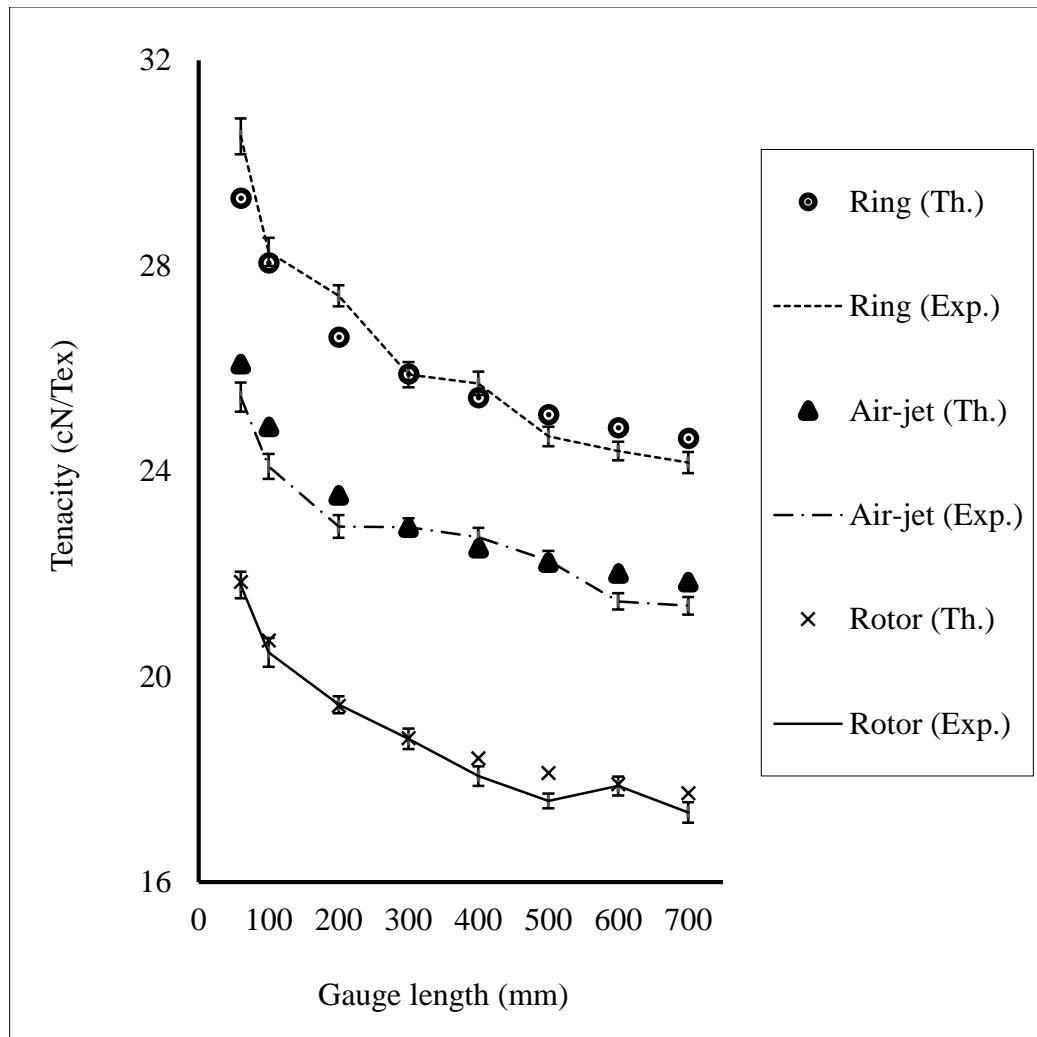


Figure 6.4 Theoretical and experimental values of yarn strength at different gauge lengths.

By comparing the twist distribution shown in *Figure 6.5* and both air jet and rotor yarns longitudinal and cross-sectional view shown in *Figure 6.6*, and in case of the rotor yarn, the thin strand of fibers (before twisting) has hooked ends as well as fibers migration is high, therefore, the fiber length is not fully utilized. Twisting during rotor spinning takes place from the outside inwards. The core fibers are in a helical form

but less parallel, in the sheath, fibers are arranged randomly (Klein, 1987). Fibers are not parallelly arranged as well as they are not so straightened. Hence, utilization of fiber strength in yarn strength is low and the yarn has lower strength. Furthermore, during spinning, new fibers are brought to the point of yarn formation and fully covered it to be joined by the yarn and twisted onto its surface. The position of such fibers on the yarn surface is random, providing an uneven appearance (Rohlena, 1975).

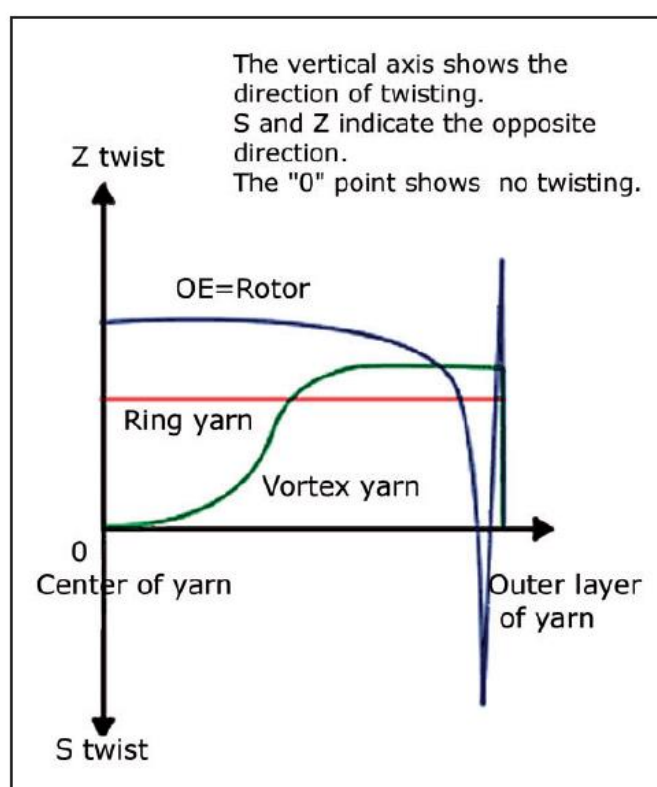


Figure 6.5 Twist distribution through the cross-section of yarns produced on different spinning systems. (N. Erdumlu, Ozipek, Oztuna, & Cetinkaya, 2009)

In case of the air jet yarn, the structure consists of two layers – a core bundle without twist, in which fibers are arranged parallel to the yarn axis, and the wrapping layer, which is twisted around the core. Fibers in wrapping layer are formed so that the top end of fibers converges to the center of the yarn while the trailing end together with other fibers wrap the core due to swirling air (*Murata Machinery Ltd. Vortex yarn guide book*, Retrieved 08 24, 2005, Web site: <http://www.muratec-vortex.com>, 2005).

Also observing the cross-sectional view shown in *Figure 6.6*, it is clear that in rotor yarns, wrapper fibers are irregularly wrapped around the core fibers with varying angles and some of them can be seen forming an angle of 90° taking the belt shape, while in air jet yarns, wrapping effect is much regular and wrapper fibers are identifiable forming a cap-like shape. These differences in structure make air jet yarn strength superior to rotor yarns.

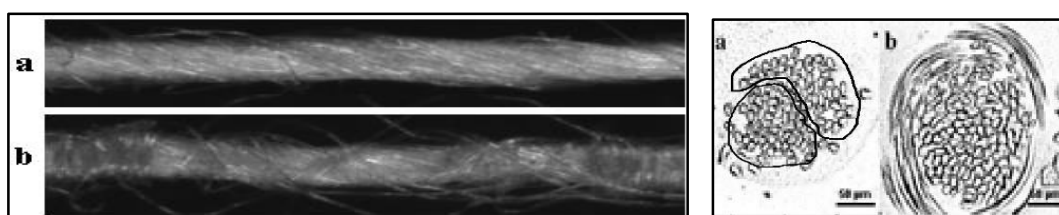


Figure 6.6 Longitudinal and cross-sectional view of yarns; (a) air jet, (b) rotor.

It is also noted from *Figure 6.4*, that the strength of all yarns decreases with increasing gauge length from 60 mm to 700 mm and this is because the probability of the existence of weak links in yarn structure is greater at higher gauge length as explained by the weak link theory (Peirce, 1926). At long gauge length, yarn thin places more likely exist which can't bear the tensile load. And most yarn failures take place when there is a sudden reduction in yarn mass (Sinha & Kumar, 2013). On the other hand, the number of thin places and its distribution along the yarn differs from one spinning method to another because of the differences in the yarn structure, consequently, the tensile behavior of each yarn differs at different gauge length.

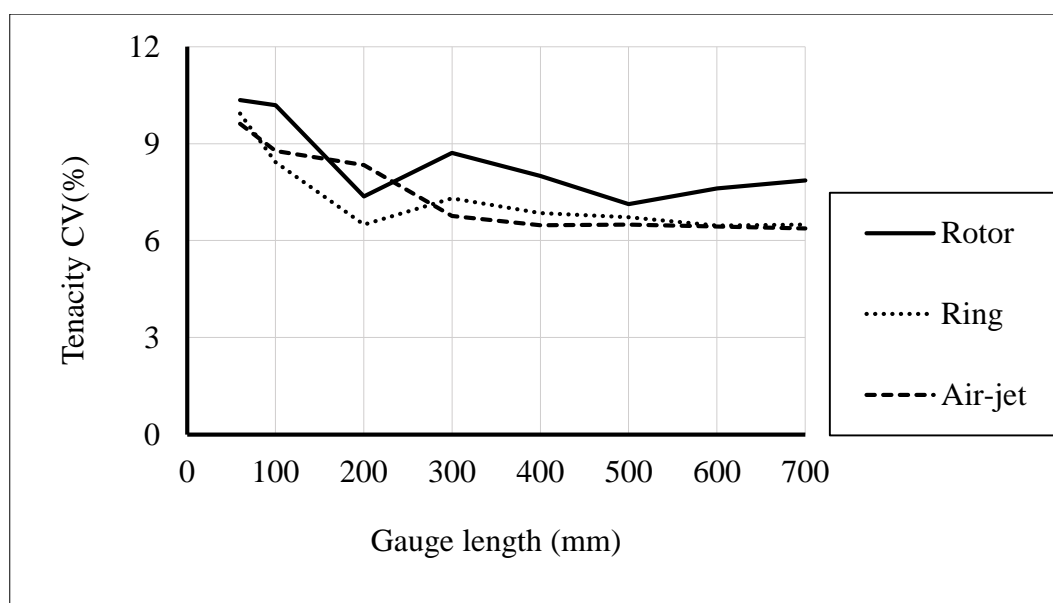
6.2.2 Coefficient of variation of yarn strength

The experimental and predicted relationship between the coefficient of variation of yarn tenacity ($CV\%$ tenacity) and gauge length is presented in *Figure 6.7*. It is observed from *Figure 6.7-a* that $CV\%$ tenacity of rotor yarn is the highest, followed by the air jet yarn and ring yarn at most gauge lengths. In the past, $CV\%$ tenacity as well as $CV\%$ mass of open end rotor spun yarns were low compared to ring spun yarns because low rotor speed along with high rotor diameter were used. Recently, high rotor speed (about 100,000 rpm) along with low rotor diameter are being used for

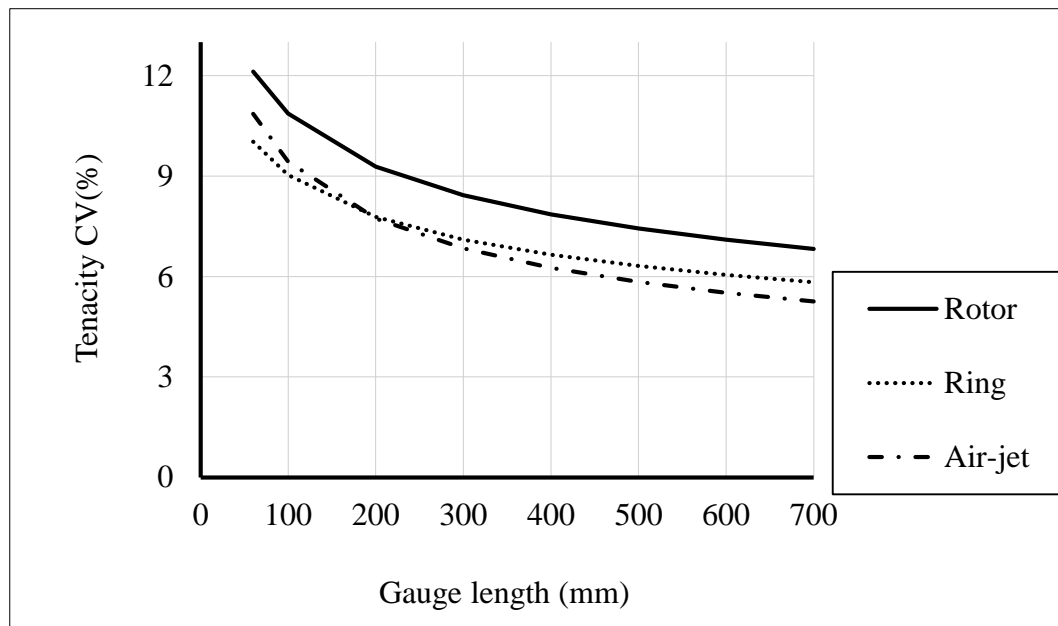
rotor yarn production which results in high $CV\%$ mass and $CV\%$ tenacity of rotor-spun yarns compared to ring spun yarns.

It is also clear that $CV\%$ tenacity for all yarns is higher at shorter gauge length. The observed higher coefficient of variation in tenacity might be attributed to the higher variation of yarn mass at shorter gauge length which is related to the role of random distribution of fibers in yarn cross-section. Theoretical results shown in *Figure 6.7-b* indicate that the reduction in coefficient of variation is the highest in case of air jet yarns (approximately 51.6%). At shorter gauge length, the air jet yarn has variability in its internal structure (classes of irregular wraps and unwrapped core fibers and such classes negatively influences the yarn irregularity). This variance clearly decreases at longer gauge length.

Figure 6.8 reveals the correlation between the experimental and theoretical $CV\%$ tenacity. Results reveal that the proposed model captured well the change in $CV\%$ tenacity over different gauge lengths for all tested yarns. The R-squared value is the highest in case of air jet yarn followed by ring spun yarn, then rotor yarn. The low R-squared value of rotor yarns may be explained by their high experimental values of $CV\%$ tenacity (08-11%) as well as the irregular nature of rotor yarn structure.



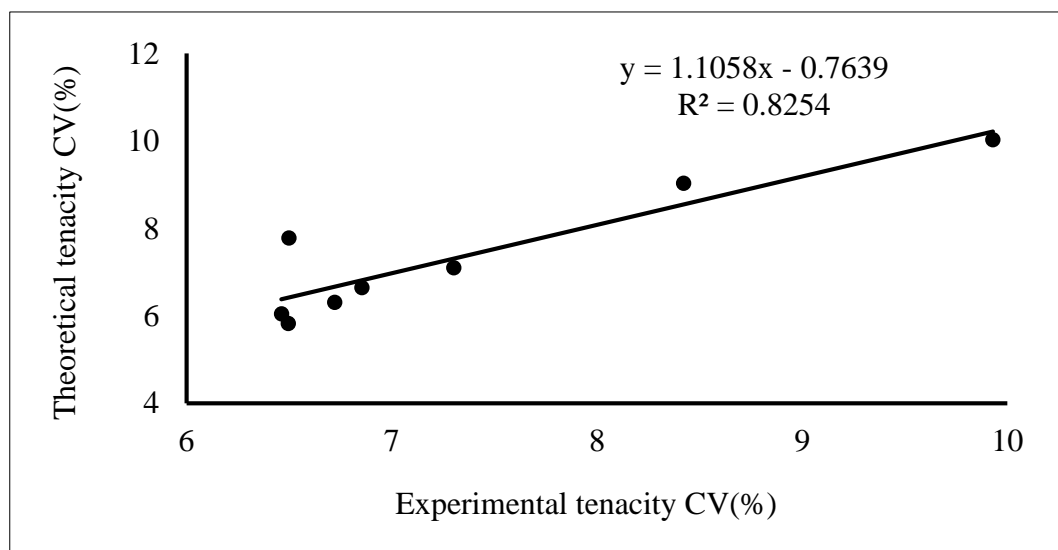
(a)



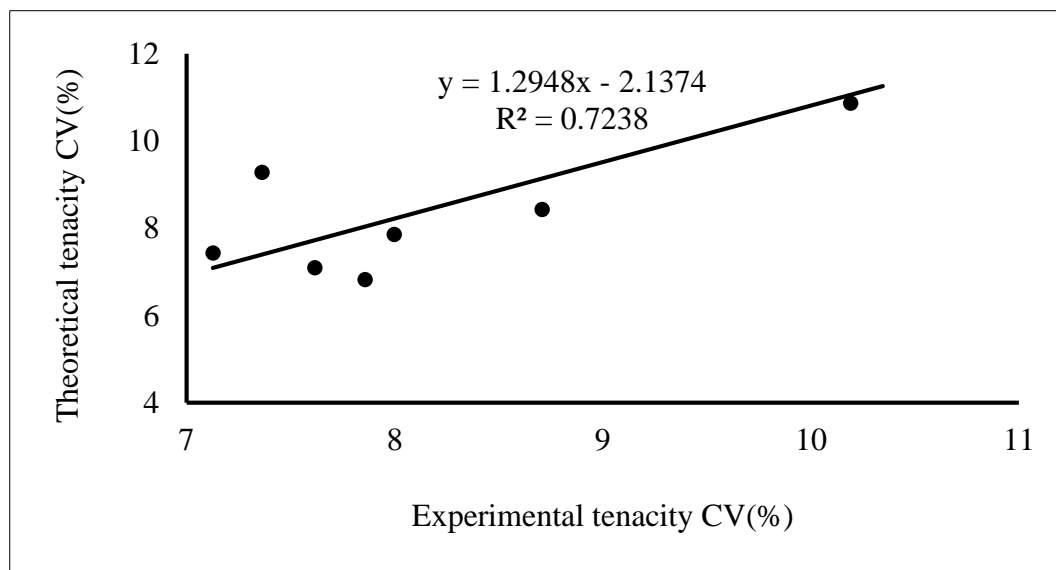
(b)

Figure 6.7 Coefficient of variation of yarn strength at different gauge lengths; (a) experimental, (b) theoretical.

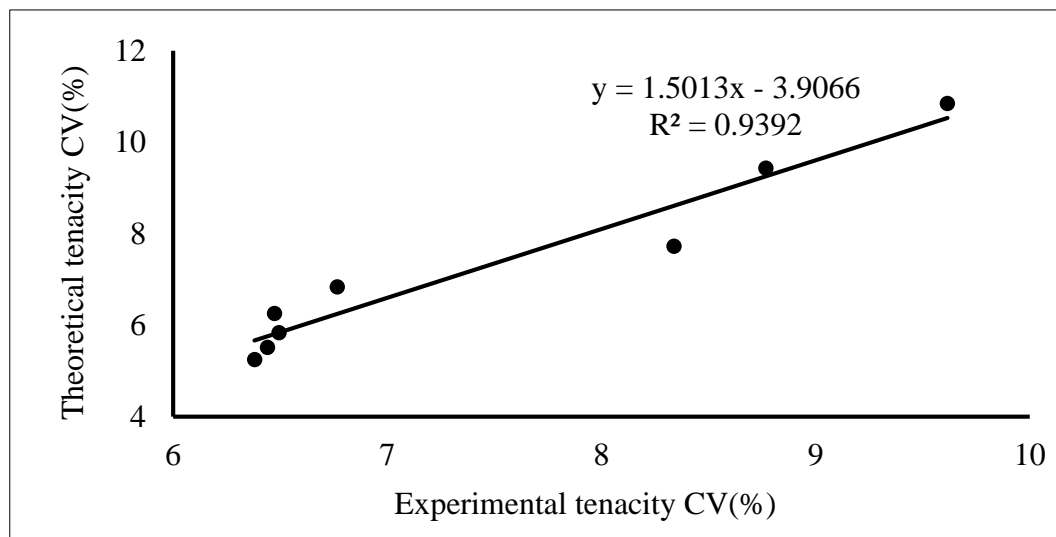
However, generally, the difference between experimental and theoretical values of coefficient of variation is attributed to the assumption that the probability of breakage of all short yarn segments is mutually independent. Another model that hypothesizes the dependency of each segment on the adjacent segments may be developed to obtain more precise results.



(a)



(b)



(c)

Figure 6.8 Experimental versus calculated results of coefficient of variation of yarn strength at different gauge lengths; (a) ring, (b) rotor, (c) air jet.

7. Conclusions and Recommendations

This thesis contributed to the knowledge of the air jet yarn formation process, particularly Rieter air jet spinning technology by investigating the influence of selected technological parameters of the spinning machine on yarn properties, especially its strength. Furthermore, it shed light on the problem of the prediction of yarn strength by trying different approaches to establish models that can be used for prediction of air jet spun yarns strength.

7.1 Summary and conclusions

In the first part, a 3D simulation process was carried out to study the principle of yarn formation of the Rieter air jet spinning machine. The following conclusions can be drawn.

- The air stream is ejected from the 4 jet orifices at a high speed. This speed decreases when it reaches the vortex chamber. As a result, a swirling airflow is generated in a thin layer near the vortex chamber wall.
- This airflow whirls inside the nozzle and move downstream and finally is expelled from the nozzle outlet. In the twisting passage, a suction airflow is created and flows into the vortex chamber enabling the drafted fiber strand to enter the nozzle.
- Another airflow is created inside the hollow spindle and flows from the hollow spindle outlet upstream to the vortex chamber and this can help in controlling the trailing ends of the spun yarn.
- These two mentioned airflows meet and become a single airflow. At this stage, the velocity of the airflow reduced near the nozzle inlet and near the hollow spindle inlet.
- Because of the specific geometry of the Rieter nozzle, the fiber strand is not sucked uniformly at the nozzle inlet where fibers strand enters the nozzle inclined to the nozzle axis so a certain number of fibers are separated from the main fiber strand and do not expose to the false twist. These fiber ends are then twisted around the non-rotating yarn core at the entry of the hollow spindle by the action of the mentioned air vortex.

- Three velocity components exist which influence the air jet yarn quality; the axial velocity component that forces the fibers to move downstream towards the hollow spindle outlet; the tangential velocity component that causes the fibers trailing ends to rotate tangentially to the nozzle inner wall leading to fiber twisting, hence, yarn wrapping; and the radial velocity component that separates the fibers and affects the yarn compactness.
- The tangential velocity component has the maximum value, followed by the axial velocity, then the radial velocity and this is ascribed to a big inclination angle of the jet orifices to the nozzle axis.

Along with the theoretical study, an experimental investigation was carried out to study the effect of the nozzle pressure on yarn tenacity. The following conclusions can be drawn.

- It is clear that yarn tenacity increases when nozzle pressure increases from 4 to 5 bar, then tenacity decreases gradually when it reaches 6 bar. The structural analyses showed that when spinning using nozzle air pressure of 4, 5 and 6 bar, the corresponding wrapper fibers ratio is 30.7, 32.7 and 29.3% respectively, however, the coefficient of variation was quite high.
- The initial increase in air pressure (4 and 5 bar) increases the intensity of the above-mentioned reverse flow in the hollow spindle which contributes to the vortex creation, the tangential velocity in the region near the nozzle entrance increases gradually, the negative pressure in the area in the vicinity of the vortex chamber outlet increases and its area shifts towards outside. All these factors contribute to the fiber separation process and the regular twist. Consequently, the yarn structure has tight regular wrappings and more wrapped portions.
- On the other hand, When the pressure reaches 6 bar, it is obvious that the reverse flow reached the nozzle inlet which could obstruct the spinning process because its direction is opposite to the strand movement direction, the tangential velocity becomes very high, the tangential velocity in the region between the wall of the hollow spindle and the inner wall of the nozzle increases and its area enlarges. This can lead to turbulence in this zone. All these factors contribute to less fiber control and

obstruction of fibers movement influencing yarn formation process negatively. Consequently, the yarn structure contains wild fibers, irregular wrapping, and less wrapped portions (less wrapper ratio).

- The experimental findings agreed with the numerical simulation results.
- According to the numerical simulation results and the experimental results, the optimal nozzle pressure is 5 bar.

In the second part, the effect of yarn linear density, nozzle pressure and delivery speed on Rieter air jet spun yarn tenacity was investigated and a statistical model that predicts the yarn tenacity was presented. The following conclusions can be drawn.

- The linear density has the maximum effect on yarn tenacity where coarser yarns 30 Tex have higher tenacity by about 29% than finer yarns 16 Tex and this is due to the increase in the number of fibers in yarn cross-section, thus, the number of core and wrapper fibers in yarn cross-section that bear the load exerted on the yarn.
- Increasing the yarn delivery speed from 350 to 400 m/min results in increasing yarn tenacity, but when using high delivery speed of 450 m/min a deterioration in yarn tenacity occurs by about 3.5% and this is a consequent of the insufficient time for the whirling action to take place in the vortex chamber which could result in an increment of the number of wild fibers and the regions of unwrapped core fibers.
- Yarn tenacity increases when nozzle pressure increases from 4 to 5 bar, then decreases gradually when it reaches 6 bar and this is because the increase in air pressure initially causes tight regular wrappings and more wrapped portions of the yarn (more wrapper ratio), but higher air pressure creates irregular wrappings and increases the wild fibers (less wrapper ratio).
- For the investigated nozzle geometry, material, selected variables range and seeking the optimal machine setting, it is suggested to adjust delivery speed within the range of 350 to 400 m/min and nozzle pressure to 5 bar.
- The general trend of the influence of the studied parameters on Rieter air jet yarn tenacity was found similar to its corresponding MVS yarn.

- The response surface equations obtained by using multiple regression enabled the prediction of air jet yarn tenacity as well as the other yarn properties based on process parameters; yarn linear density, nozzle pressure, and delivery speed.

In the third part, a prediction of air jet spun yarn strength at short gauge length was presented. The following conclusions can be drawn.

- Based on fiber parameters, namely, friction coefficient, length, length distribution, breaking load, breaking elongation, fineness and air jet spun yarn structural parameters, namely, wrapper fiber helix angle, wrapper fiber ratio and number of warps per unit length, it is possible to predict air jet spun yarn strength at short gauge length using the presented model.
- The model calculated three components of strength; core strength as a parallel bundle of fibers, wrapper fibers pressure on core fibers and wrapper fiber strength.
- The proposed model exhibited good agreement with the experimental results of yarn breaking load where the prediction error varies from (1.62-16.17%) The higher values of prediction error could be ascribed to the variation in the measured values of wrapper fiber helix angle (CV%=08-31%), the measured values of pitch (CV%=05-43%) and the wrapper fibers ratio (CV%=09-42%).

The results obtained from the theoretical model confirmed the following known facts.

- Yarn strength improves significantly with the increase of interfiber friction coefficient. Because the increase in friction reduces the slippage in the wrapper and core fibers, hence, increases the number of the wrapper and core fibers that resist load then break during the extension process.
- When spinning air jet yarn using coarser fibers, the ratio of core to wrapper fibers changes and the overall number of fibers in yarn cross-section decreases and yarn strength drops significantly.
- Yarn strength improves by increasing the wrapper ratio as this increases the total number of wrapper fibers that exert the normal forces on the core strand causing more frictional forces that resist the tensile load.

- When wraps per meter increase, yarn breaking load increases. However, unlike ring and rotor yarns, the strength of air jet yarn does not decrease significantly, but it levels off at high twist (wraps per meter). This is because approximately 70% of the yarn structure is untwisted core fibers.

In the fourth part, a new statistical model based on Peirce model was validated which is capable of capturing the change of ring, rotor, and air jet yarn strength and its coefficient of variation at different gauge lengths. The following conclusions can be drawn.

- The probability density function of the linearly transformed yarn strength as defined according to Peirce model was calculated at different gauge lengths. When the gauge length increases, yarn strength decreases including its mean value, strength variability decreases where the area under the curve decreases and asymmetry of this function slightly increases. Also, the distribution shape changes at different gauge lengths and it follows the Gaussian distribution approximately only at short gauge length.
- Weibull distribution fit well the yarn strength values at 300 mm gauge length. However, the irregular nature and the variability in rotor yarn structure causes difficulty in obtaining the Weibull distribution accurately.
- At all gauge lengths, the ring spun yarn tenacity is the strongest yarn followed by the air jet yarn then the rotor yarn. This is attributed to the uniform twist exists in ring spun yarn, which improves fiber gripping, interlocking and migration characteristics.
- The strength of all yarns decreases with increasing gauge length from 60 mm to 700 mm and this is because the probability of the existence of weak links in yarn structure is greater at higher gauge length as explained by the weak link theory. At long gauge lengths, fiber discontinuity exists, also yarn thin places more likely exist which can't bear the tensile load. And most yarn failures take place when there is a sudden reduction in yarn mass. On the other hand, the number of thin places and its distribution along the yarn differs from one spinning method to another because of the differences in yarn structure, consequently, the tensile behavior of each yarn differs at different gauge length.

- The predicted and experimental strength values are in a good agreement for all tested spun yarns.
- The $CV\%$ tenacity of rotor yarn is the highest, followed by the air jet yarn and ring yarn at most gauge lengths. It is also clear that $CV\%$ tenacity for all yarns is higher at shorter gauge length. The observed higher coefficient of variation in tenacity might be attributed to the higher variation of yarn mass at shorter gauge length which is related to the role of random distribution of fibers in yarn cross-section.
- At long gauge length, theoretical results indicate that the reduction in the coefficient of variation is the highest in case of air jet yarns (approximately 51.6%). At shorter gauge length, the air jet yarn has variability in its internal structure (classes of irregular wraps and unwrapped core fibers and such classes negatively influences the yarn irregularity). This variance clearly decreases at longer gauge length.
- The correlation between experimental and theoretical $CV\%$ tenacity is acceptable over different gauge lengths for all tested yarns and the R-squared value of the correlation between experimental and theoretical $CV\%$ tenacity is the highest in case of air jet yarn followed by ring spun, then rotor yarn. The low R-squared value of rotor yarns may be explained by their high experimental values of $CV\%$ tenacity (08-11%) as well as the irregular nature of rotor yarn structure.

7.2 Recommendations for future work

The following recommendations can be drawn.

- As far as the prediction of yarn strength using numerical simulation is concerned, the model is limited where it is not able to give a specific value for yarn strength, instead, it just predicts the change in the strength. Therefore, it is suggested to simulate the process using fibers along with the air flow.
- The mathematical model that predicts the air jet yarn strength at short gauge length may be developed to calculate the yarn strength at longer gauge length (500 mm) which is the most commonly used gauge length.
- It is important to point out the disadvantages of the used method which calculates the wrapper ratio W . Therefore, another method could be used to obtain less variance and more accurate results.

- The statistical model that predicts the air jet yarn strength at different gauge length assumed that the probability of breakage of all short yarn segments is mutually independent. Another model that hypothesizes the dependency of each segment on the adjacent segments may be developed to obtain more accurate results.

References

- Aggarwal, S. K. (1989). A model to estimate the breaking elongation of high twist ring spun cotton yarns, part I: derivation of the model for yarns from single cotton varieties. *Textile Research Journal*, 59(11), 691–695. <https://doi.org/10.1177/004051758905901112>
- Ahmad, K. E. (1994). Modified weighted least-squares estimators for the three-parameter Weibull distribution. *Applied Mathematics Letters*, 7(5), 53–56. [https://doi.org/10.1016/0893-9659\(94\)90072-8](https://doi.org/10.1016/0893-9659(94)90072-8)
- ASTM D1425, *Standard test method for evenness of textile strands using capacitance testing equipment*. (2009).
- ASTM D2256 - 10(2015), *Standard test method for tensile properties of yarns by the single-strand method*. (2015).
- ASTM D 1447, *Standard test method for length and length uniformity of cotton fibers by photoelectric measurement*. (2012).
- Basal, G. (2003). The structure and properties of vortex and compact spun yarns.
- Basal, G. (2006). Effects of some process parameters on the structure and properties of vortex spun yarn. *Textile Research Journal*, 76(6), 492–499. <https://doi.org/10.1177/0040517506064253>
- Basu, A. (1999). Progress in air-jet spinning. *Textile Progress*, 29(3), 1–38.
- Bhortakke, M. K., Nishimura, T., & Matsuo, T. (1999). The structure of polyester/cotton blended air-jet spun yarn. *Textile Research Journal*, 69(2), 84–89. <https://doi.org/10.1177/004051759906900202>
- Bogdan, J. F. (1956). The characterization of spinning quality. *Textile Research Journal*, 26(9), 720–730.
- Chasmawala, R. J., Hansen, S. M., & Jayaraman, S. (1990). Structure and properties of air-jet spun yarns. *Textile Research Journal*, 60(2), 61–69. <https://doi.org/10.1177/004051759006000201>
- Chu, C. C., Cummings, C. L., & Teixeira, N. A. (1950). Mechanics of elastic performance of textile materials, part V: a study of the factors affecting the drape of fabrics-the development of a drape meter. *Textile Research Journal*, 20(8), 539–548.

- Demir, A. (2009). *Technological status report on air-jet/vortex spinning process*. Istanbul.
- Eldeeb, M. (2016). Theoretical analyses of air jet yarn strength. In *21st Conference STRUTEX* (pp. 131–136). Liberec, ISBN 978-80-7494-269-3: Technical University in Liberec.
- Eldeeb, M., & Moučková, E. (2017). Numerical simulation of the yarn formation process in Rieter air jet spinning. *The Journal of The Textile Institute*, 108(7), 1219–1226.
- Eldeeb, M., & Neckář, B. (2017). Prediction of spun yarn strength at different gage lengths. *The Journal of The Textile Institute*, 1–6.
- Erdumlu, N., & Ozipek, B. (2010). Effect of the draft ratio on the properties of vortex spun yarn. *Fibres and Textiles in Eastern Europe*, 80(3), 38–42.
- Erdumlu, N., Ozipek, B., & Oxenham, W. (2012a). The structure and properties of carded cotton vortex yarns. *Textile Research Journal*, 82(7), 708–718. <https://doi.org/10.1177/0040517511433150>
- Erdumlu, N., Ozipek, B., & Oxenham, W. (2012b). Vortex spinning technology. *Textile Progress*, 44(3–4), 141–174. <https://doi.org/10.1080/00405167.2012.739345>
- Erdumlu, N., Ozipek, B., Oztuna, a. S., & Cetinkaya, S. (2009). Investigation of vortex spun yarn properties in comparison with conventional ring and open-end rotor spun yarns. *Textile Research Journal*, 79(7), 585–595. <https://doi.org/10.1177/0040517508093590>
- FLUENT. (2013). Theory guide. *Ansys Inc*, 5.
- Frydrych, I. (1992). A new approach for predicting strength properties of yarn. *Textile Research Journal*, 62(6), 340–348.
- Frydrych, I. (1995). Relation of single fiber and bundle strengths of cotton. *Textile Research Journal*, 65(9), 513–521.
- Ghosh, A., Ishtiaque, S. M., & Rengasamy, R. S. (2005). Analysis of spun yarn failure, part II: the translation of strength from fiber bundle to different spun yarns. *Textile Research Journal*, 75(10), 741–744.
- Ghosh, A., Ishtiaque, S. M., & Rengasamy, R. S. (2005). Stress–strain characteristics of different spun yarns as a function of strain rate and gauge length. *Journal of the Textile Institute*, 96(2), 99–104.
- Ghosh, A., Ishtiaque, S. M., Rengasamy, R. S., Mal, P., & Patnaik, A. (2004). Spun yarn strength as a function of gauge length and extension rate: a critical review. *Text*

- Apparel, Technol Management*, 4(2), 1–13.
- Ghosh, A., Ishtiaque, S., Rengasamy, S., Mal, P., & Patnaik, A. (2005). Predictive models for strength of spun yarns: an overview. *AUTEX Research Journal*, 5(1), 20–29.
- Ghosh, a. (2005). Analysis of spun yarn failure, part I: tensile failure of yarns as a function of structure and testing parameters. *Textile Research Journal*, 75(10), 731–740. <https://doi.org/10.1177/0040517505053956>
- Gordon, S. (2001). The effect of short fibre and nep levels on Murata vortex spinning efficiency and product quality. *Final Report To CanC, CSIRO Textile and Fibre Technology (2002/1)*, (October), 1–14.
- Grant, J. N., & Morlier, O. W. (1948). Relation of specific strength of cotton fibers to fiber length and testing method. *Textile Research Journal*, 18(8), 481–487.
- Guha, A., Chattopadhyay, R., & Jayadeva. (2001). Predicting yarn tenacity: a comparison of mechanistic, statistical, and neural network models. *Journal of the Textile Institute*, 92(2), 139–145.
- Günaydin, G. K., & Soydan, A. S. (2017). Vortex spinning system and vortex yarn structure. In *Vortex Structures in Fluid Dynamic Problems*. InTech.
- Guo, H., An, X., Yu, Z., & Yu, C. (2008). A numerical and experimental study on the effect of the cone angle of the spindle in Murata vortex spinning machine. *Journal of Fluids Engineering*, 130(3), 31106.
- Guo, H. F., Chen, Z. Y., & Yu, C. W. (2010). Numerical study on the effect of geometric parameters of the second nozzle in air-jet spinning. *The Journal of The Textile Institute*, 101(6), 575–582.
- Harris, J. W., & Stocker, H. (1998). Maximum likelihood method. *Handbook of Mathematics and Computational Science*, 1, 824.
- <http://www.rieter.com/cz/rikipedia/articles/alternative-spinning-systems/the-various-spinning-methods/air-jet-spinning/development/>. (2016).
- <http://www.textileworld.com/textile-world/features/2012/03/spinning-with-an-air-jet/>. (2016).
- Huh, Y., Kim, Y. R., & Oxenham, W. (2002). Analyzing structural and physical properties of ring, rotor, and friction spun yarns. *Textile Research Journal*, 72(2), 156. <https://doi.org/10.1177/004051750207200212>
- Huifen, G. U. O., Xianglong, A. N., & Chongwen, Y. U. (2007). Numerical study on the

- principle of yarn formation in Murata air-jet spinning. *Journal of Textile Engineering*, 53(5), 173–178.
- Hussain, G. F. S., Nachane, R. P., Krishna Iyer, K. R., & Srinathan, B. (1990). Weak-link effect on tensile properties of cotton yarns. *Textile Research Journal*, 60(2), 69–77. <https://doi.org/10.1177/004051759006000202>
- Ishtiaque, S. M., Salhotra, K. R., & Kumar, A. (2006). Analysis of spinning process using the Taguchi method, part II: effect of spinning process variables on fibre extent and fibre overlap in ring, rotor and air-jet yarns. *Journal of the Textile Institute*, 97(4), 285–294.
- ISO, E. N. (1995). 2062. Textiles–yarn from packages–determination of single end breaking force and elongation at break. *International Organization for Standardization*.
- ISO 1973:1995, *Textile fibres, determination of linear density, gravimetric method and vibroscope method*. (1995).
- J. Kapadia, D. F. (1935). ., 26, T142–T266.
- Jiang, X. Y., Hu, J. L., & Postle, R. (2002). A new tensile model for rotor spun yarns. *Textile Research Journal*, 72(10), 892–898. <https://doi.org/10.1177/004051750207201007>
- Johnson, W. M. (2002). The impact of MVS machine settings and finishing applications on yarn quality and knitted fabric hand. MSc Thesis, Institute of Textile Technology, Charlottesville, Virginia, USA.
- Klein, W. (1987). The technology of short staple spinning, in: manual of textile technology, short-staple spinning series. *The Textile Institute*.
- Krause, H. W., & Soliman, H. a. (1990). Theoretical study of the strength of single jet false twist spun yarns. *Textile Research Journal*, 60(6), 309–318. <https://doi.org/10.1177/004051759006000601>
- Kumar, A., Ishtiaque, S. M., & Salhotra, K. R. (2006). Analysis of spinning process using the Taguchi method, part III: effect of spinning process variables on migration parameters of ring, rotor and air-jet yarn. *Journal of the Textile Institute*, 97(5), 377–384.
- Kumar, A., Salhotra, K. R., & Ishtiaque, S. M. (2006). Analysis of spinning process using the Taguchi method, part V: effect of spinning process variables on physical

- properties of ring, rotor and air-jet yarns. *Journal of the Textile Institute*, 97(6), 463–473.
- Kumar, a., Ishtiaque, S. M., & Salhotra, K. R. (2006). Analysis of spinning process using the Taguchi method, part IV: effect of spinning process variables on tensile properties of ring, rotor and air-jet yarns. *Journal of the Textile Institute*, 97(5), 385–390. <https://doi.org/10.1533/joti.2006.0106>
- Lawrence, C. A. (2010). *Advances in yarn spinning technology*. Elsevier.
- Li, M., Yu, C., & Shang, S. (2013). A numerical and experimental study on the effect of the orifice angle of vortex tube in vortex spinning machine. *The Journal of The Textile Institute*, 104(12), 1303–1311.
- Łukaszewicz, G., & Kalita, P. (2016). Navier–Stokes Equations. <https://doi.org/10.1007/978-3-319-27760-8>
- Majumdar, P. K., & Majumdar, A. (2004). Predicting the breaking elongation of ring spun cotton yarns using mathematical, statistical, and artificial neural network models. *Textile Research Journal*, 74(7), 652–655.
- Muhammad Zubair, Bohuslav Neckar, Moaz Eldeeb, G. A. B. (2017). Tensile behavior of staple fiber yarns, part IV: experimental verification of predicted stress–strain curves. *The Journal of The Textile Institute*, 108(8), 1291–1296.
- Murata Machinery Ltd. *Vortex yarn guide book*, Retrieved 08 24, 2005, Web site: <http://www.muratec-vortex.com>. (2005).
- Neckar, B., & Das, D. (2003). A stochastic approach to yarn strength. In *Seventh Asian Textile Conference*.
- Neckář, B., & Das, D. (2017). Tensile behavior of staple fiber yarns, part I: theoretical models. *The Journal of The Textile Institute*, 108(6), 922–930.
- Neckar B. and Das D. (2016). *Theory of structure and mechanics of yarns*, Manuscript of the book. Technical University of Liberec.
- Ning, P. (1993). Development of a constitutive theory for short fiber yarns, part II: mechanics of staple yarn with slippage effect. *Textile Research Journal*, 63(9), 504–514. <https://doi.org/10.1177/004051759306300902>
- Onder, E., & Baser, G. (1996). A comprehensive stress and breakage analysis of staple fiber yarns, part I: stress analysis of a staple yarn based on a yarn geometry of conical helix fiber paths. *Textile Research Journal*, 66(10), 634–640.

- <https://doi.org/10.1177/004051759606601004>
- Ortlek, H. G. (2005). Effect of some variables on properties of 100% cotton vortex spun yarn. *Textile Research Journal*, 75(6), 458–461. <https://doi.org/10.1177/0040517505053835>
- Ortlek, H. G., Nair, F., Kilik, R., & Guven, K. (2008). Effect of spindle diameter and spindle working period on the properties of 100% viscose MVS yarns. *Fibres and Textiles in Eastern Europe*, 16(3), 17–20.
- Oxenham, W., & Basu, A. (1993). Effect of jet design on the properties of air-jet spun yarns. *Textile Research Journal*, 63(11), 674–678. <https://doi.org/10.1177/004051759306301109>
- Oxenham, W., Zhu, R. Y., & Leaf, G. A. V. (1992). Observations on the tensile properties of friction-spun yarns. *J. Textile Inst.*, 83, 621–623.
- Pan, N. (1992). Development of a constitutive theory for short fiber yarns: mechanics of staple yarn without slippage effect. *Textile Research Journal*, 62(12), 749–765.
- Pan, N., Hua, T., & Qiu, Y. (2001a). Prediction of statistical strengths of twisted fibre structures. *Textile Research Journal*, 28(11), 960–964.
- Pan, N., Hua, T., & Qiu, Y. (2001b). Relationship between fiber and yarn strength. *Textile Research Journal*, 71(11), 960–964.
- Pei, Z., Hu, B., Diao, C., & Yu, C. (2012). Investigation on the motion of different types of fibers in the vortex spinning nozzle. *Polymer Engineering & Science*, 52(4), 856–867.
- Pei, Z., & Yu, C. (2009). Study on the principle of yarn formation of Murata vortex spinning using numerical simulation. *Textile Research Journal*, 79(14), 1274–1280.
- Pei, Z., & Yu, C. (2010). Numerical and experimental research on the influence of parameters on the tensile properties of Murata vortex yarn. *Journal of the Textile Institute*, 101(10), 931–940. <https://doi.org/10.1080/00405000903031228>
- Pei, Z., & Yu, C. (2011a). Investigation on the dynamic behavior of the fiber in the vortex spinning nozzle and effects of some nozzle structure parameters. *J Eng Fiber Fabr*, 6, 16–29.
- Pei, Z., & Yu, C. (2011b). Numerical simulation of fiber motion in the nozzle of Murata vortex spinning machine. *The Journal of the Textile Institute*, 102(4), 281–292.
- Pei, Z., & Yu, C. (2011c). Numerical study on the effect of nozzle pressure and yarn

- delivery speed on the fiber motion in the nozzle of Murata vortex spinning. *Journal of Fluids and Structures*, 27(1), 121–133.
- Peirce, F. T. (1926). Tensile tests for cotton yarns - the weakest link, theorems on the strength of long and of composite specimens. *Journal of the Textile Institute Transactions*, 17(7), T355–T368. <https://doi.org/10.1080/19447027.1926.10599953>
- Pillay, K. P. R. (1965). Seventh Tech. Conf. In *ATIRA, BTRA, and SITRA* (pp. 15–30).
- Punj, S. K., Mukhopadhyay, A., & Chakraborty, A. (1998). Effect of extension rate and gauge length on tensile behaviour of ring and air-jet spun yarns. *Indian Journal of Fibre & Textile Research*, 23, 19–24.
- Rajamanickam, R., Hansen, S. M., & Jayaraman, S. (1997a). A computer simulation approach for engineering air-jet spun yarns. *Textile Research Journal*, 67(3), 223–230. <https://doi.org/10.1177/004051759706700311>
- Rajamanickam, R., Hansen, S. M., & Jayaraman, S. (1997b). Analysis of the modeling methodologies for predicting the strength of air-jet spun yarns. *Textile Research Journal*, 67(1), 39–44. <https://doi.org/10.1177/004051759706700109>
- Rajamanickam, R., Hansen, S. M., & Jayaraman, S. (1998a). A model for the tensile fracture behavior of air-jet spun yarns. *Textile Research Journal*, 68(9), 654–662. <https://doi.org/10.1177/004051759806800906>
- Rajamanickam, R., Hansen, S. M., & Jayaraman, S. (1998b). Studies on fiber–process–structure–property relationships in air-jet spinning. part II: model development. *Journal of the Textile Institute*, 89(2), 243–265. <https://doi.org/10.1080/00405009808658614>
- Realff, M. L., Seo, M., Boyce, M. C., Schwartz, P., & Backer, S. (1991). Mechanical properties of fabrics woven from yarns produced by different spinning technologies: yarn failure as a function of gauge length. *Textile Research Journal*, 61(9), 517–530.
- Recommended procedure for preparation of samples. Soft and hard sections (slices). Internal standard no. 46-108-01/01, Faculty of Textile, Technical University of Liberec.* (2004).
- Rieter. (2017a). Air-jet spinning development. Retrieved from <http://www.rieter.com/cz/rikipedia/articles/alternative-spinning-systems/the-various-spinning-methods/air-jet-spinning/development/>
- Rieter. (2017b). Two nozzle air-jet spinning. Retrieved January 1, 2017, from

- <http://www.rieter.com/cz/rikipedia/articles/alternative-spinning-systems/the-various-spinning-methods/the-false-twist-process/two-nozzle-air-jet-spinning/operating-principle/>
- Rohlana, V. (1975). *Open-end spinning*. Elsevier Science Ltd.
- Rosen, B. W. (1983). *Mechanics of composite materials. recent advances*, Pergamon Press, Oxford, 105.
- Salhotra, K. R., Ishtiaque, S. M., & Kumar, A. (2006). Analysis of spinning process using the Taguchi method, part I: effect of spinning process variables on fibre orientation and tenacities of sliver and roving. *Journal of the Textile Institute*, 97(4), 271–284.
- Seo, M. H., Realff, M. L., Pan, N., Boyce, M., Schwartz, P., & Backer, S. (1993). Mechanical properties of fabric woven from yarns produced by different spinning technologies: yarn failure in woven fabric. *Textile Research Journal*, 63(3), 123–134. <https://doi.org/10.1177/004051759306300301>
- Sharma, D. (2004). Performance and low-stress characteristics of polyester-cotton MVS yarns. *Indian Journal of Fibre & Textile Research*, 29(September), 301–307.
- Sinha, S. K., & Kumar, P. (2013). An investigation of the behavior of thin places in ring spun yarns. *Journal of Textile and Apparel, Technology and Management*, 8(2).
- Spencer-Smith, J. L. (1947). The estimation of fibre quality. *Journal of the Textile Institute Proceedings*, 38(8), P257–P272.
- Suzuki, Y., & Sukigara, S. (2012). Mechanical and tactile properties of plain knitted fabrics produced from rayon vortex yarns. *Textile Research Journal*, 83(7), 740–751. <https://doi.org/10.1177/0040517512467132>
- Tyagi, G. K., Sharma, D., & Salhotra, K. R. (2004a). Process-structure-property relationship of polyester-cotton MVS yarns, part I: influence of processing variables on yarn structural parameters. *Indian Journal of Fibre and Textile Research*, 29(4), 419–428.
- Tyagi, G. K., Sharma, D., & Salhotra, K. R. (2004b). Process-structure-property relationship of polyester-cotton MVS yarns: part II: influence of process variables on yarn characteristics. *Indian Journal of Fibre and Textile Research*, 29(4), 429.
- United States Patent and Trademark Office, US Patent 2007/0125062 A1, <http://www.uspto.gov>. (2007). Retrieved from <http://www.uspto.gov>
- Xie, Y., Oxenham, W., & Grosberg, P. (1986). 25—A study of the strength of wrapped

- yarns, part II: computation and experimental. *Journal of the Textile Institute*, 77(5), 305–313. <https://doi.org/10.1080/00405008608658425>
- Zeguang Pei, & Chongwen Yu. (2011). Prediction of the vortex yarn tenacity from some process and nozzle parameters based on numerical simulation and artificial neural network. *Textile Research Journal*, 81(17), 1796–1807. <https://doi.org/10.1177/0040517511411970>
- Zeng, Y. C., Wan, Y.-Q., Yu, C. W., & He, J.-H. (2005). Controlling the air vortex twist in air-jet spinning. *Textile Research Journal*, 75(2), 175–177.
- Zeng, Y. C., & Yu, C. W. (2003). Numerical simulation of air flow in the nozzle of an air-jet spinning machine. *Textile Research Journal*, 73(4), 350–356.
- Zeng, Y. C., & Yu, C. W. (2004). Numerical simulation of fiber motion in the nozzle of an air-jet spinning machine. *Textile Research Journal*, 74(2), 117–122.
- Zhu, G., & Ibrahim, S. (2012). Optimization application of air-jet nozzle in ring spinning system, 9(5), 455–461.
- Zhuanyong Zou, Jianyong Yu, Wenliang Xue, Yunde Zhu, Jianming Wu, & Longdi Cheng. (2009). Analysis of the fiber spatial trajectory in vortex spun yarn. *Textile Research Journal*, 79(10), 924–929. <https://doi.org/10.1177/0040517508095609>
- Zhuanyong Zou, Longdi Cheng, Wenliang Xue, & Jianyong Yu. (2008). A study of the twisted strength of the whirled airflow in Murata vortex spinning. *Textile Research Journal*, 78(8), 682–687. <https://doi.org/10.1177/0040517508089753>
- Zou, Z., Liu, S., Zheng, S., & Cheng, L. (2010). Numerical computation of a flow field affected by the process parameters of Murata vortex spinning. *Fibres Text. East. Eur*, 18(2), 35–39.
- Zubair, M., Eldeeb, M., & Neckar, B. (2017). Tensile behavior of staple fiber yarns, part III: comparison of mathematical models. *The Journal of The Textile Institute*, 108(7), 1234–1237.
- Zurek, W., Frydrych, I., & Zakrzewski, S. (1987). A method of predicting the strength and breaking strain of cotton yarn. *Textile Research Journal*, 57(8), 439–444. <https://doi.org/10.1177/004051758705700802>
- Zurek, W., Malinowski, L., & Plotka, E. (1976). Analytical technological method of prediction of strength and breaking strain of cotton yarn. *Technical University of Lodz*, 33, 62–73.

Publications

Published articles

1. **Eldeeb M.**, Ismael Rakha, Fawkia Fahim, and Eman Elshahat, "Comparative study between plied "conventional and compact" spun yarns characteristics", Mansoura Engineering Journal, 2010, Vol. 35(2).
2. **Eldeeb M.**, Sayed Ibrahim, Ismael Rakha, Fawkia Fahim, and Eman Elshahat, "Effect of finishing process on plied compact and conventional ring spun yarn properties", Vlakna a Textila, 2015, Vol. 22(1), 5-8. ISSN 1335-0617.
3. **Eldeeb M.**, Ismael Rakha, Fawkia Fahim, and Eman Elshahat. "Optimizing the production process of conventional ring spun and compact plied yarns", Journal of Textile & Apparel, 2016, Vol. 26(1), 48-54.
4. **Eldeeb M.**, and Eva Moučková. "Numerical simulation of the yarn formation process in Rieter air jet spinning", The Journal of The Textile Institute, 2017, Vol. 108(7), 1219-1226.
5. **Eldeeb M.** and Bohuslav Neckář, "Prediction of spun yarn strength at different gauge lengths", The Journal of the Textile Institute, 2017, Vol. 0(0), 1-6.
6. **Eldeeb M.**, Eva Moučková, and Petr Ursíny, "Properties of Viscose Rieter air jet spun plied yarns", Indian Journal of Fiber & Textile Research, 2015, accepted.
7. Muhammad Zubair, **Eldeeb M.**, and Bohuslav Neckar, "Tensile behavior of staple fiber yarns, part III: comparison of mathematical models", The Journal of the Textile Institute, 2017, Vol. 108(7), 1234-1237.
8. Zuhaib Ahmed, **Eldeeb M.**, Shoaib Iqbal, and Adnan Mazari, "Cover factor of airjet and rotor fabrics by light transmission", Industria Textila, 2017, accepted.
9. Zuhaib Ahmad, Brigita Kolčavová Sirková, and **Eldeeb M.** "Yarn cross-sectional deformation in woven fabric", Vlakna a Textil, 2016, Vol. 23(4), 36-41. ISSN 1335-0617.
10. Muhammad Zubair, Bohuslav Neckar, **Eldeeb M.**, and Gulzar A. "Tensile behavior of staple fiber yarns, part IV: experimental verification of predicted stress–strain curves", The Journal of the Textile Institute, 2016, Vol. 108(8), 1291-1296.

11. Hafiz Shahzad Maqsood, Jakub Wiener, Vijaykumar Baheti, **Eldeeb M.**, and Jiri Militky. "Ozonation: a green source for oxidized cotton", FIBERS & TEXTILES in Eastern Europe 2016, Vol. 24(1), 19-21.

Articles under review

1. **Eldeeb M.**, and Eva Moučková, "Predicting the strength of air jet spun yarns using mathematical modeling", Autex Research Journal.
2. **Eldeeb M.**, and Ali Demir "Optimizing the production process of Rieter air jet spun yarns and a model for prediction of its strength", FIBERS & TEXTILES in Eastern Europe.
3. Shoaib Iqbal, **Eldeeb M.**, Zuhaib Ahmed and Adnan Mazari, "Comparative study on yarn and knitted fabric made from Open end and Rieter airjet spun system", Journal of Textile & Apparel.

Conferences and workshops

1. **Eldeeb M.**, Sayed Ibrahim, Ismael Rakha, Fawkia Fahim, and Eman Elshahat, "Effect of finishing process on plied compact and conventional ring spun yarn properties", 20th Conference STRUTEX (proceedings), Liberec: Technical University in Liberec, 2014. Not paged 4 pages. ISBN 978-80-7494-139-9.
2. **Eldeeb M.**, Sayed Ibrahim, Ismael Rakha, Fawkia Fahim, and Eman Elshahat, "Comparative study on finished compact and conventional ring spun yarn properties", 4th International Conference of Applied Arts (proceedings). Damietta: Damietta University, 2015, not paged 11 pages.
3. **Eldeeb M.**, "Theoretical analyses of air jet yarn strength", 21st Conference STRUTEX (proceedings), Liberec: Technical University in Liberec, 2016, 131-136 ISBN 978-80-7494-269-3.
4. **Eldeeb M.**, Eva Moučková, and Petr Ursíny, "Effect of plying process parameters on air jet spun yarn properties", Světlanka Workshop (Proceedings), Rokytnice Nad Jizerou: Světlanka, 2015, 37-42. ISBN 978-80-7494-229-7
5. **Eldeeb M.**, "Air Jet yarn properties based on structure", a presentation at the Bílá Voda Workshop, Harrachov, 20th - 23rd September, 2016.

6. Zuhaib Ahmad, Brigita Kolčavová Sirková, and **Eldeeb M.**, “Influence of weft setting on shape of yarn cross-section in woven fabrics”, Světlanka Workshop (Proceedings), Rokytnice Nad Jizerou: Světlanka, 2015, 08-14. ISBN 978-80-7494-229-7.

Other research activities

1. **Eldeeb M.**, Shoaib Iqbal, and Zuhaib Ahmed, A project entitled, “Effect of plying process on air jet yarn properties”, supported by “Student Grant Competition 2015”, Technical University of Liberec, Czech Republic, project no. 21086.
2. Zuhaib Ahmed, **Eldeeb M.**, and Shoaib Iqbal, A project entitled, “3D construction and structure of woven fabric”, supported by “Student Grant Competition 2015”, Technical University of Liberec, Czech Republic, project no. 21153.

Appendices

Appendix 1: 23 Tex Viscose yarns tenacity

Nozzle pressure (bar)	4		5		6	
	16.41	13.46	16.85	15.18	13.53	14.12
	13.27	15.13	15.54	16.74	15.69	13.64
	13.85	15.24	16.45	16.2	14.26	15.73
	15.19	12.94	16.09	15.03	14.25	15.25
	16.16	13.59	15.64	16.39	16.19	15.87
	13.12	13.37	16.35	16.5	14.89	15.18
	14.99	13.05	15.04	16.03	14.76	15.97
	15.03	14.71	15.47	15.36	14.01	15.87
	13.15	13.33	16.67	16.66	14.07	16.54
	13.28	13.4	15.48	16.75	14.99	16.63
	13.46	13.78	15.28	16.89	14.36	15.41
	13.65	12.89	16.32	16.39	15.1	14.81
	13.16	13.14	15.87	16.44	14.45	13.78
	13.63	15.02	15.97	16.54	16.26	14.49
	15.75	16.41	16.18	16.25	16.64	14.39
	15.13	14.83	16.26	16.11	16.57	14.17
	16.5	14.6	14.91	15.43	16.44	15.29
	15.68	15.2	15.78	15.77	14.68	15.73
	16.21	14.54	16.39	15.47	14.88	14.84
	14.01	15.75	15.23	16.77	15.94	15.89
	15.12	14.84	15.51	15.27	15.96	13.9
	15.37	14.89	15.63	15.83	14.23	15.87
	13.84	12.89	15.15	15.18	15.24	14.4
	15.25	13.89	15.2	15.83	14.25	13.74
	14	13.02	16.12	15.23	14.19	15.79
Average (cN/Tex)	14.4		15.9		15.1	
Confidence level (95%)	0.31		0.16		0.26	
Standard deviation	1.09		0.57		0.91	
Coefficient of variation (%)	7.6		3.6		5.9	

ANOVA summary: Single Factor

Groups	Count	Sum	Average	Variance		
P4	50	719.12	14.3824	1.201757		
P5	50	795.62	15.9124	0.327186		
P6	50	753.13	15.0626	0.814958		
Source of Variation	SS	df	MS	F	P-value	F crit
Between Groups	58.7622	2	29.3811	37.60537	6.47E-14	3.057621
Within Groups	114.8512	147	0.781301			
Total	173.6134	149				

Appendix 2: Wrapper ratio W% of 23 Tex Viscose yarns

Nozzle pressure (bar)	4				5				6	
	38.08	38.13	22.51	27.90	22.01	18.53	20.47	44.23	29.64	
	39.15	39.23	21.38	35.33	43.67	27.90	35.48	20.95	27.19	
	24.65	35.40	39.15	33.05	38.50	24.34	34.85	28.93	20.47	
	25.73	24.18	22.51	21.09	41.36	43.67	36.51	29.40	18.88	
	29.85	34.81	33.85	42.01	33.35	36.21	20.47	42.61	27.81	
	39.46	23.10	38.13	29.10	41.07	39.02	30.94	43.78	20.47	
	23.11	21.68	39.15	25.12	24.34	43.67	32.52	20.47	27.19	
	21.38	23.65	21.38	21.72	35.72	24.34	33.47	32.11	28.19	
	42.23	33.85	33.85	44.61	37.40	27.90	29.64	35.49	27.19	
	42.39	10.81	22.51	28.75	36.21	39.02	28.19	29.40	20.47	
	24.26	32.82	38.13	38.36	44.52	25.12	35.33	41.65	27.19	
	30.45	22.36	39.15	36.16	4.44	43.67	20.47	34.33	31.78	
	34.10	22.51	23.65	26.16	44.24	27.90	27.19	35.12	29.64	
	43.39	28.16	33.85	33.27	26.16	26.16	18.88	29.40	27.81	
	26.98	44.92	21.38	39.02	24.34	43.67	27.81	38.69	28.19	
	21.38	24.59	38.13	32.25	25.12	26.16	30.03	25.67	31.78	
	42.73	26.19	23.65	37.93	43.67	18.53	31.78	36.26	32.11	
	21.38	41.25	22.51	38.43	39.02	39.02	37.70	18.88	29.64	
	23.13	44.79	39.15	31.26	27.90	43.67	25.09	27.19	29.40	
	19.54	28.67	21.38	41.11	24.34	36.21	41.56	29.64	31.78	
	29.29	29.97	33.85	22.48	18.53	43.67	20.47	27.81	32.11	
	23.33	43.76	39.15	18.53	25.12	36.21	28.30	18.88	28.19	
	32.57	44.50	42.22	42.12	39.02	43.67	30.25	25.67	20.47	
	25.32			22.87			26.55			
Average (%)	30.70				32.7				29.3	
Confidence level (95%)	1.99				2.11				1.51	
Standard deviation	9.04				9.62				7.17	
Coefficient of variation (%)	29.39				29.44				24.51	

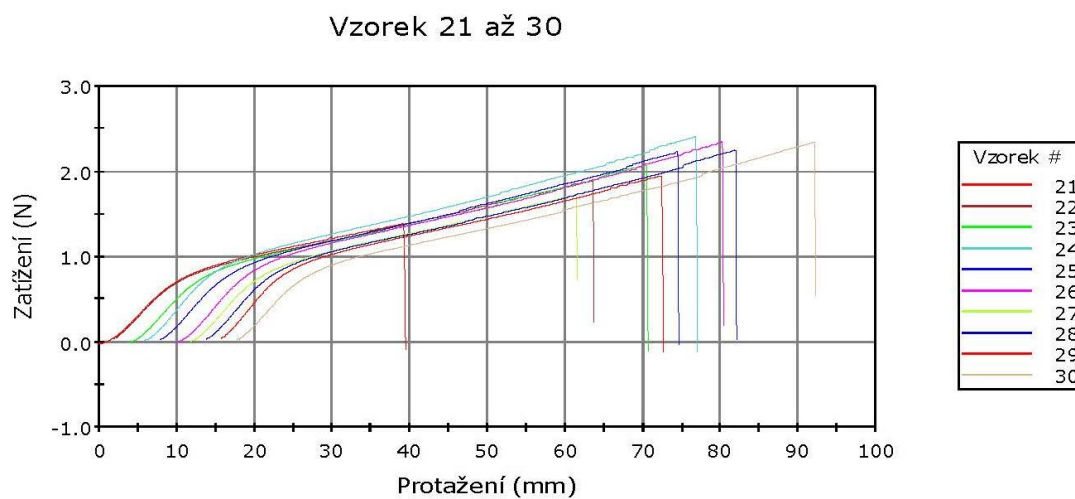
ANOVA summary: Single Factor

Groups	Count	Sum	Average	Variance		
P4	70	2153.853	30.76933	69.45831		
P5	70	2286.923	32.67033	78.59915		
P6	70	2048.05	29.25785	39.93206		
Source of Variation	SS	df	MS	F	P-value	F crit
Between Groups	409.3469	2	204.6735	3.266248	0.040124	3.039508
Within Groups	12971.28	207	62.66317			
Total						

Appendix 3: Average tested properties of Viscose yarn

Sample	Tenacity (cN/Tex)	Breaking elongation (%)	Irregularity (CVm %)	Thin places (-50%/km)	Thick places (+50%/km)	Neps (+140%/km)	Total imperfections (/km)	Hairiness (H)	Abrasive length (m)
1	12.9	12.34	14.12	35.6	29.2	166	230.8	3.96	1449
2	16.28	14.31	10.67	0	3.2	76.4	79.6	3.96	57
3	16.31	14.15	10.97	0	2.4	158.8	161.2	4.66	88
4	11.9	11.95	14.6	44.4	56.4	249.6	350.4	5.09	183
5	15.41	14.96	10.8	0.4	2	176.4	178.8	4.51	93
6	12.77	11.86	14.29	41.2	30.8	194.4	266.4	4.19	1154
7	16.5	13.95	10.63	0	5.2	77.2	82.4	4.06	95
8	15.35	14.02	12.48	15.6	5.2	187.6	208.4	4.29	324
9	14.26	12.86	12.06	0.8	6	154.8	161.6	5.94	500
10	14.15	14.06	12.26	4	5.6	242.8	252.4	3.78	226
11	14.41	13.25	12.21	12.4	12.4	238	262.8	4.59	405
12	15.64	13.67	12.25	3.2	6.8	202	212	4.42	298

Appendix 4: Stress-strain curves of Viscose yarn (16 Tex, pressure 5 bar, and delivery speed 350 m/min)



Appendix 5: Combined effect of yarn linear density, delivery speed, and nozzle pressure on yarn properties

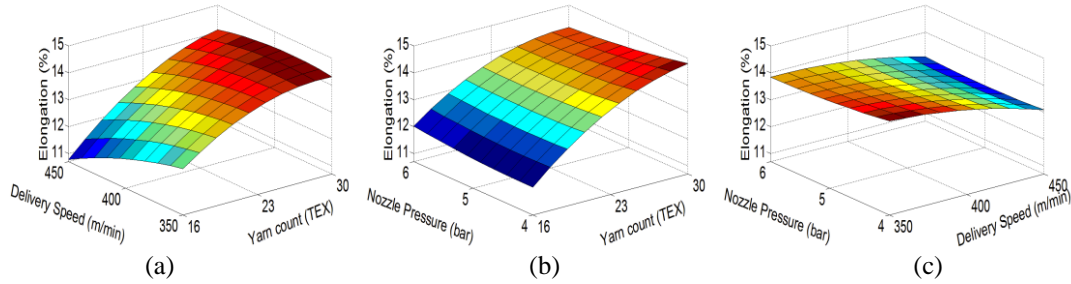


Figure 5.1 Interaction effect of (a) yarn linear density and delivery speed, (b) yarn linear density and nozzle pressure, and (c) nozzle pressure and yarn delivery speed on yarn breaking elongation.

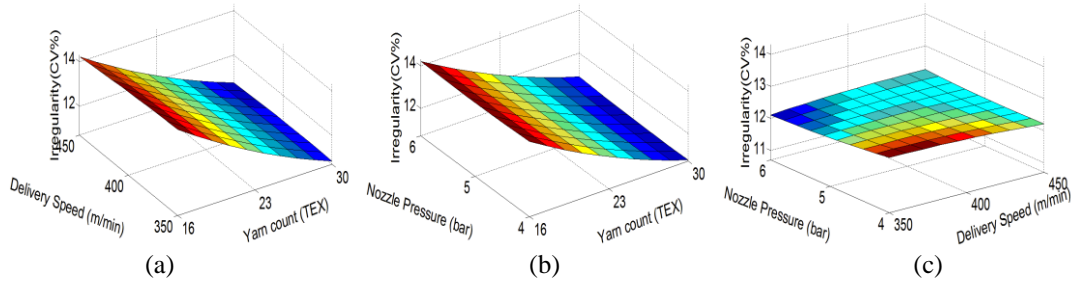


Figure 5.2 Effect of (a) yarn linear density and delivery speed, (b) yarn linear density and nozzle pressure, and (c) nozzle pressure and yarn delivery speed on yarn irregularity.

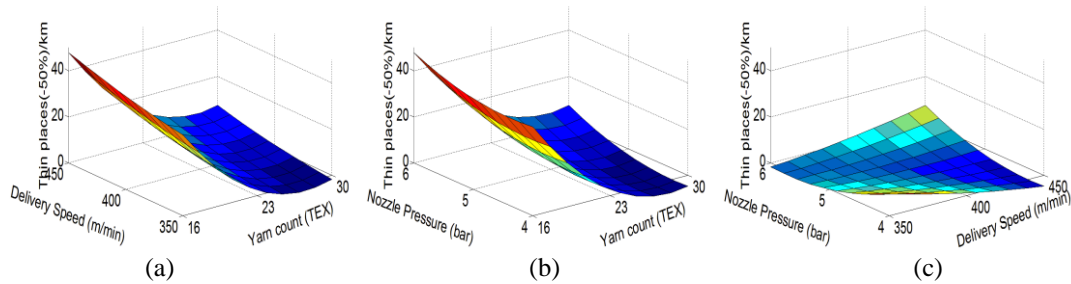


Figure 5.3 Effect of (a) yarn linear density and delivery speed, (b) yarn linear density and nozzle pressure, and (c) nozzle pressure and yarn delivery speed on yarn thin places.

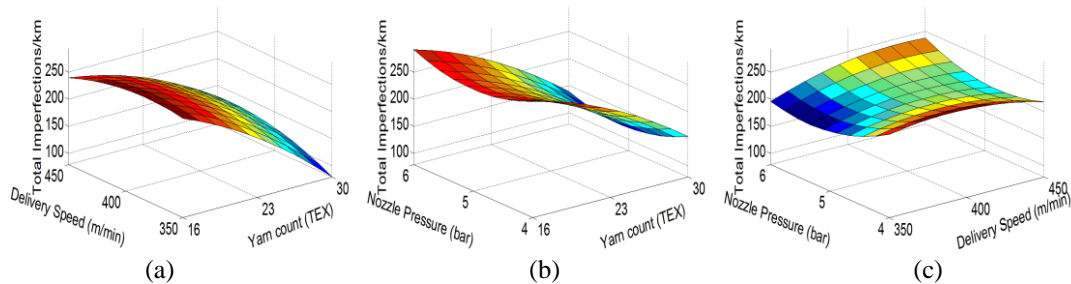


Figure 5.4 Effect of (a) yarn linear density and delivery speed, (b) yarn linear density and nozzle pressure, and (c) nozzle pressure and yarn delivery speed on yarn total imperfection.

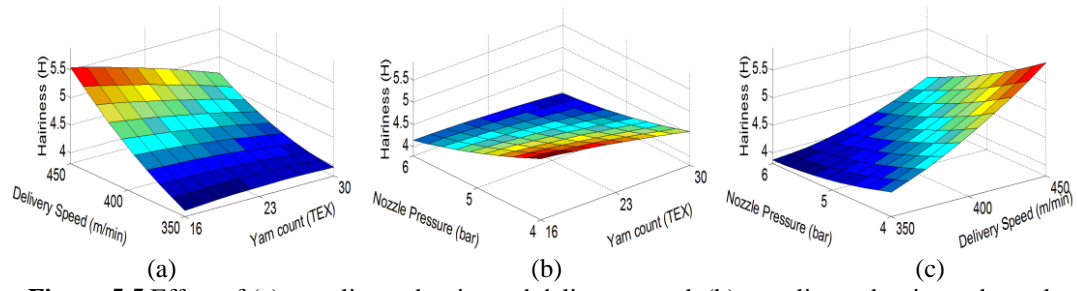


Figure 5.5 Effect of (a) yarn linear density and delivery speed, (b) yarn linear density and nozzle pressure, and (c) nozzle pressure and yarn delivery speed on yarn hairiness.

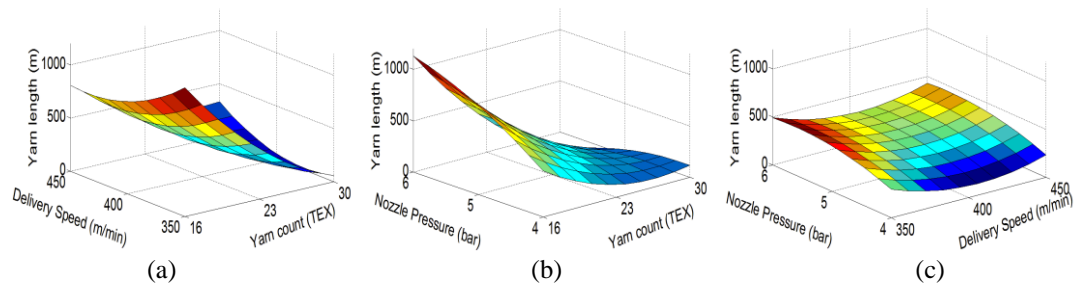


Figure 5.6 Combined effect of (a) yarn linear density and delivery speed, (b) yarn linear density and nozzle pressure, and (c) nozzle pressure and yarn delivery speed on yarn abrasiveness.

Appendix 6: Calculation of Viscose fiber length utilization factor

From equation (5.13)

$$(1 + e_f) = \frac{l_u}{l_{uo}} \quad (6.1)$$

Also, from Figure (5.3),

$$(1 + e_f)^2 = \frac{l_u^2}{l_{uo}^2} = \frac{2\pi r^2 + pi^2}{l_{uo}^2} = \frac{(2\pi r)^2}{l_{uo}^2} + \frac{pi^2}{l_{uo}^2} \quad (6.2)$$

It is valid that,

$$(1 + e_f)^2 = \frac{(2\pi r)^2}{l_{uo}^2} \cdot \frac{r_o^2}{r_o^2} + \frac{pi^2}{l_{uo}^2} \cdot \frac{p_o^2}{p_o^2} = \frac{(2\pi r_o)^2}{l_{uo}^2} \cdot \frac{r^2}{r_o^2} + \frac{p_o^2}{l_{uo}^2} \cdot \frac{pi^2}{p_o^2} \quad (6.3)$$

From Figure (5.3), equation (5.14), and equation (5.15),

$$(1 + e_f)^2 = (\sin \alpha_o)^2 (1 + e_r)^2 + (\cos \alpha_o)^2 (1 + e_y)^2 \quad (6.4)$$

From equation (5.19),

$$(1 + e_f)^2 = (\sin \alpha_o)^2 (1 - e_y)^2 + (\cos \alpha_o)^2 (1 + e_y)^2 \quad (6.5)$$

$$(1 + e_f)^2 = (1 - e_y)^2 (\sin \alpha_o)^2 + (1 + e_y)^2 (1 - (\sin \alpha_o)^2) \quad (6.6)$$

$$1 + 2e_f + e_f^2 = (1 - 2e_y + e_y^2)(\sin \alpha_o)^2 + (1 + 2e_y + e_y^2)(1 - (\sin \alpha_o)^2) \quad (6.7)$$

$$e_y^2 + e_y(2 - 4(\sin \alpha_o)^2) - e_f(2 + e_f) = 0 \quad (6.8)$$

$$e_y = \frac{-2 + 4(\sin \alpha_o)^2 \pm \sqrt{4 - 16(\sin \alpha_o)^2 + 16(\sin \alpha_o)^4 + 4e_f(2 + e_f)}}{2.1} \quad (6.9)$$

$$e_y = 2(\sin \alpha_o)^2 - 1 \pm \frac{\sqrt{4(\sin \alpha_o)^2 - 2)^2 + 4e_f(2 + e_f)}}{2} \quad (6.10)$$

As e_y is a positive value,

$$e_y = 2(\sin \alpha_o)^2 - 1 + \frac{\sqrt{4(2(\sin \alpha_o)^2 - 1)^2 + 4e_f(2 + e_f)}}{2} \quad (6.11)$$

And finally,

$$e_y = 2(\sin \alpha_o)^2 - 1 + \sqrt{(2(\sin \alpha_o)^2 - 1)^2 + e_f(2 + e_f)} \quad (6.12)$$

Appendix 7: Viscose and Tencel fibers tensile properties

Sample no.	Tencel			Viscose		
	Fineness (dtex)	Breaking force (cN)	Breaking elongation (%)	Fineness (dtex)	Breaking force (cN)	Breaking elongation (%)
1	1.15	5.25	9.20	1.41	2.42	14.40
2	1.16	4.82	10.10	1.39	3.08	21.90
3	1.15	5.25	9.20	1.37	2.91	14.70
4	1.31	5.74	4.30	1.15	2.55	24.10
5	1.15	5.72	9.20	1.35	3.12	21.70
6	1.56	6.46	12.60	1.20	2.75	14.70
7	1.16	4.33	11.60	1.52	3.55	15.60
8	1.55	5.74	9.90	1.56	2.28	12.70
9	1.36	5.40	5.70	1.36	3.19	18.40
10	1.46	5.72	10.60	1.29	2.83	22.90
11	1.38	5.25	5.36	1.40	3.59	21.20
12	1.41	4.34	9.10	1.23	2.47	18.90
13	1.18	5.25	9.15	1.49	2.93	19.10
14	1.51	4.81	8.20	1.18	2.41	21.10
15	1.17	5.74	9.16	1.46	3.54	18.70
16	1.30	5.72	9.25	1.02	2.41	16.20
17	1.20	4.71	9.40	1.29	2.78	19.70
18	1.33	4.10	9.30	1.20	3.29	21.10
19	1.40	4.35	9.10	1.18	2.39	16.10
20	1.20	4.45	9.10	1.40	3.48	20.60
21	1.15	5.25	9.20	1.31	3.30	20.90
22	1.29	4.14	7.10	1.16	2.45	21.60
23	1.20	5.40	9.25	1.51	3.10	23.40
24	1.16	4.33	9.28	1.15	2.40	21.10
25	1.18	5.72	9.16	1.16	3.19	22.60
26	1.56	5.72	5.36	1.55	3.61	22.60
27	1.32	5.60	9.13	1.12	3.07	20.10
28	1.30	5.40	9.14	1.56	3.43	19.70
29	1.15	4.50	8.10	1.46	3.93	21.10
30	1.42	4.63	6.78	1.38	3.47	17.40
31	1.23	4.60	7.44	1.38	3.32	18.70
32	1.24	5.30	8.26	1.39	3.90	20.30
33	1.33	5.20	7.10	1.28	3.98	19.30
34	1.39	5.60	7.46	1.12	3.91	17.80
35	1.28	5.30	8.20	1.15	3.84	16.90
36	1.15	5.63	5.32	1.16	3.96	14.90
37	1.09	5.42	7.10	1.26	3.30	18.60
38	1.20	5.12	7.42	1.16	3.94	18.80
39	1.23	5.29	7.46	1.39	3.86	16.90
40	1.28	5.28	8.20	1.52	3.00	16.70
41	1.30	5.63	8.60	1.53	3.90	20.10
42	1.31	5.61	7.46	1.40	3.95	20.50
43	1.32	5.45	6.43	1.10	3.60	19.50

44	1.32	5.40	7.10	1.12	3.70	20.50
45	1.34	5.20	8.20	1.16	3.55	21.30
46	1.31	5.23	6.38	1.12	3.70	21.90
47	1.36	5.36	5.26	1.18	3.95	21.40
48	1.42	5.12	7.10	1.17	3.93	22.60
49	1.45	5.16	6.43	1.22	3.80	19.80
50	1.44	5.44	6.23	1.24	3.15	19.10
Average	1.30	5.20	8.10	1.30	3.28	19.40
Confidence level (95%)	0.03	0.14	0.48	0.04	0.15	0.74
Standard deviation	0.12	0.51	1.68	0.15	0.54	2.61
Coefficient of variation (%)	9.38	9.77	20.76	11.44	16.36	13.46

Appendix 8: 16 Tex Viscose yarn structural parameters (Sample no. 1)

Sample no.	A	B	C	D	Helix diam eter	Pitch	Number of coils
1	57	67	231	496	62.0	496.0	1.0
2	75	88	258	532	81.5	532.0	1.0
3	71	90	59	128	80.5	128.0	1.0
4	54	69	218	438	61.5	438.0	1.0
5	60	73	226	573	66.5	573.0	1.0
6	60	68	361	628	64.0	628.0	1.0
7	70	91	254	522	80.5	522.0	1.0
8	60	79	210	476	69.5	476.0	1.0
9	53	63	225	470	58.0	470.0	1.0
10	60	70	410	510	65.0	510.0	1.0
11	49	67	109	402	58.0	402.0	1.0
12	48	59	115	217	53.5	217.0	1.0
13	56	79	78	195	67.5	195.0	1.0
14	47	53	226	550	50.0	550.0	1.0
15	63	88	98	299	75.5	299.0	1.0
16	49	89	30	313	69.0	313.0	1.0
17	39	53	83	443	46.0	443.0	1.0
18	61	85	97	240	73.0	240.0	1.0
19	56	75	159	432	65.5	432.0	1.0
20	52	65	163	462	58.5	462.0	1.0
21	57	75	181	607	66.0	607.0	1.0
22	61	78	162	539	69.5	539.0	1.0
23	61	72	221	490	66.5	490.0	1.0
24	62	78	94	244	70.0	244.0	1.0
25	56	69	215	408	62.5	408.0	1.0
26	57	78	69	145	67.5	145.0	1.0
27	45	72	61	240	58.5	240.0	1.0
28	64	76	156	252	70.0	252.0	1.0
29	41	58	62	284	49.5	284.0	1.0
30	47	58	206	394	52.5	394.0	1.0
31	61	74	177	393	67.5	393.0	1.0
32	63	77	196	556	70.0	556.0	1.0
33	73	87	355	593	80.0	593.0	1.0
34	85	104	132	664	94.5	664.0	1.0
35	60	76	190	658	68.0	658.0	1.0
36	51	61	277	717	56.0	717.0	1.0
37	67	79	311	884	73.0	884.0	1.0
38	48	70	30	172	59.0	172.0	1.0

39	67	72	554	931	69.5	931.0	1.0
40	78	91	373	858	84.5	858.0	1.0
41	54	77	39	205	65.5	205.0	1.0
42	63	74	220	437	68.5	437.0	1.0
43	55	67	166	453	61.0	453.0	1.0
44	60	70	254	637	65.0	637.0	1.0
45	72	81	170	401	76.5	401.0	1.0
46	67	86	231	598	76.5	598.0	1.0
47	65	78	95	128	71.5	128.0	1.0
48	61	71	341	601	66.0	601.0	1.0
49	65	76	164	341	70.5	341.0	1.0
50	60	78	188	442	69.0	442.0	1.0
51	69	80	323	635	74.5	635.0	1.0
Average		59.5	74.8	192.6	455.5	67.1	
Confidence level (95%)		2.60	2.90	30.20	53.69	2.62	
Standard deviation		9.3	10.3	107.4	190.9	9.3	
Coefficient of variation (%)		15.6	13.8	55.7	41.9	13.9	

Sample no.	Coil length	Cross section area	Wrapper volume	Core volume	Wrapper ratio (%)	Helix angle (°)	Number of wraps/m
1	532.8	1155.0	615427.9	1266181.7	32.7	22.0	Scale
2	590.4	1677.0	990018.1	2351250.0	29.6	24.0	200 Micron: 77.6 Unit
3	283.3	560.5	158807.2	506980.6	23.9	52.0	? Micron: 24928 Unit
4	478.7	1635.0	782643.4	1003520.6	43.8	27.0	
5	609.9	1469.0	895886.0	1620771.4	35.6	25.0	Total length=64.2 mm
6	659.4	1444.0	952130.4	1776342.9	34.9	21.0	
7	580.0	2667.0	1546806.4	2009700.0	43.5	24.0	53 Wrap: 64.2 mm
8	523.6	1995.0	1044664.6	1346400.0	43.7	25.0	? Wrap: 1000 mm
9	504.1	1125.0	567057.7	1037323.6	35.3	29.0	
10	549.3	2050.0	1126114.1	1442571.4	43.8	25.0	Number of wraps/m=
11	441.3	981.0	432944.2	758373.0	36.3	23.0	825.0
12	274.4	632.5	173574.5	392832.0	30.6	16.0	
13	288.0	897.0	258341.9	480480.0	35.0	26.0	
14	572.0	678.0	387795.3	954603.6	28.9	21.0	
15	381.6	1225.0	467435.3	932431.5	33.4	28.0	
16	380.7	600.0	228402.7	590474.5	27.9	27.0	
17	466.0	581.0	270718.5	529416.6	33.8	17.0	
18	331.9	1164.0	386303.9	701674.3	35.5	19.0	
19	478.5	1510.5	722714.1	1064448.0	40.4	28.0	
20	497.2	1059.5	526760.1	981552.0	34.9	36.0	
21	641.4	1629.0	1044845.0	1549540.9	40.3	31.0	
22	581.5	1377.0	800729.2	1575843.5	33.7	28.0	
23	532.6	1215.5	647419.6	1432585.0	31.1	29.0	

24	328.4	752.0	246958.5	736949.7	25.1	23.0
25	452.7	1397.5	632711.2	1005312.0	38.6	28.0
26	256.8	724.5	186053.8	370153.9	33.5	35.0
27	302.2	823.5	248885.1	381857.1	39.5	25.0
28	334.4	936.0	312988.2	811008.0	27.8	26.0
29	323.8	527.0	170616.6	375103.1	31.3	26.0
30	427.1	1133.0	483900.5	683843.3	41.4	21.0
31	446.5	1150.5	513710.6	1148991.6	30.9	28.0
32	597.9	1372.0	820277.1	1733886.0	32.1	24.0
33	644.0	2485.0	1600367.9	2482933.4	39.2	22.0
34	727.3	1254.0	912016.4	3769385.7	19.5	20.0
35	691.8	1520.0	1051500.4	1861200.0	36.1	23.0
36	738.2	1385.0	1022472.2	1465291.9	41.1	21.0
37	913.2	1866.0	1704096.1	3117931.1	35.3	21.0
38	252.8	330.0	83422.3	311369.1	21.1	34.0
39	956.2	1385.0	1324385.4	3283703.5	28.7	21.0
40	898.1	2424.5	2177417.0	4101485.1	34.7	27.0
41	290.4	448.5	130239.0	469684.3	21.7	39.0
42	487.1	1210.0	589349.1	1362784.5	30.2	36.0
43	491.8	996.0	489862.5	1076683.9	31.3	20.0
44	668.9	1270.0	849501.7	1801800.0	32.0	28.0
45	467.4	765.0	357593.0	1633330.3	18.0	25.0
46	644.4	2194.5	1414226.9	2109188.7	40.1	32.0
47	258.4	617.5	159583.7	424914.3	27.3	24.0
48	635.7	1705.0	1083915.3	1757109.4	38.2	24.0
49	406.6	902.0	366711.2	1131998.2	24.5	26.0
50	492.2	1692.0	832879.3	1250228.6	40.0	21.0
51	676.7	1776.5	1202190.8	2375398.9	33.6	25.0
Average	509.6	1262.2	705791.6	1359584.8	33.4	26.0
Confidence level (95%)	48.24	153.15	131844.65	245198.50	1.80	1.71
Standard deviation	171.5	544.5	468773.4	871802.8	6.4	6.1
Coefficient of variation (%)	33.7	43.1	66.4	64.1	19.2	23.4

Appendix 9: Calculation of Viscose fibers length utilization factor

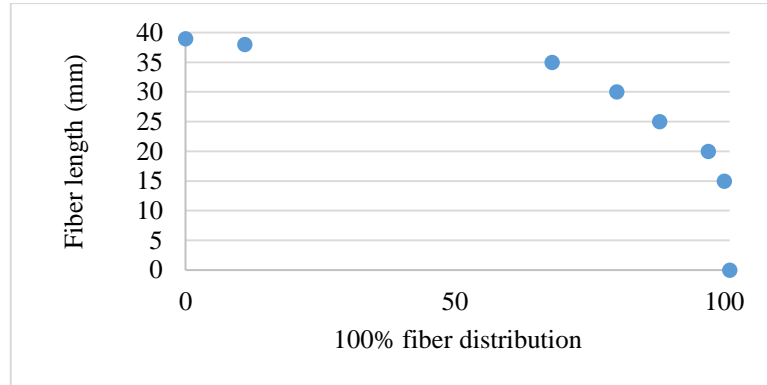


Figure 9.1 Fibrograph (fiber distribution by length).

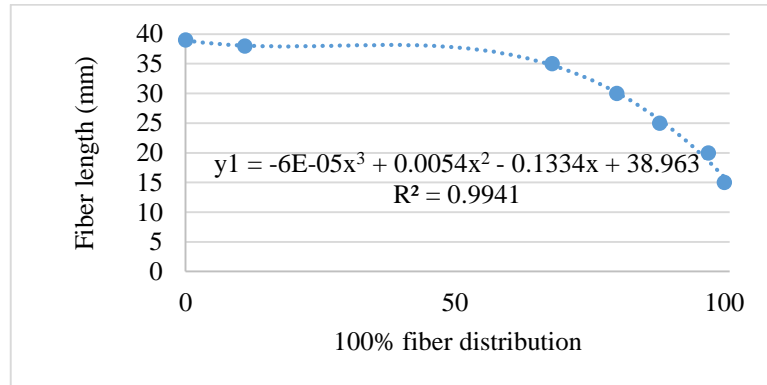


Figure 9.2 1st part of the Fibrograph (fiber distribution by length).

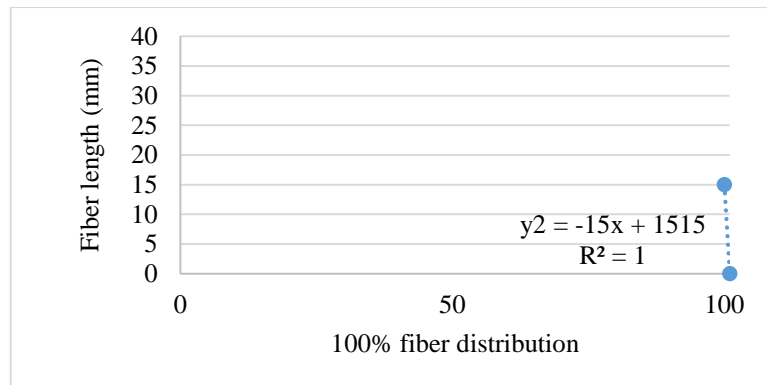


Figure 9.3 2nd part of the Fibrograph (fiber distribution by length).

$$\gamma(l) = \left(\int_0^{95} (y1) dx + \int_{95}^{100} (y2) dx \right) / (100 * 38) \quad (9.1)$$

$$\eta = \left(1 - \frac{30}{38} \right) \gamma(l) \quad (9.2)$$

Appendix 10: Tenacity values of 23 Tex Tencel yarns

Gauge length (mm)	Air jet spun yarn							
	60	100	200	300	400	500	600	700
23.26	25.55	22.69	22.25	21.81	20.88	21.28	21.63	
23.74	20.09	22.51	22.20	21.67	21.98	20.18	21.45	
25.24	20.22	26.04	21.06	23.57	21.85	21.45	24.05	
25.33	22.95	24.05	22.03	23.13	21.10	20.84	21.01	
27.67	23.08	23.08	22.38	21.01	21.23	19.60	17.49	
26.30	24.45	18.41	22.11	23.92	22.51	21.37	21.89	
24.19	23.00	19.47	22.16	23.17	24.85	22.60	21.50	
27.18	25.24	23.39	27.05	22.07	22.95	22.64	23.30	
25.99	24.36	22.51	25.51	23.00	20.93	22.56	20.93	
26.12	24.93	23.13	23.22	24.54	20.53	23.52	22.29	
24.80	24.45	22.95	23.83	23.74	21.76	22.73	19.52	
25.02	25.95	23.39	21.63	19.82	22.47	21.76	22.47	
21.89	24.41	21.89	20.75	23.52	21.15	24.71	21.89	
30.09	22.47	26.30	22.51	22.25	23.92	21.10	19.56	
23.70	20.88	25.90	23.44	22.64	23.79	20.75	21.01	
22.07	23.74	24.05	23.17	20.48	23.57	23.17	21.01	
22.86	21.67	22.42	21.28	23.30	20.75	23.00	20.48	
23.22	25.73	23.13	21.98	22.29	22.78	21.50	21.01	
26.83	24.98	22.64	21.94	17.89	23.66	22.86	21.15	
25.24	25.68	20.93	22.56	22.03	22.03	23.00	20.84	
27.05	29.03	19.60	22.73	23.17	21.85	22.69	20.88	
28.77	29.03	21.89	24.32	21.59	24.58	22.03	20.66	
30.84	26.48	23.00	23.22	23.48	24.67	22.82	21.41	
27.05	25.15	21.63	22.07	22.16	22.69	21.19	22.64	
23.92	24.27	24.85	25.37	19.87	22.73	19.60	20.84	
23.96	23.35	23.22	20.62	22.95	24.76	21.67	20.62	
25.55	24.63	23.57	24.98	22.91	22.07	24.67	21.85	
27.44	24.45	25.29	20.70	23.66	22.25	22.69	23.79	
26.65	23.30	21.98	26.83	23.44	22.86	22.33	22.60	
24.41	25.24	23.70	23.88	23.30	22.42	22.29	22.86	
25.55	22.38	24.36	24.71	23.00	21.67	20.22	21.67	
24.41	25.42	22.11	24.23	25.07	21.10	21.45	21.81	
23.30	22.95	24.63	24.63	22.38	23.26	19.96	23.48	
30.57	25.64	22.11	23.00	21.59	22.03	21.41	21.76	
25.95	24.93	19.52	20.62	22.82	25.07	21.59	20.88	
24.89	20.79	21.63	24.89	20.18	23.88	22.95	21.28	
33.61	24.49	25.37	22.25	23.04	21.85	20.48	22.73	
28.59	25.68	19.96	21.63	22.29	22.07	20.97	19.74	
24.98	22.82	22.51	25.20	24.01	21.10	20.88	21.72	

	26.43	21.89	22.60	22.03	22.20	18.63	19.56	22.56
	19.87	22.47	23.44	23.22	22.56	20.88	24.10	22.38
	21.59	27.18	21.06	21.54	25.37	21.89	20.13	22.33
	25.24	23.96	20.48	21.85	24.41	24.71	21.63	20.53
	28.15	24.10	23.48	23.66	22.82	23.88	23.00	21.76
	25.99	27.14	20.62	21.23	22.33	22.20	23.30	22.78
	22.25	22.38	23.52	22.91	25.02	21.98	22.38	23.48
	25.46	23.74	24.89	23.00	25.99	22.25	21.19	20.97
	29.21	25.29	23.30	23.79	22.03	20.93	19.03	21.19
	30.57	21.76	20.31	22.69	21.76	23.00	21.81	21.45
	23.57	24.76	26.43	23.57	21.63	24.05	22.20	20.66
	26.61	22.47	23.61	23.08	22.38	20.26	21.98	21.59
	26.83	26.61	19.91	22.82	25.02	24.76	20.75	23.04
	24.71	24.67	23.79	20.93	25.51	20.44	19.30	21.28
	23.92	23.26	24.76	21.89	21.67	23.26	21.59	21.01
	22.11	24.32	26.39	22.56	22.33	21.76	22.86	17.18
	27.14	25.42	25.55	24.27	22.73	23.96	22.29	22.56
	22.42	23.66	18.33	23.39	24.63	23.04	20.40	19.82
	22.82	27.44	23.48	21.67	20.40	22.03	19.38	21.41
	25.29	21.50	24.05	20.66	22.29	23.44	22.07	21.98
	26.65	24.27	24.89	27.14	24.14	23.44	22.03	20.79
	26.39	21.50	22.51	22.33	23.08	22.64	19.82	23.04
	21.19	25.46	21.50	23.57	20.48	21.45	21.23	19.91
	27.53	22.60	22.42	21.54	23.04	19.25	19.78	17.53
	24.85	28.41	26.87	23.00	22.60	18.99	23.00	19.65
	23.61	29.25	25.02	23.57	23.66	20.53	20.09	21.89
	26.34	21.54	21.32	23.96	23.17	21.50	21.45	22.91
	26.65	20.88	21.45	21.10	23.35	21.89	21.76	20.93
	24.41	20.97	24.41	24.76	23.04	20.79	20.53	19.69
	24.36	24.27	21.50	19.34	18.81	19.52	19.87	
	26.78	26.26	22.25	24.76	22.73	23.26	18.24	
	24.01	21.41	22.95	22.42	24.14	22.56	20.35	
	23.44	25.51	24.63	22.03	23.39	21.94	18.37	
	22.33	20.13	21.06	23.66	22.69		21.15	
	25.90	23.30	22.11	23.61	23.00		19.87	
	25.42	23.44	24.58	21.63			21.06	
Average (cN/Tex)	25.44	24.09	22.92	22.91	22.72	22.26	21.47	21.38
Confidence level (95%)	0.56	0.49	0.44	0.36	0.34	0.34	0.32	0.33
Standard deviation	2.45	2.11	1.91	1.55	1.47	1.45	1.38	1.36
Coefficient of variation (%)	9.62	8.77	8.34	6.77	6.47	6.49	6.44	6.38


Open end rotor spun yarn								
Gauge length (mm)	60	100	200	300	400	500	600	700
	18.17	21.27	20.83	19.78	19.00	16.86	15.81	19.78
	17.21	21.31	21.09	18.60	17.60	17.03	17.29	16.46
	24.10	21.70	21.44	16.29	16.99	16.90	18.95	16.29
	26.20	16.59	19.48	16.59	19.26	17.38	16.68	19.08
	25.68	19.04	21.53	20.61	17.12	18.21	18.08	17.55
	20.31	21.18	18.86	20.17	18.30	16.46	18.82	20.00
	22.97	21.88	19.91	18.73	17.60	17.12	17.34	18.34
	20.61	22.45	21.66	18.17	16.81	17.90	17.51	16.77
	14.72	22.66	19.21	16.94	17.82	17.29	18.91	18.17
	19.17	20.83	17.38	21.14	16.16	17.95	16.64	17.60
	20.83	19.91	19.00	15.76	18.69	15.28	18.38	16.90
	21.57	23.01	16.51	19.17	17.95	19.13	15.98	16.24
	24.85	20.35	18.25	17.38	16.59	18.47	16.99	17.73
	21.18	19.61	19.56	16.94	18.69	17.77	18.86	17.47
	19.91	17.90	20.00	19.17	16.86	16.90	19.91	15.24
	19.26	23.97	18.69	20.17	17.99	16.16	16.51	17.42
	18.65	23.62	18.82	18.82	20.09	19.91	15.55	17.12
	20.13	21.40	20.87	21.62	16.42	16.72	20.74	15.85
	19.00	21.83	18.91	19.00	18.38	17.07	18.30	16.24
	22.97	16.46	19.43	17.16	14.63	16.94	17.82	16.42
	18.82	19.34	21.09	18.52	18.95	17.82	18.03	16.42
	24.10	19.48	19.43	15.98	19.13	16.64	16.20	19.00
	23.45	20.09	18.43	19.39	19.21	19.78	18.86	15.50
	19.17	22.84	20.66	17.12	19.13	17.73	19.74	19.56
	23.41	21.09	21.22	21.53	18.73	18.43	18.21	18.34
	23.54	20.87	19.48	17.60	19.30	19.00	17.51	17.03
	22.97	22.49	18.34	19.61	16.94	19.13	19.26	19.78
	22.14	20.31	21.22	18.78	14.85	16.86	19.61	16.99
	23.54	18.82	19.78	20.26	20.83	17.25	17.77	16.72
	26.81	23.06	20.04	19.34	17.69	18.69	20.87	17.95
	22.75	18.69	19.69	20.04	16.11	18.17	15.46	16.11
	24.54	17.29	20.39	16.99	16.59	14.19	16.42	16.90
	20.70	19.26	17.03	17.03	18.78	17.90	16.77	15.59
	21.44	20.70	20.39	15.94	20.09	17.47	18.52	15.81
	21.00	18.65	19.39	18.34	18.38	17.03	18.56	17.12
	20.09	17.03	18.47	20.35	19.43	15.46	16.42	17.60
	22.45	22.01	17.69	16.46	16.59	17.29	20.39	15.98
	18.69	24.24	22.10	16.86	16.94	19.21	17.95	18.82
	19.65	22.01	22.75	19.61	14.89	16.99	17.51	19.34
	22.75	20.66	19.04	19.08	19.87	18.95	17.77	19.61
	22.79	21.09	21.40	19.91	18.47	17.77	16.24	16.99
	18.65	19.13	20.48	20.92	14.72	18.47	16.16	18.08

	21.53	20.13	19.39	21.88	19.30	16.11	15.90	17.60
	23.93	24.72	17.69	18.56	16.94	16.59	19.48	16.29
	24.24	17.82	18.78	17.82	20.09	18.30	18.38	17.38
	19.52	23.58	18.52	17.95	20.09	17.34	18.17	16.46
	20.92	21.83	18.08	21.31	18.65	17.38	17.38	16.24
	20.31	20.17	19.96	19.04	18.69	16.51	18.73	15.90
	21.70	19.65	20.35	19.43	16.20	18.95	19.65	15.33
	23.10	19.21	17.69	19.65	19.04	17.12	17.16	16.55
	23.10	17.55	17.77	19.13	15.98	18.47	18.56	15.63
	22.27	18.95	17.07	20.39	17.07	15.90	20.09	19.13
	23.28	22.45	19.43	20.22	18.38	16.33	19.17	16.72
	18.52	20.31	19.87	17.90	18.82	19.52	15.90	18.95
	19.83	21.00	18.25	18.30	19.48	19.83	15.72	16.86
	24.41	17.42	17.86	19.83	17.38	17.29	17.99	15.15
	23.62	19.65	20.44	20.83	19.74	18.03	20.26	18.65
	22.58	18.30	22.53	15.98	16.81	18.08	16.55	18.73
	21.79	18.12	17.16	18.43	18.52	17.42	17.82	16.81
	22.05	17.51	19.83	18.34	19.13	17.82	18.82	16.16
	22.18	19.83	20.17	16.90	18.38	18.65	15.63	15.55
	22.84	17.86	19.74	19.83	18.78	17.69	18.78	19.04
	24.15	23.76	18.91	20.96	20.66	18.08	19.17	16.51
	20.09	20.66	20.31	21.44	18.91	16.29	17.42	17.60
	20.74	21.97	17.86	16.46	17.03	15.24	18.03	16.33
	23.76	24.15	19.00	17.34	19.87	18.95	16.59	19.48
	23.14	20.83	17.60	16.55	16.90	19.17	17.25	19.52
	21.83	18.08	18.65	19.78	17.29	17.60	18.82	19.96
	24.24	24.19	20.57	18.56	17.38	15.90	17.99	
	22.97	17.51	19.91	20.48	18.82	15.02	17.60	
	20.87	20.48	21.27	19.96	19.78	17.51	16.77	
	20.52		19.43	18.34	18.12	20.04		
	21.31		16.20	20.92		16.16		
	21.18		21.00	16.16		20.31		
	26.42		17.95			17.38		
Average (cN/Tex)	21.78	20.48	19.46	18.79	18.07	17.58	17.87	17.36
Confidence level (95%)	0.52	0.49	0.33	0.38	0.34	0.29	0.32	0.33
Standard deviation	2.25	2.09	1.43	1.64	1.44	1.25	1.36	1.36
Coefficient of variation (%)	10.35	10.19	7.36	8.71	8.00	7.13	7.62	7.86

Ring spun yarn								
Gauge length (mm)	60	100	200	300	400	500	600	700
27.63	31.08	27.11	26.77	24.83	25.43	26.03	25.30	
27.63	25.13	26.94	23.62	25.99	24.66	25.56	21.72	
33.28	34.27	29.87	25.78	28.19	24.70	22.33	24.09	
35.52	29.44	27.03	28.10	24.22	24.40	22.46	25.17	
30.95	26.81	26.64	22.63	26.51	25.52	22.72	25.65	
31.55	28.49	28.79	27.11	25.47	25.86	22.24	26.42	
35.04	27.46	26.51	25.82	23.23	26.51	22.11	20.13	
29.27	23.66	25.99	22.20	25.47	23.41	22.93	25.69	
27.97	26.59	26.29	25.00	27.89	26.72	23.79	23.79	
27.20	29.87	25.13	26.55	26.68	27.80	27.41	23.75	
36.68	29.27	27.63	25.30	25.22	26.42	24.31	24.22	
30.82	25.00	27.50	25.13	24.22	25.60	25.73	25.30	
29.96	27.93	28.75	25.52	25.30	25.47	21.77	23.49	
34.70	28.10	28.79	22.07	24.40	24.57	23.28	23.92	
29.22	28.19	25.60	23.45	27.63	23.19	23.32	24.83	
34.18	30.00	25.43	25.39	28.32	25.95	23.62	21.98	
28.28	31.90	27.11	27.16	25.99	25.52	25.00	23.45	
33.75	30.91	27.63	28.28	23.19	25.04	24.48	24.27	
32.59	31.59	27.76	26.34	26.29	23.88	22.37	24.61	
30.34	28.58	30.47	28.23	23.49	26.42	24.61	25.04	
27.07	27.03	23.62	25.91	29.18	23.84	24.66	25.00	
33.41	28.28	30.22	23.79	24.87	22.84	23.75	24.40	
28.28	28.75	27.50	24.66	25.95	26.47	24.87	23.53	
30.95	27.37	26.47	25.86	25.52	26.12	25.26	24.61	
27.03	25.86	29.83	25.17	26.59	21.68	23.28	26.38	
28.23	30.13	27.89	24.87	27.63	24.70	24.44	21.90	
34.53	34.48	26.42	23.75	29.40	25.65	22.54	24.01	
25.47	29.44	28.49	27.72	23.75	23.92	25.73	25.34	
29.78	27.16	30.34	26.25	26.21	24.96	25.99	24.40	
28.75	28.23	23.02	29.31	24.96	25.73	24.96	26.25	
32.41	28.10	27.84	29.35	24.74	23.58	24.27	26.38	
33.15	27.03	27.16	26.85	28.23	22.72	24.83	21.85	
30.78	29.09	30.47	27.97	24.61	23.19	26.85	25.17	
33.10	31.12	27.93	27.72	25.95	26.77	25.22	23.71	
25.22	27.28	26.38	23.62	25.22	23.92	22.72	25.73	
26.94	28.92	28.84	25.65	27.24	21.85	23.45	24.44	
34.35	28.02	25.52	26.90	25.78	25.78	26.25	23.45	
29.78	27.07	27.50	26.12	25.39	24.18	23.62	24.27	
33.45	29.57	30.52	28.58	25.91	22.20	21.25	24.83	
25.09	28.02	28.97	28.79	25.78	25.17	26.94	23.41	
26.81	26.72	24.78	24.27	25.65	25.60	23.06	23.36	
28.97	25.39	26.34	27.07	27.72	26.98	26.38	23.58	

	36.34	31.98	28.49	28.92	25.04	25.56	23.19	20.82
	29.31	23.53	27.72	24.14	24.48	25.04	26.25	25.26
	31.38	25.60	25.95	26.29	26.51	24.48	27.59	26.03
	22.72	34.18	24.53	27.97	22.41	23.45	24.48	25.78
	37.37	26.81	24.53	22.97	26.59	28.41	25.86	25.82
	28.71	28.62	29.09	24.09	29.44	26.42	22.84	20.52
	28.88	26.59	29.27	27.50	24.78	26.12	25.13	25.99
	28.10	25.95	25.34	24.01	25.52	24.74	25.30	26.81
	29.70	29.09	25.17	25.86	28.58	26.47	23.49	24.31
	29.78	26.47	27.20	25.13	24.27	19.70	24.27	23.41
	27.67	27.54	28.36	24.87	24.53	25.09	25.39	25.47
	28.45	29.01	25.09	24.96	26.21	27.59	24.57	25.34
	32.89	27.33	30.65	26.64	26.03	22.80	23.75	24.01
	33.84	28.10	26.90	29.09	23.23	24.44	23.41	24.44
	33.32	27.59	28.58	24.57	25.43	25.04	26.77	24.96
	28.97	29.01	29.05	28.92	22.93	24.53	23.88	23.28
	29.18	26.25	28.10	25.82	26.68	25.56	25.60	24.05
	30.65	31.25	30.13	26.34	24.09	23.49	25.22	23.49
	32.76	29.70	29.78	23.62	22.76	23.71	20.56	25.17
	31.81	30.78	28.79	27.07	28.23	24.53	24.44	20.60
	33.58	30.34	28.10	27.11	24.14	22.67	25.04	21.64
	31.51	30.52	25.99	22.89	27.93	26.08	25.39	21.25
	28.49	28.10	29.31	26.81	28.41	24.01	23.28	21.98
	31.98	23.49	27.84	25.09	22.97	25.95	20.99	26.21
	28.15	31.98	27.72	25.34	23.28	23.02	25.26	23.62
	36.59	26.94	27.54	22.37	22.59	22.54	22.80	24.40
	31.38	24.22	26.85	26.03	27.54	24.96	27.46	
	26.85	25.86	26.90	28.23	24.87	23.10	25.30	
	29.61	29.61	24.53	27.33	27.93	23.58	26.72	
	29.09	24.01	23.88	22.84	24.83	25.47	24.70	
	29.09	28.41	27.37			23.10	24.53	
	30.34	26.64	27.24			24.74	26.08	
	30.26	27.46	27.16			19.53	23.58	
Average (cN/Tex)	30.52	28.27	27.42	25.88	25.71	24.68	24.39	24.17
Confidence level (95%)	0.70	0.55	0.41	0.44	0.41	0.38	0.36	0.38
Standard deviation	3.03	2.38	1.78	1.89	1.76	1.66	1.58	1.57
Coefficient of variation (%)	9.93	8.42	6.50	7.30	6.85	6.72	6.46	6.50

Curriculum Vitae

Personal information			
Name	Moaaz Eldeeb		
Address	5 Elmotaz Bellah St, Mansoura, Egypt		
Phone	+420 776 714 456		
E-mail	eldeeb.moaaz@gmail.com		
Nationality	Egyptian		
Marital status	Married		
Date of birth	23.11.1983		
Work Experience			
• Textile Technology Department, Faculty of Textile Engineering, Technical University of Liberec, Liberec, Czech Republic.	PhD scholar	2013-2017	
• Textile Technology Department, Faculty of Engineering, Mansoura University, Mansoura, Egypt.	Teacher	2011-2013	
• K.C.G Textile Egypt S.A.E Company for home textiles, El Asher men Ramadan, Egypt.	Teaching assistant	2009-2011	
• Oriental Weavers Company for carpets, El Asher men Ramadan, Egypt.	Quality assurance supervisor	2008-2009	
• El Gazar Company for ready-made garments, Mansoura, Egypt.	Maintenance and production Engineer	2006-2008	
	Planning Engineer	2005-2006	
Academic Profile and Fellowship Period			
• Mansoura University, Mansoura, Egypt	Textile Engineering Department, Faculty of Engineering	MSc Degree, Awarded	2011
• Küçükçalık company for home textiles, İnegöl, Turkey	Quality control	Training	2008
• Mansoura University, Mansoura, Egypt	Textile Engineering Department, Faculty of Engineering	BSc Degree, Very Good with honor (First of class)	2005
• Masr Company for spinning and weaving, El Mahala El Kobra, Egypt.	Maintenance	Training	2004
• El Nasr Company for spinning, weaving and dying, El Mahala El Kobra, Egypt	Production	Training	2003
Personal skills and competences			
• Ability to work in a team and utilize the team spirit to achieve good contributions to a specific project aim.			
• Ability to deal with different nationalities with a different background gained through my work with British, Turkish, Czech and other nationalities. Moreover, good communication skills, dedication, patience.			
Languages			
Arabic	Mother tongue	Turkish	Little
English	Good	French	Little

Social skills and competences	
Institutional skills and competence	A Strong tendency towards the rationalization of goals.
	Ability to work with others in a team environment with minimum supervision.
	Competence for analysis, improvement of current product configuration, and product and material innovation.
	Ability to define problems, collect, analyze data, identify and validate root cause.
Technical skills and competences	Aware of the total quality management system.
	Good command of quality control processes (quality audits).
	Aware of Sulzer weaving machine maintenance.
	Aware of basic yarn structural testing methods using microscopic analyses (optical and SEM).
Computer skills and competences	Aware of fiber and yarn physical testing instruments.
	Basic knowledge of yarn cross-section analysis.
	Writing skills, public relations and events management.
	Professional knowledge of AutoCAD 2D, 3D, and Auto Lisp.
	Basic knowledge of graphic design applications (ACDSee, Adobe Photoshop).
	Aware of Matlab (image processing, artificial neural network analysis, mathematical computation, data processing, 2d curves and 3D surface plotting).
	Good command of Microsoft Office tools (Word, Excel, and PowerPoint).
	Basic knowledge of ANSYS software.
Awards and honor's	
First of class award during Bachelor study (2002, 2003 and 2004)	